Vascular Fto has cell-type specific functions in regulation of myogenic tone

Inaugural dissertation

for the attainment of the title of doctor
in the Faculty of Mathematics and Natural Sciences
at the Heinrich Heine University Düsseldorf

presented by

Nenja Anita Krüger
from Düsseldorf

Düsseldorf, November 2016

from the Institute for Animal Developmental and Molecular Biology (EMT)
at the Heinrich Heine University Düsseldorf

Published by permission of the
Faculty of Mathematics and Natural Sciences at
Heinrich Heine University Düsseldorf

Supervisor: Prof. Dr. Ulrich Rüther
Co-supervisor: Prof. Dr. Axel Gödecke

Date of the oral examination: 01.12.2016

Für meine Eltern

Acknowledgement

First of all, I would like to thank my supervisor Prof. Dr. Ulrich Rüther for giving me the opportunity to work on this project. Thank you for all your guidance, advice and support throughout this project. Furthermore, I would like to thank my co-supervisor Prof. Dr. Axel Gödecke for always finding time for productive discussions to my project and for being a great head of the IRTG. I would also like to thank PhD Brant Isakson for being more than just a cooperation partner, but a mentor for me and my project- not just during my time in Charlottesville, but also back in Düsseldorf. I could not imagine how I could have had a better exchange phase as I had.

Furthermore, I would like to thank the whole Isakson lab for supporting me throughout good and bad times, for making me feel being a part of the lab, all the ideas and the great times we had. Especially, I would like to thank Lauren, Miranda and Daniela who became real friends so far away from home. For all your support during day and night times, keeping my back and for all the fun times we had (although, I admit: a lot of time was in the lab). I would also like to thank Tzu-Ying for offering me a place to stay in Charlottesville. We became much more than just roommates; you are such a lovely person and you always made me feel home!

I would like to also thank the whole Rüther lab, especially Steffi S., Jule, Mel, André, Andreas and Antonia for a supportive and great time together here in the lab. Furthermore, I would like to thank the IRTG 1902 for funding me and giving me the opportunity of being part of such a great exchange program. Sandra, Janett, and Steffi, thank you for all support in coordinating and planning everything so great. Furthermore, I would like to thank Lucia and Sofia for the great time we had here in Düsseldorf and Charlottesville!

I would like to also thank my friends Ina, Kerstin, Cora, Edwina, Svenja and Theresa for all the support and all the great time we had together in so many years. I know, we will just have even more fun together in the future.

Schlussendlich möchte ich meinen Eltern danken: Ich weiß, dass es nicht selbstverständlich ist, Eltern zu haben, die einen so aufrichtig lieben und einen immer unterstützen, wie sie nur können. Mein Leben lang wart ihr immer für mich da, habt mich gefördert und mich zu dem Menschen gemacht, der ich heute bin. Ich danke euch von ganzem Herzen für alles und freue mich, dass ich voller Glück sagen kann, dass ihr meine Eltern seid. Ich würde euch für nichts in der Welt hergeben wollen!

Table of content

I Statutory declaration

Statutory declaration

I hereby assure that I wrote the dissertation "Vascular Fto has cell-type specific functions in regulation of myogenic tone" independently and without other resources as indicated in compliance with "Grundsätze zur Sicherung guter wissenschaftlicher Praxis an der Heinrich-Heine Universität Düsseldorf".
Furthermore, I assure that I did not submit this dissertation, either in full or in part, to any other academic institution and did not absolve any promotion trials before.

Düsseldorf,

_____

Nenja Anita Krüger

Eidesstattliche Erklärung

Ich versichere an Eides Statt, dass die Dissertation „Vascular Fto has cell-type specific functions in regulation of myogenic tone" von mir selbstständig und ohne unzulässige fremde Hilfe unter Beachtung der „Grundsätze zur Sicherung guter wissenschaftlicher Praxis an der Heinrich-Heine Universität Düsseldorf" erstellt worden ist.
Darüber hinaus versichere ich, dass ich die Dissertation weder in der hier vorgelegten noch in einer ähnlichen Form bei einem anderen Institut eingereicht habe und bisher keine Promotionsversuche unternommen habe.

Düsseldorf, den

_____

Nenja Anita Krüger

II List of abbreviations

Special characters

%	Percentage
∆P	Pressure gradient
°C	Degree Celsius
α_1	alpha1
β_2	β_2

A

AA	Arachidonic acid
ACE	Angiotensin converting enzyme
ACh	Acetylcholine
ADP	Adenosine diphosphate
AlkB	Alpha-ketoglutarate dependent dioxygenase
AlkBH5	AlkB Homolog 5
AngII	Angiotensin II
ANS	Autonomous nervous system
Approx.	Approximately
APS	Ammonium persulfate
AT_1 receptor	Angiotensin II receptor 1
ATP	Adenosine triphosphate
AUC	Area under curve

B

$BaCl_2$	Bariumchloride
BK_{Ca}	Large-conductance Ca^{2+}-activated potassium channel
BMFZ	Biological-medical research center
BMI	Body mass index
Bp	Blood pressure
BSA	Bovine serum albumin

C

Ca^{2+}	Calcium
cAMP	Cyclic adenosine monophosphate
cDNA	Copy DNA

cGMP	Cyclic guanosine monophosphate
CNS	Central nervous system
CO_2	Carbon dioxide
COX	Cyclooxygenase
Cre+	Cre-recombinase expression
Cre-ER^{T2}	Tamoxifen-inducible Cre recombinase
cRNA	Copy RNA
CV	Cardiovascular
CVD	Cardiovascular disease
Cx	Connexin
D	
Da	Dalton
DAPI	4‘6-diamidino-2-phenylindole
DMEM	Dulbecco’s modified eagle medium
DMSO	Dimethyl sulfoxide
DMT	Danish Myo Technologies
DNA	Deoxyribonucleic acid
dNTP	Deoxyribose nucleotide triphosphate
DP	Prostaglandin D2 receptor
DTT	Dithiotreitol
E	
E	Epinephrine
e.g.	*exempli gratia*, for example
EC Cre-; $Fto^{fl/fl}$ +Tmx	Tamoxifen-injected VeCadherin-$CreER^{T2}$- ;$Fto^{flox/flox}$
EC Cre+; $Fto^{fl/fl}$ +Po	Peanut oil-injected VeCadherin-$CreER^{T2}$+ ;$Fto^{flox/flox}$
EC Cre+; $Fto^{fl/fl}$ +Tmx	Tamoxifen-injected VeCadherin-$CreER^{T2}$+ ;$Fto^{flox/flox}$
EC	Endothelial cell
ECE	Endothelin-converting enzyme
EDH	Endothelial derived hyperpolarization
EDHF	Endothelial derived hyperpolarization factor
EDTA	Ethylene diamine tetra acetic acid
EEL	External elastic lamina
EGTA	Ethylene glycol tetra acetic acid

ENaC	Epithelial Na^+ channel
eNOS	Endothelial nitric oxide synthase
EP	Prostaglandin E2 receptor
Et *al.*	*Et alii/ et aliae*, and others
ET-1	Endothelin-1
ET_A	Endothelin receptor A
ET_B	Endothelin receptor B
F	
F	Blood flow
F-actin	Filamentous actin
FBS	Fetal bovine serum
FCS	Fetal calf serum
FFA	Free fatty acid
Fig.	Figure
Fl	Floxed
FOR	Forward
FP	Prostaglandin F2 receptor
Ft	Fused toes
Fto/FTO	Fat mass and obesity associated gene
G	
g	Gram
g	Gravity
GAPDH	Glyceraldehyde 3-phosphate dehydrogenase
GDP	Guanine diphosphate
GPRC	G-protein coupled receptor
GTP	Guanine triphosphate
GTT	Glucose tolerance test
GWAS	Genome wide association studies
H	
HAoEC	Human aortic endothelial cells
HBSS	Hanks balanced salt solution
HCoSMCs	Human coronary smooth muscle cells
HDL	High density lipoprotein cholesterol

HEPES	4-(2-hydroxyethyl)-1-piperazineethanesulfonic acid
HFD	High fat diet
HR	Heart rate
I	
i.p.	Intraperitoneally
IB	Immunoblot
IEL	Internal elastic lamina
IF	Immunofluorescence
IgG	Immunoglobulin G
IK_{Ca}	Intermediate Ca^{2+} -activated potassium channel
IL-6	Interleukin 6
iNOS	Inducible nitric oxide synthase
IP	Prostacyclin receptor
IP3	Inositol-triphosphate
IR	Insulin resistance
Irx3	Iroquois-class homeodomain protein 3
ITT	Insulin tolerance test
J	
K	
K^+	Potassium
kb	Kilobase
Kg	Kilogram
K_{ir}	Inward rectifier potassium channel
L	
L	Liter
LD	Inner lumen diameter
LDL	Low-density lipoprotein
L-NAME	NG-nitro-L-arginine methyl ester
M	
M	Mole
M3	Muscarinic acetylcholine receptor type 3
M6A	N6-methyladenosine
MAP	Mean arterial pressure

MEJ	Myoendothelial junction
MeRIP-sequencing	Methylated RNA immunoprecipitation followed by sequencing
MetS	Metabolic syndrome
Mettl14	Methyltransferase-like 14
Mettl3	Methyltransferase-like 3
Min	Minute
miRNA	Micro RNA
MLC 20	Myosin light chain 20
MLCK	Myosin light chain kinase
MLCP	Myosin light chain phosphatase
mmHg	Millimeter mercury, unit of pressure
mRNA	Messenger RNA
N	
n.a.	Not applicable
Na^+	Sodium
Na^+/K^+- ATPase	Sodium-potassium adenosine triphosphatase
NC	Normal chow
NE	Norepinephrine
NEAA	Non-essential amino acids
NLS	Nuclear localization sequence
nNOS	Neuronal nitric oxide synthase
NO	Nitric oxide
NS309	6,7-dichloro-1*H*-indole-2,3-dione 3-oxime
O	
O_{2^-}	Superoxide
OCR	Oxygen consumption rate
P	
P	Prostanoid
P/S	Penicillin and streptomycin solution
PBS	Phosphate-buffered saline
PCR	Polymerase chain reaction
PE	Phenylephrine
PFA	Paraformaldehyde

Pgd2	Prostaglandin D2
Pgds	Prostaglandin D2 synthase
Pge2	Prostaglandin E2
Pges	Prostaglandin E2 synthase
Pgf2	Prostaglandin F2
Pgfs	Prostaglandin F2 synthase
Pgg2	Prostaglandin G2
Pgh2	Prostaglandin H2
Pgi2	Prostacyclin
Pgis	Prostacyclin synthase
Pgj2	Prostaglandin J2
P_i	Phosphate
Pkg	Protein kinase G
Pla2	Phospholipase A2
Plc	Phospholipase C
Po	Peanut oil
Ppar-γ	Peroxisome proliferator- activated receptor-gamma
Q	
qRT-PCR	Quantitative real time polymerase chain reaction
R	
R	Vascular resistance
r	Vessel radius
RAAS	Renin angiotensin aldosterone system
Rev	Reverse
RhoA	Ras homolog gene family member A
RhoGEF	Rho Guanine exchange factor
RIN	RNA integrity number
RM	Repeated measurements
RNA	Ribonucleic acid
ROCK	Rho-associated protein kinase
ROS	Reactive oxygen species
RT	Room temperature
Runx1	Runt-related transcription factor 1

S

SAC	Stretch-activated channel
SDS	Sodium dodecyl sulfate
Ser	Serine
sGC	Soluble guanylate cyclase
siRNA	Small interfering RNA
SK_{Ca}	Small Ca^{2+} -activated potassium channel
SMC	Smooth muscle cell
SMMHC	Smooth muscle myosin, heavy polypeptide 11
SNP	Single nucleotide polymorphism
SNP	Sodium nitroprusside
SR	Sarcoplasmic reticulum
Srf	Serum response factor

T

Tab.	Table
Thr	Threonine
Tmx	Tamoxifen
TNF- α	Tumor necrosis factor-alpha
TP	Thromboxane A2 receptor
TRPC6	Transient receptor potential channel homologue 6
TRPV4	Transient receptor vanilloid channel 4
Txa2	Thromboxane A2
Txs	Thromboxane A2 synthase

U

U	Units

V

V	Volt
v/v	Volume percent
VDCC	Voltage-dependent calcium channel
VeCadherin	Vascular endothelial cadherin

W

w/v	Mass percent
wt	Wildtype

WTAP	Wilms tumour 1-associated protein
X	
Y	
YTHDF2	YTH domain family 2 protein
Z	

III List of figures

Supplements

IV List of tables

1 Summary

Genetic variations within the *Fat mass and obesity associated* (*FTO*) gene have been linked to obesity and cardiovascular diseases in humans. In line with this linkage, global *Fto* deficiency in mice was found to protect against the development of obesity and obesity-induced metabolic changes such as hyperglycemia. These effects have been reported to have a significant and direct effect on cardiovascular health. Indeed, human studies have linked *FTO* to hypertension. Although *FTO* is clearly associated with obesity and hypertension, there have not been any mechanistic studies analyzing a role of *Fto* in blood pressure regulation. In order to accomplish this, the influence of vascular Fto on myogenic tone (MT) in resistance arterioles should be investigated, as MT directly regulates blood pressure by altering peripheral resistance.

A role of vascular Fto in myogenic tone was initially indicated by microarray analysis of thoracic aortae of $Fto^{+/+}$ and $Fto^{-/-}$ mice, as pathway analysis revealed that *Fto* deficiency affected SMC contraction. Because of this, endothelial cell (EC)- and smooth muscle cell (SMC)- specific *Fto* deficient mice were generated. In both mouse models, there was a strong influence on MT, but not on body weight by *Fto* deficiency. While EC-specific *Fto* deficient mice were protected from high fat diet- (HFD-) induced changes on MT, SMC-specific *Fto* deficiency significantly reduced MT in normal chow- (NC-) fed mice. Further metabolic analysis in HFD-fed mice revealed that EC-specific *Fto* deficiency significantly improved glucose and insulin tolerance, while dyslipidemia was not affected. Data from our initial microarray analysis helped us to identify a mechanism whereby this could be occurring and pointed to a role of the Prostaglandin D2 synthase in ECs and the Serum response factor in SMCs.

In conclusion, these data revealed that vascular Fto is not only important in regulation of MT, but also in HFD-induced metabolic changes. EC-specific *Fto* deficiency protected from HFD-induced changes on MT and improved glucose homeostasis indicating it may be important in the development of obesity-induced insulin resistance, hyperglycemia and hypertension. Remarkably, collaborative studies could verify a reduced blood pressure in EC-specific *Fto* deficient HFD-fed mice suggesting that EC-specific *Fto* deficiency protected from obesity-induced hypertension. In contrast, SMC-specific *Fto* deficiency reduced MT in NC-fed mice. Also here, collaborative studies verified that SMC-specific *Fto* deficiency significantly reduced blood pressure in mice.

These data show for the first time that vascular Fto is important in regulation of MT and blood pressure in both NC-fed and HFD-fed mice independent from its known protective effects on obesity. Furthermore, endothelial *Fto* appeared to be central in mediating obesity-induced metabolic changes in glucose homeostasis in HFD-fed mice.

2 Zusammenfassung

Genetische Variationen innerhalb des „*Fat mass and obesity associated*" (*FTO*) Gens sind dafür bekannt, mit Übergewicht und kardiovaskulären Krankheiten im Menschen zu korrelieren. In Übereinstimmung mit diesen Daten sind globale *Fto*-defiziente Mäuse nicht nur vor Übergewicht geschützt, sondern auch vor der Entstehung von übergewichtsbedingten metabolischen Veränderungen wie beispielsweise Hyperglykämie. Diese metabolischen Veränderungen sind dafür bekannt, einen signifikanten und direkten Einfluss auf die kardiovaskuläre Gesundheit zu haben. In der Tat zeigen humane Studien eine Korrelation von genetischen Variationen des *FTO* Locus mit Bluthochdruck. Obwohl *FTO* mit Übergewicht und Bluthochdruck assoziiert ist, gab es noch keine mechanistischen Analysen darüber, ob und wie Fto den Blutdruck beeinflusst. Um dies herauszufinden, soll die Rolle von vaskulärem Fto in der Regulation von myogenen Ton (MT) in Resistenzarterien analysiert werden, da dieser den Blutdruck durch eine Änderung der peripheren Resistenz direkt beeinflusst.

Dass vaskuläres Fto in der Regulation von myogenen Ton von Bedeutung sein könnte, wurde durch initiale Microarray-Analysen von thorakalen Aorten aus *Fto* wildtypischen und *Fto*-defizienten Mäusen angedeutet, da Signalwegsanalysen zeigten, dass *Fto* Defizienz glatte Muskelzellkontraktion beeinflusst. Daraufhin wurden endotheliale und glattmuskuläre *Fto*-defiziente Mäuse generiert. In beiden Mausmodellen zeigte eine *Fto* Defizienz starken Einfluss auf den MT, aber nicht auf das Körpergewicht. Während endothelial *Fto*-defiziente Mäuse vor den Einflüssen einer hochkalorischen Diät (HD) auf den MT geschützt waren, bedingte die glattmuskuläre *Fto*-Defizienz einen signifikant reduzierten MT in Mäusen auf einer normalen Diät (ND). Weitere metabolische Analysen in HD-gefütterten Mäusen konnten zeigen, dass endotheliale *Fto*-Defizienz Glukose- und Insulintoleranz verbesserte, wobei es keinen Einfluss auf die Dyslipidemie hatte. Daten des initialen Microarrays halfen bei der Identifizierung möglicher zellulärer Mechanismen und deuteten auf eine Rolle der Prostaglandin D2 Synthase in Endothelzellen und des „Serum response factors" in glatten Muskelzellen hin.

Schlussfolgernd zeigen diese Daten, dass vaskuläres Fto nicht nur wichtig ist in der Regulation von MT, sondern auch in der Entwicklung von HD-induzierten metabolischen Veränderungen. Endotheliale *Fto*-Defizienz in HD-gefütterten Mäusen schützte vor den durch eine HD ausgelösten Veränderungen auf den MT und verbesserte den Glukosehaushalt signifikant. Diese Daten deuten darauf hin, dass endotheliales *Fto* in der Entstehung von übergewichtsbedingter Insulinresistenz, Hyperglykämie und Bluthochdruck wichtig sein könnte. In Kollaboration durchgeführte Blutdruckmessungen konnten bestätigen, dass endotheliale *Fto*-Defizienz den Blutdruck in HD-gefütterten Mäusen signifikant reduzierte und lässt vermuten, dass endotheliale *Fto*-Defizienz vor der Entstehung von übergewichtsbedingtem Bluthochdruck schützen kann. Im Gegensatz dazu führte eine *Fto* Defizienz in glatten Muskelzellen zu signifikant reduziertem MT in ND-gefütterten Mäusen. Auch hier konnte eine Reduktion des Blutdrucks durch eine glattmuskuläre *Fto*-Defizienz bestätigt werden.

Diese Daten zeigen zum ersten Mal, dass vaskuläres Fto wichtig ist in der Regulation von MT in mesenterialen Arterien und im Blutdruck in ND- und HD-gefütterten Mäusen, unabhängig von dem bekannten protektiven Effekt gegenüber Übergewicht. Darüber hinaus scheint endotheliales *Fto* zentral an der Entstehung von übergewichtsbedingten metabolischen Veränderungen im Glukosehaushalt in HD-gefütterten Mäusen beteiligt zu sein.

3 Introduction

3.1 Mesenteric arteries are key regulators of peripheral vascular resistance

Mesenteric arteries are small resistance arteries which are the most important vascular regulators of blood pressure. Pathophysiological changes in mesenteric artery function are known to cause hypertension which is a risk factor for cardiovascular diseases (CVDs), the global number 1 cause of death [1-4]. Therefore, it is important to understand the mechanisms leading to mesenteric artery dysfunction which would allow the development of new therapeutics for treating hypertension and resulting CVDs.

3.1.1 Anatomy of mesenteric arteries

Mesenteric arteries are located within the gastrointestinal tract. Arising from the abdominal aorta, the superior and inferior mesenteric artery branch into smaller arteries and arterioles with subsequent capillaries to allow proper distribution of blood to different parts of the gut. As mesenteric arteries branch into smaller arterioles, the lumen size and vessel properties change to fulfill their physiological roles. While bigger vessels such as the thoracic aorta function as a balloon reservoir for blood leaving the heart, smaller vessels are more important in regulating blood flow to protect the following organs. To fulfill these demands, large vessels have a different vessel wall composition compared to smaller vessels.

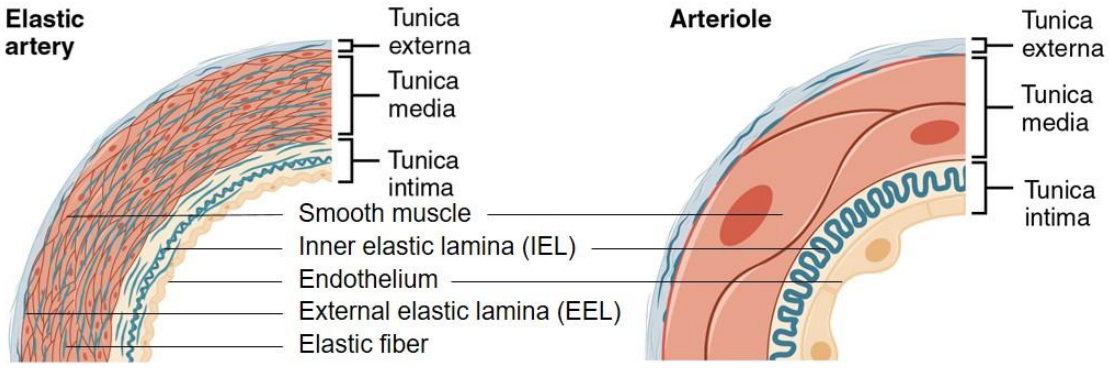

Fig. 1: Vessel wall structure of an elastic artery and arteriole in comparison
Both an elastic artery (left) and an arteriole (right) vessel wall are composed of three layers: the tunica intima, the tunica media and the tunica externa. Starting from the lumen, the first layer is the tunica intima which consists of endothelial cells (ECs) followed by an elastic layer, the internal elastic lamina (IEL). The next layer, the tunica media, shows vessel-type specific differences: while elastic arteries have various layers of smooth muscle cells (SMCs) and a high percentage of elastic fibers, arterioles have nearly no

elastic fibers and usually one to two layers of SMCs. The last elastic layer of the tunica media is the external elastic lamina (EEL) which is only present in elastic arteries and separates the SMCs from the outermost layer, the tunica externa. The tunica externa of both vessel types consists of loose collagen fibers and anchors the vessel to the surrounding tissue (Modified, [5]).

As illustrated in Figure 1 (Fig. 1), in large vessels close to the heart, which are also called elastic arteries (e.g. the aorta), the vessel wall has a high percentage of elastic fibers surrounding the smooth muscle cells (SMCs). Starting from the lumen, the innermost part of the vessel wall, the tunica intima consists of endothelial cells (ECs) which line the lumen of the artery and represent the cell type being in contact to the flowing blood. This one cell layer is surrounded by loose connective tissue and followed by an internal elastic lamina (IEL) that consists of elastic fibers and delimits the tunica intima from the next layer, the tunica media. The tunica media of elastic arteries is compared to other vessel types very thick as it consists of repetitive sheets of circumferential ordered SMCs and elastic laminae layers. The last elastic layer which is called the external elastic lamina (EEL) separates the tunica media from the outermost layer, the tunica adventitia. This layer consists of loose collagen fibers, anchors the vessel to adjacent tissue and contains exclusively in large vessels "vasa vasori", which are small arteries and veins needed to supply nutrients to the different vascular cell types within large vessels [6].

In contrast to elastic arteries, resistance arteries (e.g. 3rd order mesenteric arteries) are part of the microcirculation and have a lumen diameter between 15 and 300 μm depending on species. They derive from arteries and branch out to subsequent capillaries. As their physiological role is to propagate sufficient blood supply depending on the metabolic need of the following organs, their main function is to regulate blood flow and pressure by changing their lumen diameter. To allow proper regulation of blood flow, these vessels have a comparatively low amount of elastic fibers. The only elastic layer present in this vessel type is the IEL (see Fig. 1). Furthermore, these vessels are characterized by a thin tunica intima consisting of a monolayer of ECs with nearly no surrounding connective tissue. Also, the tunica media is comparatively thinner and consists nearly exclusively of SMCs. Depending on the vessel size, the SMCs can build up one to two repetitive layers which allow a fast constriction of these vessels [6]. In addition, resistance arteries are characterized by a high number of myoendothelial junctions (MEJs). MEJs are projections of mainly ECs, but also of SMCs through the IEL to the other respective cell type and connect the cells directly via gap junctions [7]. As the contractile status of resistance vessels is a highly regulated process, MEJs allow heterocellular crosstalk

between ECs and SMCs of these vessels revealing the importance of different cell types in regulating SMC contraction in resistance arteries.

3.1.2 Physiological role of mesenteric arteries

Resistance arteries, such as 3rd order mesenteric arteries, are the main contributor to vascular resistance. The importance of vascular resistance is apparent, if considering the equation between blood flow (F), blood pressure (bp) and vascular resistance (R) which is comparable to Ohm's law for the relation of current, resistance and voltage:

$$F = \frac{\Delta P}{R}$$

This equation says that the blood flow is equal to the quotient of the pressure gradient (∆P) and the resistance inside the system. For example in the systemic circulation the blood flow is equal to the pressure gradient between the root of the thoracic aorta and the right atrium, while the resistance is equal to the systemic vascular resistance. Thereby, higher resistance is reducing blood flow, if the pressure gradient is kept constant. Vice versa, an increase in resistance is affecting the pressure gradient, if the flow is constant. The dependence of these variables shows the importance of vascular resistance as this can be adapted to the metabolic need in a rapid and efficient way.

In detail, the first equation can be extended to Pouseuille's law to understand the importance of different factors attributing to resistance: the vessel radius (r), the viscosity of blood and the length of all tubes inside the system. This leads to the following equation:

$$F = \frac{\pi \times \Delta P \times r^4}{8 \times (viscosity\ of\ blood) \times length\ of\ tube}$$

This equation says that blood flow is equal to the pressure gradient multiplied with the vessel radius to the power of 4 divided by the viscosity of blood and the length of tubes inside the system. In the circulation, neither length of tubes nor blood viscosity can be changed (quickly). However, it is possible to alter the diameter of vessels by either increasing lumen diameter (vasodilation) or decreasing lumen diameter (vasoconstriction), especially in resistance arteries. Furthermore, this equation emphasizes the importance of the radius on blood flow and vice versa blood pressure, as doubling the radius leads to a 16-fold increase in blood flow or pressure, respectively [8].

3.2 Vasoactive properties of mesenteric arteries

The importance of resistance arteries (e.g. 3rd order mesenteric arteries) in vascular resistance is becoming obvious by contemplating their vessel properties to other vessel types (e.g. thoracic aorta). In 1902, Bayliss observed that if the pressure in resistance vessels is increased causing a stretch of the vessel, the vessel starts to constrict to decrease the lumen diameter and thereby increasing the resistance [9]. Although this Bayliss effect, known as myogenic tone, is not unique to resistance arteries, it gains importance with decreasing vessel size and only small resistance arteries can provoke a substantial decrease of lumen diameter in response to pressure increases [10, 11].

Interestingly, further studies could reveal that neither ECs nor neuronal input are mandatory for myogenic tone as their removal does not inhibit myogenic tone development; however, they are important in proper regulation of myogenic tone [12]. The only obligatory cell type for myogenic tone are SMCs which induce contraction by a cellular signaling pathway. Briefly, an increased intraluminal pressure leads to stretching of the vessel wall which is sensed by mechanosensitive receptors. Their activation induces a Calcium (Ca^{2+})-dependent SMC contraction and therewith decrease of lumen diameter. As seen in Fig. 2 A, an incremental increase of intraluminal pressure of a resistance artery from 10 mmHg to 100 mmHg induces an incremental increase of lumen diameter from 100 µm to 194 µm if no Ca^{2+} is present. However, with normal extracellular Ca^{2+} concentration, the lumen diameter does not increase if pressure is increased higher than 40 mmHg, but slightly decreases to a lumen diameter of 133 µm at 100 mmHg (Fig. 2 A). This observation is caused by myogenic tone and is important in autoregulation of flow. As illustrated in Fig. 2 B, blood flow is constantly increasing in both fully constricted and fully dilated vessels with increasing pressure, but myogenic tone allows autoregulation of flow. This leads to a nearly constant flow over a range of pressure to allow proper nutrient supply of the following organs and to protect downstream capillaries from elevated pressure. Its limitations are only reached if the vessel is either fully dilated or fully constricted.

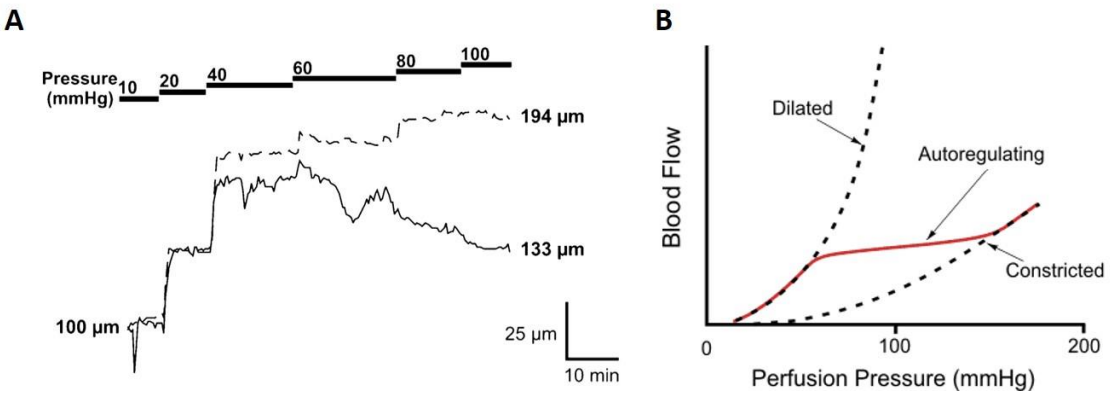

Fig. 2: The Bayliss effect influences vessel diameter of resistance arteries with increasing pressure (A) and the relationship between blood flow and perfusion pressure (B)
(A) Recording of the lumen diameter of a resistance artery with increasing intraluminal pressure from 10 mmHg up to 100 mmHg with Ca^{2+} (solid line) and without Ca^{2+} (dashed line). Without Ca^{2+} the lumen diameter incrementally increases with pressure from 100 µm at 10 mmHg to 194 µm at 100 mmHg. In contrast, the lumen diameter starts to decrease if the pressure is increased to more than 40 mmHg resulting in a lumen diameter of 133 µm at 100 mmHg when Ca^{2+} is present. The difference between these curves is called the Bayliss effect (or myogenic tone). (B) The Bayliss effect leads to a non-linear relation between blood flow and perfusion pressure of a resistance artery. If a vessel is fully dilated (no constriction of SMCs), an increase of pressure induces increased flow (dashed line). Also, if a vessel is fully constricted, increased pressure leads to an increased blood flow (dashed line). Comparing these two curves, it is obvious that the dilated vessel has a higher blood flow at each pressure compared to the constricted vessel. The Bayliss effect (red line) induces that a resistance vessel is keeping blood flow nearly constant between a high range of perfusion pressure, which limits are if the vessel is fully vasodilated or fully vasoconstricted (Modified, from [13] (A) and [6] (B)).

3.2.1 Myogenic tone

Although myogenic tone is still present even if ECs or nerves are not functional, both cell types can regulate myogenic tone by a variety of factors. This is necessary as the physiological role of resistance arteries is to allow proper nutrient supply depending on the tissues demand. For instance, when a person is digesting food, the gastrointestinal tract needs a higher blood supply to allow transportation of all nutrients as compared to a person not digesting food. Therefore, resistance arteries can either constrict leading to higher vascular resistance and reduced blood flow or dilate inducing decreased vascular resistance and increased blood flow. This mechanism should allow a proper distribution of blood to all organs.

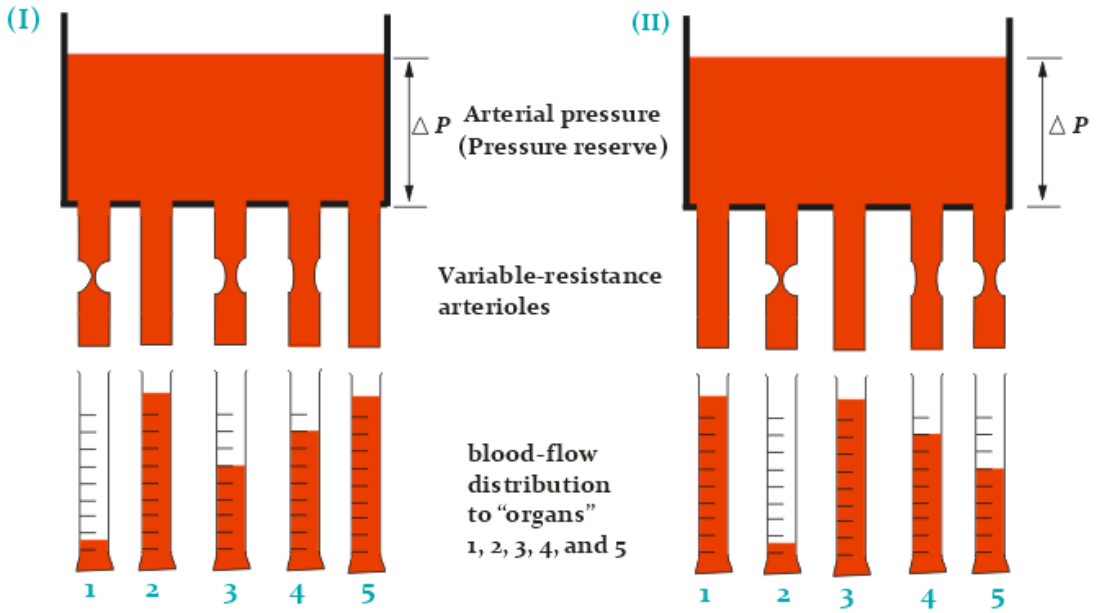

Fig. 3: Schematic illustration of the relationship between arterial pressure, resistance artery radius and blood supply of the following organs
In both conditions (I and II), the arterial pressure is the same. While in (I) resistance arteries to organs 1, 3 and 4 are constricted leading to a reduced blood flow and supply of their following organs, in (II) resistance artery to organs 2, 4, and 5 are constricted resulting in reduced blood supply of their following organs. In this way, resistance arteries can influence the distribution of blood depending on the tissues demand (Modified, from [14]).

As illustrated in Fig. 3, vasoconstriction of resistance arteries affects blood flow and supply to their following organs while the arterial pressure is constant. In (I) vessels 1, 3 and 4 are more constricted compared to vessel 2 and 5 which causes a reduced blood supply to the following organs of the constricted resistance arteries. In contrast, in (II) the blood supply is highest for organs 1 and 3, whose resistance arteries are less constricted compared to organ 2, 4 and 5. This illustrates the physiological role of resistance arteries in regulation of blood flow and blood supply by changing lumen diameter.

To allow constriction of resistance arteries depending on the local and systemic situation, the "basal" myogenic tone can be modulated by various stimuli such as neurohumoral, mechanical, metabolic, local as well as paracrine mechanisms, which all together define vascular tone. At a specific pressure, myogenic tone induces a partial vasoconstriction of the resistance artery. Depending on the influencing factors, the vessel can then either vasodilate to increase blood flow or further constrict inducing less blood flow. In this way, the lumen diameter of resistance arteries is adapted to both, systemic and local requirements.

3.2.2 Regulation of vascular tone in mesenteric arteries

Both ECs and SMCs in resistance arteries have important roles in the regulation of vascular tone. As ECs are in contact with blood, they can sense factors such as blood flow (in particular shear stress), metabolites and nutrients in the blood. The ECs can then transduce the stimulus into a cellular mechanism via the release of vasoactive compounds or electrical signals to the adjacent SMCs which can react with increased or decreased vasoconstriction. Similar to ECs, also SMCs themselves are able to initiate vasoconstriction, e.g. via activation of cell surface receptors.

To understand the effect of different factors on vascular tone, it is first important to understand the cellular signaling in both ECs and SMCs in regulation of vascular tone.

In both cell types, the regulation of cytosolic Ca^{2+} (via internal store release or from extracellular sources) and membrane potential are important in regulation of vascular tone. However, an increase of intracellular Ca^{2+} in ECs induces vasodilation while respective increase of Ca^{2+} in SMCs induces vasoconstriction revealing cell-type specific differences. Therefore, the following two chapters (3.3 and 3.4) will explain the role of both cell types in regulation of vascular tone in more detail.

3.3 Smooth muscle cells in regulation of vascular tone

Smooth muscle cells are crucial to vascular tone generation. Their constriction depends on the crossbridge-cycle of sliding actin and myosin filaments. To allow binding of actin and myosin filaments, myosin has to be in a high-energy form where the myosin head is bound to adenosine diphosphate (ADP) and phosphate (P_i). In the next step, the "power stroke", ADP and P_i get released from the myosin head and the free energy is used to move the myosin head with the attached actin filament. Now, myosin is in its low-energy form until adenosine triphosphate (ATP) binds to the myosin head inducing a conformational change and releasing the bound actin filament. To get back in its high-energy status, the myosin ATPase hydrolyzes bound ATP to ADP and P_i to allow new binding of actin for starting a new crossbridge-cycle.

Regulation of the crossbridge-cycle is mainly dependent on the phosphorylation of the myosin light chain 20 (MLC 20). MLC 20 phosphorylation can be regulated by different pathways including pressure-induced constriction (myogenic tone) or agonist-induced

constriction. While myogenic tone is induced by a cellular cascade following an increase in intraluminal pressure, agonist-induced constriction is mainly dependent on activation of G protein coupled receptors (GPCR). Both pathways influence intracellular Ca^{2+} concentration and Ca^{2+} sensitivity to regulate the phosphorylation of MLC 20 and reveal the dependence of both pathways.

3.3.1 Agonist-induced smooth muscle cell contraction

Agonist-induced contraction of smooth muscle cells is primarily initiated by activation of GPRCs or membrane depolarization and transduces intracellular effects via two pathways: A Ca^{2+}-dependent pathway and a Ca^{2+}-independent (Ca^{2+}-sensitization) pathway (see Fig. 4).

In the Ca^{2+}-dependent pathway, intracellular Ca^{2+} levels can be increased by two different mechanisms. First, membrane-depolarization induces opening of voltage-dependent Ca^{2+} channels (VDCC) allowing influx of extracellular Ca^{2+}. Second, activation of phospholipase C (PLC) leads to increased levels of inositol-triphosphate (IP3) which subsequently activates ryanodine receptors on the sarcoplasmic reticulum (SR) inducing SR-stored Ca^{2+}-release. The increased cytosolic Ca^{2+} concentration then induces binding of Ca^{2+} to Calmodulin which activates the Myosin light chain kinase (MLCK). MLCK in turn is phosphorylating MLC 20 on Serine 19 (Ser 19) and Threonine 18 (Thr 18) to initiate contraction [15].

In comparison, the Ca^{2+}-sensitization pathway affects MLC 20 phosphorylation by inhibiting the Myosin light chain phosphatase (MLCP) resulting in increased levels of phosphorylated MLC 20. This inactivation of MLCP is induced by the Ras homolog gene family member A- (RhoA-) dependent pathway. Activation of various GPRCs induces activation of their coupled G-protein. Coupled $G_{q/11}$ and $G_{12/13}$ proteins are known to activate Rho-Guanine exchange factors (RhoGEFs) which sequentially activate the monomeric GTPase RhoA by exchanging bound GDP to GTP. GTP-bound RhoA can then in turn activate the Rho-associated protein kinase (ROCK) which phosphorylates and thereby inhibits MLCP leading to more phosphorylated MLC 20 (reviewed in [16]).

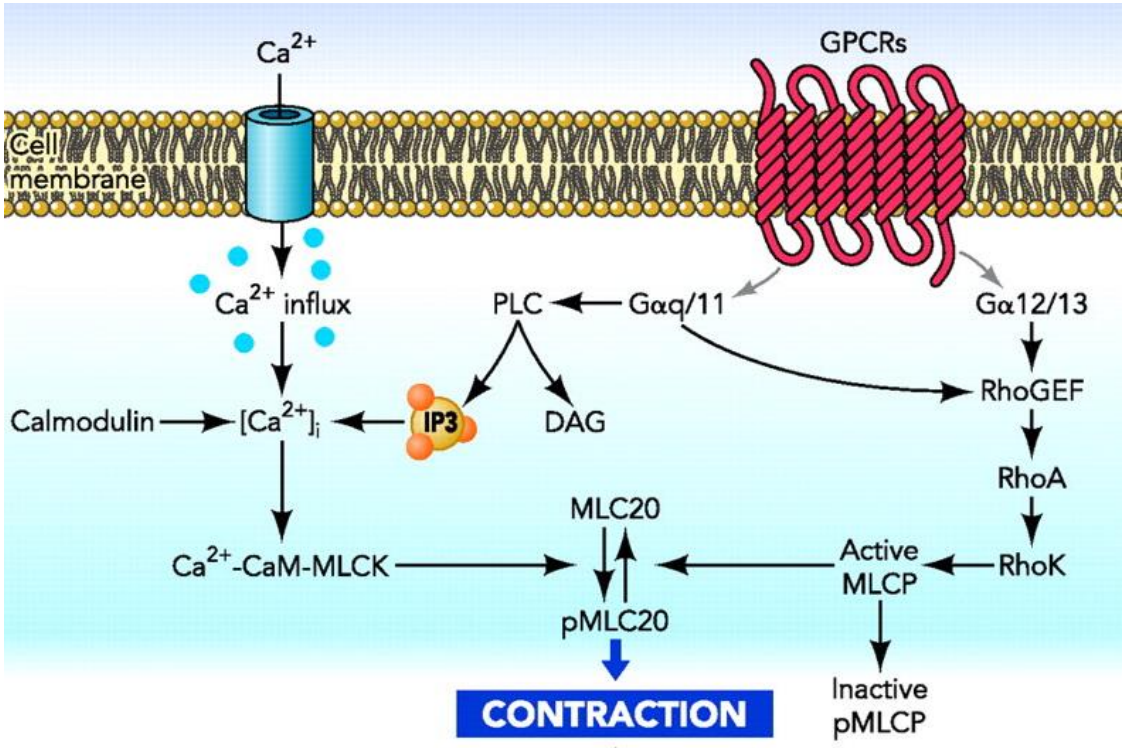

Fig. 4: Schematic illustration of cellular pathways regulating smooth muscle cell contraction
Smooth muscle cell contraction is mainly dependent on the myosin light chain 20 phosphorylation (MLC20). This phosphorylation is regulated by two antagonists- the myosin light chain kinase (MLCK) which is inducing the phosphorylation and the myosin light chain phosphatase (MLCP) which dephosphorylates MLC20. Both enzymes are regulated by different cellular pathways. While the MLCK is activated by increased Ca^{2+} levels, the MLCP is inactivated by a phosphorylation. An increase of intracellular Ca^{2+} can be achieved by two pathways: Activation of voltage-operated Ca^{2+} channels (VDCC) leading to Ca^{2+} influx from extracellular space or by IP3-dependent activation of ryanodine receptors on sarcoplasmic reticulae inducing release from intracellular Ca^{2+} stores (not shown). While VDCC are regulated by membrane potential, IP3 is being released by activation of the PLC which is activated by GPCR coupled to $G_{q/11}$ heterotrimeric proteins.
In contrast, the phosphorylation of MLCP is conducted by the Rho-Kinase (ROCK) which is activated by GPCR coupled to $G_{12/13}$ proteins. They activate different RhoGEFs which are activating RhoA and subsequently ROCK. In addition to these classical pathways, also $G_{q/11}$ heterotrimeric proteins can activate RhoGEF demonstrating a crosstalk between both pathways (Modified, from [16]).

Not only the phosphorylation of MLC20 is affecting SMC contraction, also cytoskeletal properties are important. For instance, inhibition of actin stress fiber assembly is known to drastically reduce SMC contraction [17-19]. Interestingly, a main factor in regulation of a “contractile” phenotype is the transcription factor Serum response factor (Srf). Srf activates transcript expression of various contractile proteins such as calponin and vimentin and different myosin light and heavy chain proteins inducing a more “contractile” phenotype [20]. In line, inhibition of Srf activity or of Srf-regulated transcripts does not only affect agonist-induced SMC contraction, but also pressure-induced SMC contraction revealing the importance of the cytoskeleton in both processes [20-22].

3.3.2 Pressure-induced smooth muscle cell contraction

Compared to agonist-induced SMC contraction, in pressure-induced SMC contraction the SMCs "sense" altered intraluminal pressure and subsequent vessel wall stretching to transfer a mechanical stimulus into a cellular pathway rather than stimulus-induced activation of a GPCR.

Stretch-activated ion channels (SAC) are thought to be the first step in this process as a "sensor" of the stretch and their activation induces membrane depolarization and influx of extracellular Ca^{2+}. Similar to agonist-induced contraction, SAC-induced membrane depolarization activates VDCC leading to a further increase of intracellular Ca^{2+} levels which induces increased MLCK activity and MLC20 phosphorylation. Comparable to agonist-induced SMC contraction, not only Ca^{2+}-dependent pathways are important in myogenic tone. Also Ca^{2+}-sensitization could be shown to be important in regulation of myogenic tone as inhibition of ROCK activity decreased myogenic tone [23, 24]. However, the cellular pathways underlying myogenic tone are rather complex and still not fully understood.

Although myogenic tone was discovered more than 100 years ago, the identity of SACs is still under investigation. Until now, two candidates as putative SAC channels could be identified: the epithelial Na^+ channel (ENaC) and the transient receptor potential channel homologue 6 (TRPC6). ENaC channels are mechanosensitive non-voltage gated sodium channels and are thought to initiate membrane depolarization by cation influx (most likely Ca^{2+} or sodium (Na^+)) [25]. Similarly for TRPC6, it is postulated that their activation induces cation influx inducing membrane depolarization [26].

But not only SACs are important in regulation of myogenic tone. Also other ion channels influence SMC contraction such as the sodium-potassium adenosine triphosphatase (Na^+/K^+- ATPase) and the large conductance Ca^{2+}-activated potassium channel (BK_{Ca}). While the Na^+/K^+- ATPase is important in maintaining the resting potential of the cell, activation of BK_{Ca} induces potassium (K^+) efflux and thus membrane hyperpolarization and termination of contraction. Na^+/K^+- ATPase influences resting potential by pumping K^+ ions out and Na^+ into the cell- both against their concentration gradient by using ATP. In contrast, BK_{Ca} channels are activated by membrane depolarization and/or increased intracellular Ca^{2+} leading to K^+ efflux from the cell and membrane hyperpolarization to terminate contraction [27].

Furthermore, evidence suggests that SACs are not the only mechanosensors and thus being important in "detecting" myogenic tone. It could be revealed that the cytoskeletal

proteins integrin alpha-v beta-3 and alpha-5 beta-1 and different GPCRs are also mechanosensitive [28]. For instance, the angiotensin II receptor 1 (AT_1R) can be independently activated by stretch thus revealing the importance of cytoskeletal properties and GPCR-mediated signaling in myogenic tone [29, 30].

3.4 Endothelial cell-dependent regulation of vascular tone

That ECs are important in the regulation of vascular tone was irrevocably proven by Furchgott and Zawadzki in 1980 where they showed that ECs are obligatory to induce vasodilation in response to acetylcholine (ACh). They revealed that in *ex vivo* preparations without functional ECs, ACh induced vasoconstriction. However, if the *ex vivo* preparations had functional ECs, ACh induced vasodilation and they attributed this to an unknown endothelial factor which was released and induced subsequent relaxation in adjacent SMCs [31].

Since then, researchers have been attempting to unravel the role of ECs in regulation of tone and could prove that ECs can not only induce vasodilation, but also vasoconstriction of SMCs. Among all endothelial mediators of vascular tone, the most important signaling molecules identified are nitric oxide (NO), prostaglandins, endothelial dependent hyperpolarization (EDH) and endothelin-1 (ET-1). All of them are activated by an increase of intracellular Ca^{2+} or membrane depolarization in ECs and can affect the contractile state of SMCs either by the release of substances or by generation of electrical signals.

3.4.1 Regulation of membrane potential and intracellular Calcium in ECs

Membrane potential and intracellular Ca^{2+} are not only important in SMCs, but also in ECs. However, while increases in smooth muscle intracellular Ca^{2+} induce vasoconstriction, increases of endothelial intracellular Ca^{2+} induce vasodilation.

Compared to SMCs, ECs do not express VDCC, but the Ca^{2+}-permeable TRP channel homolog called transient receptor vanilloid channel 4 (TRPV4) [32]. Similar to VDCC, activation of TRPV4 induces membrane depolarization and Ca^{2+} influx. However, while VDCCs are voltage-dependent and inhibited by membrane hyperpolarization, TRPV4 activity is additionally increased by hyperpolarization. Thus, activation of the Ca^{2+} -activated potassium channel BK_{Ca} in SMCs inhibits further Ca^{2+} influx. In contrast, hyperpolarization of ECs by activation of the endothelial small (SK_{Ca}) and intermediate

conductance (IK_{Ca}) Ca^{2+} -activated potassium channel further activates TRPV4 [32-35]. Thus, SMC hyperpolarization inhibits further Ca^{2+} influx while EC hyperpolarization favors further Ca^{2+} influx.

The importance of EC hyperpolarization and activation of SK_{Ca} and IK_{Ca} channels in regulation of vascular tone has been shown in several publications. The chemical compound 6,7-dichloro-1*H*-indole-2,3-dione 3-oxime (NS309) is a specific activator of SK_{Ca} and IK_{Ca} channels. Remarkably, 1μM NS309 is sufficient to induce up to 90% vasodilation of tone if added to mesenteric arteries with functional ECs demonstrating again the importance of ECs in regulation of tone [36, 37].

In addition to SK_{Ca} and IK_{Ca} channels, another potassium channel is important in regulation of EC membrane potential- the inward rectifier K^+ (K_{ir}) channel [38, 39]. In contrast to K_{Ca} channels, K_{ir} channels are not activated by an increased intracellular Ca^{2+} level, but by membrane hyperpolarization or increased extracellular potassium concentrations. Therefore, these channels are supposed to be "hyperpolarization booster" amplifying and stabilizing a hyperpolarization. Compared to SK_{Ca} and IK_{Ca} channels, K_{ir} channels are not activated by NS309. To analyze the functional role of K_{ir} channels, up to 100 μM barium can be used to inhibit K_{ir} channel activity [40]. Interestingly, Sonkusare et al. found that K_{ir} channels can "boost" SK_{Ca} and IK_{Ca}-induced hyperpolarization. They showed that activation of SK_{Ca} and IK_{Ca} channels by 0.3-1 μM NS309 led to subsequent hyperpolarization and vasodilation of mesenteric arteries, which could be reduced by barium-induced inhibition of K_{ir} channels. However, if the concentration of NS309 was further increased to 2 μM, inhibition of K_{ir} channels did not reduce vasodilation suggesting a "booster" effect of K_{ir} channels in SK_{Ca} and IK_{Ca}-channel induced hyperpolarization [41].

Collectively, these data show that regulation of membrane potential and intracellular Ca^{2+} is different in ECs compared to SMCs. However, ECs can influence intracellular Ca^{2+} and membrane potential of SMCs either by spreading membrane potential (e.g. EDH) or by the release of endothelial-derived factors (e.g. prostaglandins, NO, ET-1). These can either induce vasodilation or vasoconstriction, depending on their effect on intracellular Ca^{2+} in SMCs (see Fig. 5).

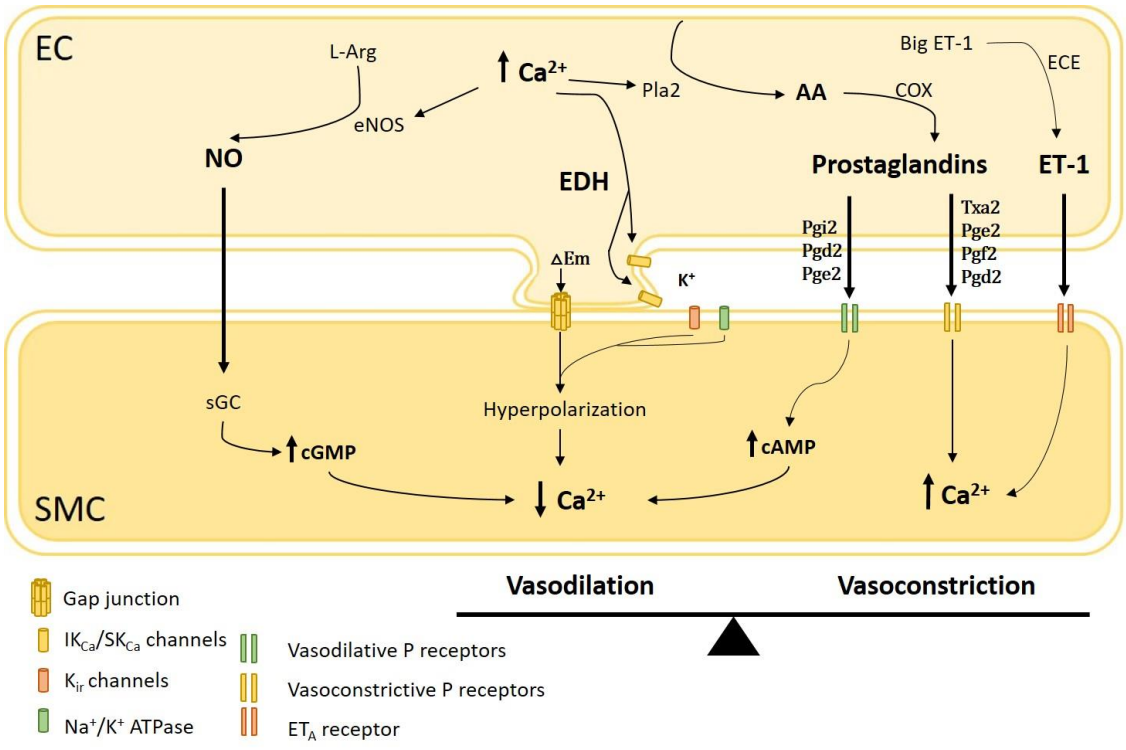

Fig. 5: Cellular pathways of endothelial-derived factors in regulation of vascular tone
A simplified schematic of different endothelial pathways in regulation of vascular tone. In the endothelial cell (EC), increased intracellular Ca^{2+} can activate eNOS, phospholipase A2 (Pla2) and IK_{Ca} as well as SK_{Ca} channels. While eNOS activation induces the formation of nitric oxide (NO) by using the substrate L-Arginine (L-Arg), Pla2 activation induces the formation of arachidonic acid (AA) by using phospholipids as substrate which is further metabolized by cyclooxygenase (COX) and different prostaglandin synthases (not illustrated) to various prostaglandins. Additionally, activation of IK_{Ca} and SK_{Ca} channels induces increase of extracellular potassium (K^+) and EC hyperpolarization (shown as ΔEm). Endothelial cells can also synthesize endothelin 1 (ET-1) by the endothelin converting enzyme (ECE) using the substrate big endothelin-1. In adjacent SMCs, all these factors can influence intracellular Ca^{2+}concentration and thus the contractile state of the cell. While NO, endothelial-dependent hyperpolarization (EDH) and some prostaglandins (Pgi2, Pgd2, Pge2) induce decreases in SMC Ca^{2+} and thus vasodilation, other prostaglandins (Txa2, Pge2, Pgf2, Pgd2) and ET-1 induce increases of SMC Ca^{2+} leading to vasoconstriction. To do so, NO activates the soluble guanylate cyclase (sGC) leading to increased cGMP levels which reduce intracellular Ca^{2+}. EDH decreases intracellular SMC Ca^{2+} by spreading endothelial hyperpolarization via gap junctions in MEJs. Parallel increases of extracellular K^+ further support SMC hyperpolarization by affecting Na^+K^+ATPase and K_{ir} channel function. Prostaglandins induce effects on SMC Ca^{2+} by activation of different prostaglandin receptors. These can either increase intracellular cAMP levels leading to decreased or increased intracellular SMC Ca^{2+}. ET-1 mediates vasoconstriction by activation of smooth muscle endothelin 1 receptor A (ET_A) and subsequent increases of SMC Ca^{2+}.

3.4.2 Endothelial nitric oxide in regulation of vascular tone

The first identified and likely the most extensively characterized endothelial factor is NO, which induces vasodilation of SMCs [42-46]. NO is a gaseous molecule synthesized by endothelial nitric oxide synthase (eNOS), inducible NOS (iNOS) and neuronal NOS (nNOS) using the amino acid L-arginine and molecular oxygen as a substrate [47]. In ECs, all three NO synthases have been detected, although eNOS is the predominant active isoform under physiological conditions [48, 49]. If intracellular Ca^{2+} levels are increasing,

eNOS is activated by a Ca^{2+}-calmodulin dependent mechanism [50]. eNOS in turn synthesizes NO which is released from ECs and activates the soluble guanylate cyclase (sGC) in adjacent SMCs leading to increased levels of the second messenger cyclic guanosine monophosphate (cGMP) [51, 52]. cGMP is activating the cGMP-dependent protein kinase G (PKG) which is attributing to the vasodilative effects of NO by two processes: a decrease in intracellular Ca^{2+} concentration and a decreased Ca^{2+}-sensitization. Decreased intracellular Ca^{2+} concentration is caused by inhibition of Ca^{2+}-release from both the SR and extracellular space [51, 53-55]. A reduced Ca^{2+} sensitization is caused by PKG-dependent activation of MLCP [56].

The importance of NO and cGMP-dependent PKG activation on vascular tone became further evident by various genetic studies and effects of drug-dependent inhibition of NO. For instance, Albertini et al. could show that inhibition of NO formation using the NOS-inhibitor NG-nitro-L-arginine methyl ester (L-NAME) significantly increased vascular resistance and arterial blood pressure in mice [57, 58]. Similarly, also inactivation of either *Pkg* or *eNOS* induced higher blood pressure in mice demonstrating the importance of NO as an influencing factor of vascular tone *in vivo* [59-62].

3.4.3 Prostaglandins in regulation of vascular tone

Prostaglandins are fatty acid derivates produced in various tissues and important in physiological and pathophysiological processes such as blood coagulation, vascular resistance, pain and asthma [63]. In ECs, prostaglandins are mostly involved in vasoconstriction or vasodilation as well as regulation of platelet aggregation [64].

To fulfill their physiological functions, prostaglandin synthesis is tightly regulated by different enzymes. In the first step, increased intracellular Ca^{2+} activates the phospholipase A2 (Pla2) which enzymatically modifies membrane phospholipids to the free fatty acid arachidonic acid (AA). Then, AA is converted into prostaglandin H2 (Pgh2) via the intermediate product prostaglandin G2 (Pgg2) which is the rate-limiting step performed by two different cyclooxygenases (COXs): COX-1 and COX-2 with COX-1 being the predominant isoform in healthy ECs [65, 66]. In the next step, Pgh2 is converted into the different prostaglandins D2 (Pgd2), E2 (Pge2), F2 (Pgf2), thromboxane A2 (Txa2) and prostacyclin (Pgi2) by prostaglandin D2 synthase (Pgds), prostaglandin E2 synthase (Pges), prostaglandin F2 synthase (Pgfs), thromboxane A2 synthase (Txs) and prostacyclin synthase (Pgis), respectively. To mediate their effect, prostaglandins can

either directly interact with prostanoid (P) receptors or can be further metabolized into other prostaglandin derivates.

As different prostaglandins exist, there are a number of P receptors found which are named correspondingly to the prostaglandin with the highest affinity to it, e.g. Pgd2 has the highest affinity to the DP receptor. However, prostaglandins do not only bind to one receptor, they can also activate other P receptors to induce other physiological effects.

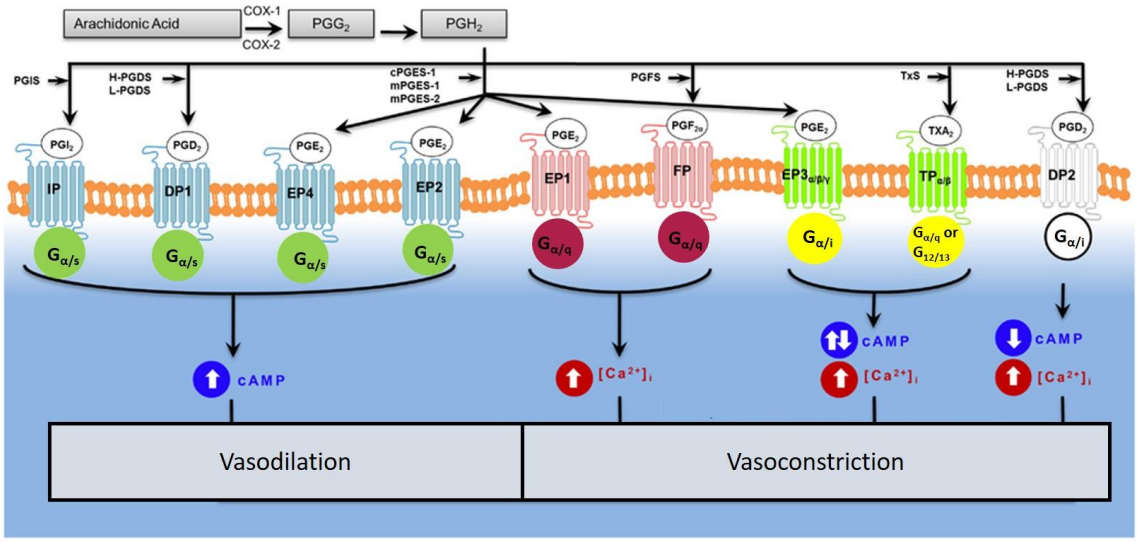

Fig. 6: Synthesis and vascular effects of prostaglandins within the vascular system
Arachidonic acid (AA) is the main substrate for the synthesis of all prostaglandins. First, COX-1 and COX-2 mediate the formation of AA to the intermediate prostaglandin Pgg2 and finally Pgh2. Pgh2 is then used by the prostaglandin-specific synthases Pgis, Pgds, Pges, Pgfs and Txs for the formation of Pgi2, Pgd2, Pge2, Pgf2 and Txa2, respectively. Their biological effect is depending on the activation of the respective prostanoid (P) receptor and its coupled heterotrimeric G-protein. In detail, IP, DP1, EP4 and EP2 activation induce vasodilation by $G_{a/s}$-mediated increase of cytosolic cAMP levels. In contrast, activation of EP1, FP, EP3, TP and DP2 receptors induce vasoconstriction. While EP1 and FP receptors are coupled to $G_{a/q}$-proteins which induce PLC-dependent increase in intracellular Ca^{2+} levels to induce vasoconstriction, EP3 and DP2 receptors decreased intracellular cAMP levels via $G_{a/i}$ proteins. TP receptors are primarily coupled to $G_{a/q}$- or $G_{12/13}$-proteins which induce constriction via increased intracellular Ca^{2+} levels or by activation of different RhoGEF-proteins, respectively (modified, from [64]).

In terms of vascular resistance, prostaglandins can be both vasoconstrictive and vasodilative depending on the receptor they activate. As all P receptors are GPCRs, the physiological effect is depending on the coupled heterotrimeric G protein and its following signaling cascade (see Fig. 6). Pgi2 which is the main prostaglandin produced in ECs is primarily vasodilative by activating IP receptors. IP receptors are coupled to $G_{a/s}$-heterotrimeric proteins leading to activation of the adenylate cyclase and subsequent increase of cyclic adenosine monophosphate (cAMP) levels which inhibit the activation of MLCK thereby inducing vasodilation [67]. In contrast to Pgi2, Txa2 induces vasoconstriction mostly by activating TP receptors in SMCs. TP receptors are mainly $G_{q/11}$- or $G_{12/13}$- coupled and induce vasoconstriction by an increase of intracellular Ca^{2+}

leading to activation of the MLCK or by ROCK-dependent inhibition of the MLCP, respectively [68].

Compared to the "classical" prostaglandins, other prostaglandins are more diverse in their effects. For example, Pge2 can be both, vasoconstrictive and vasodilative by activating different EP receptor subtypes. While EP2 and EP4 are $G_{a/s}$-coupled receptors, whose activation induces increased levels of intracellular cAMP leading to vasodilation, EP3 receptors are mainly coupled to $G_{\alpha/I}$ resulting in decreased cAMP levels and subsequent vasoconstriction [69]. Also the activation of the EP1 receptor induces vasoconstriction by activating its coupled $G_{q/11}$- protein [70]. Similar to EP1 receptors, FP receptors which are mainly activated by Pgf2 are also $G_{q/11}$-coupled leading to subsequent vasoconstriction. Additionally, Pgf2 has been shown to also activate TP receptors inducing vasoconstriction and illustrating the complexity of prostaglandin-mediated vascular effects [71]. The last prostaglandin, Pgd2, has also divergent effects on tone. Pgd2 can either increase or decrease intracellular cAMP levels in SMCs by activating $G_{a/s}$-coupled DP1 receptor or by activating $G_{\alpha/I}$-coupled DP2 receptors, respectively. Furthermore, Pgd2 can be dehydrated to produce the J series of prostaglandins (Pgj2 analogues). Pgj2 analogues are known ligands of the transcription factor peroxisome proliferator- activated receptor-gamma (Ppar-γ), whose activation is also known to reduce blood pressure [72].

Overall, prostaglandins regulate vascular resistance by activating different GPCR-coupled receptors to induce either vasodilation or vasoconstriction. As the interaction between the different prostaglandins and the P receptors is rather complex, there are still many open questions concerning their regulation and dysregulation in diseases including hypertension.

3.4.4 Endothelium-derived hyperpolarization (EDH) in regulation of vascular tone

The existence of a third endothelial vasodilative factor was discovered, because EC-dependent vasodilation could not be fully inhibited using a combination of NO- and prostaglandin- blockade [73, 74]. Therefore, it was postulated that ECs can influence SMC vasodilation via a third pathway leading to EC and subsequent SMC hyperpolarization. At that point, researchers were assuming that a diffusible factor named endothelial derived hyperpolarization factor (EDHF) is released by EC hyperpolarization to induce SMC hyperpolarization. However, it is now mostly accepted, that endothelial

derived hyperpolarization (EDH) is mediated by electrical coupling of both cell types and the parallel release of K^+ ions from ECs and not by a diffusible factor [75].

In ECs, EDH is activated by an increase of intracellular Ca^{2+} which activates endothelial SK_{Ca} and IK_{Ca} channels [76-79]. These channels are enriched in endothelial projections (MEJs) to adjacent SMCs through the IEL and they induce EC hyperpolarization via increasing extracellular K^+ concentration. The increased extracellular K^+ is thought to activate smooth muscle $Na^{+/}K^+$ ATPase and K_{ir} channels as a diffusible "K cloud" [80, 81]. In parallel, the hyperpolarization in the EC can spread to the adjacent SMC via electrical coupling of both cell types by gap junctions in the MEJs. These gap junctions are formed by connexins building a heterocellular hemichannel which allows direct electrical coupling and second messenger transfer between the cells [82-84]. It is known that the connexins (Cx) Cx37, Cx40 and Cx43 compose gap junctions in the vasculature and for Cx40 and Cx43, an essential role in EDH-mediated vasodilation could be proven in mice [85-91].

That different vessel types have diverse vasoactive properties is also emphasized by EDH. While EDH gains importance with decreasing vessel size, the opposite is true for NO [92-94]. In parallel, the number of MEJs also increases with decreasing vessel size revealing a correlation of MEJ numbers and importance of EDH signaling [93, 95].

3.4.5 Endothelin-1 in regulation of vascular tone

Endothelin-1 (ET-1) is a vasoactive peptide which is produced in ECs and presents one of the most potent vasoconstrictors, although it has only a minimal role in healthy vessels [96, 97]. ET-1 is formed from its precursors preproendothelin-1 and big endothelin-1 by proteolytic cleavage through the endothelin-converting enzyme (ECE) [96]. To induce its vascular effects, ET-1 is released from ECs primarily towards vascular SMCs to activate the GPCRs endothelin-1 receptor A (ET_A) and endothelin-1 receptor B (ET_B) [98, 99].

Under physiological conditions, the ET_A is the most important receptor which is expressed only in SMCs and its activation induces constriction via its coupled $G_{q/11}$ proteins. The ET_B receptor is less important in physiological conditions and is primarily expressed in ECs and to a lesser extent in SMCs and can induce cell type-dependent vascular effects [100]. If ET_B is activated only in SMCs or in SMCs and ECs simultaneously, it induces contraction. However, being only activated in ECs, it induces vasodilation by the release of NO and prostacyclins thereby representing a negative feedback mechanism [101].

In sum, ET-1 induces vasoconstriction in physiological conditions as the ET_A receptor is the dominant receptor. However, ET-1 is gaining importance in pathological conditions.

3.5 Modulators of vascular tone in mesenteric arteries

Both ECs and SMCs control vascular tone by their intracellular Ca^{2+} concentrations, membrane potential and associated cellular signaling pathways. Depending on the local and collective situation of the organism, vascular tone has to be adapted. Therefore, both extrinsic and intrinsic factors affect vascular tone. While intrinsic factors such as shear stress, metabolites and intraluminal pressure are reactions to the local situation, extrinsic factors mediate vascular tone by neural or humoral factors e.g. to adjust vascular resistance for maintaining blood pressure [102]. This complex network allows regulation of vascular tone dependent on both local and systemic demand.

3.5.1 Extrinsic factors in regulation of vascular tone

Extrinsic factors, namely neural and humoral factors (see Fig. 7 for illustration) are known to regulate vascular tone. Neural factors are released from the autonomous nervous system (ANS) which has a central role in adjusting cardiac output, heart rate and vascular resistance for maintenance of blood pressure. Within the cardiovascular system this is predominantly a function of sympathetic adrenergic and parasympathetic cholinergic nerves. While activation of the sympathetic system increases heart rate, cardiac contractility and vascular resistance leading to an increase of blood pressure, the parasympathetic system acts as an antagonist to decrease blood pressure mostly by decreasing the heart rate and, to a lesser impact, reducing vascular resistance [102].

The importance of the sympathetic system in regulation of vascular resistance is evident due to sympathetic neurons that have a high resting activity in “basal” vascular resistance called sympathetic tone. This high sympathetic tone together with myogenic tone are determining the “basal vascular tone” which can be adapted if needed. While increased sympathetic activity increases vascular tone, a decreased activity induces vasodilation. To persuade these effects, arteries are innervated by sympathetic adrenergic nerves which release norepinephrine (NE) as a neurotransmitter. NE in turn activates mainly $alpha_1$-adrenergic receptors on SMCs which are GPCRs coupled to $G_{q/11}$ [102, 103]. Activation of $G_{q/11}$ then induces increased intracellular Ca^{2+} levels and subsequent vasoconstriction.

Interestingly, although the sympathetic system is more important for regulation of "basal vascular tone", acetylcholine (ACh), the neurotransmitter of parasympathetic cholinergic nerves, can also affect vascular resistance. In resistance arteries, ACh induces vasodilation by activating endothelial muscarinic acetylcholine receptor type 3 (M3) [104]. As M3 receptors are $G_{q/11}$ coupled GPCRs their activation induces an increase of intracellular Ca^{2+} which primarily activates eNOS and to a lesser extent IK_{Ca} and SK_{Ca} channels. Activation of eNOS and IK_{Ca} and SK_{Ca} channels in turn induces vasodilation of adjacent SMCs mostly via NO and EDH, respectively [46, 105-107].

In addition to the ANS, circulating humoral factors within the blood can influence vascular tone. The most important factors are circulating catecholamines (epinephrine (E) and NE) and the renin-angiotensin-aldosterone system (RAAS). Circulating catecholamines are produced by sympathetic activation by the adrenal medulla in response to stress [102]. Additionally, NE is also released by spillover from sympathetic nerves innervating blood vessels [102, 108]. While NE induces vasoconstriction by smooth muscle alpha1- (α_1-) adrenergic receptor stimulation, E can be either vasodilative or vasoconstrictive depending on its plasma concentration. At low concentration, E activates beta2- (β_2-) adrenergic receptors which induce vasodilation by activation of their coupled G_s proteins [109]. This leads to subsequent increase of intracellular cAMP concentration which decreases intracellular Ca^{2+} levels. At higher concentrations, E mainly activates α_1-adrenoreceptors, thereby shutting of its antagonizing vasodilative response to further enhance NE-induced vasoconstriction [109]. Therefore, the ratio of both compounds, but also their concentrations are important to understand their physiological effect *in vivo*.

Compared to catecholamines, RAAS influences blood pressure and cardiac output by affecting blood volume and vascular resistance. RAAS is activated by sympathetic nerve activation, decreased intraluminal pressure in kidney arterioles and decreased Na^+-levels in the distal tubules [110]. Activation of RAAS leads to the release of renin from the kidney, which proteolytically cleaves circulating angiotensinogen to angiotensin 1. Angiotensin 1 in turn is enzymatically cut to angiotensin II (Ang II) by the angiotensin converting enzyme (ACE), e.g. in vascular endothelium [110]. In regulation of vascular resistance, Ang II actives AT_1Rs on SMCs which induces vasoconstriction. The AT_1R is also a GPCR coupled to $G_{q/11}$ or G_i which can result in increased IP3-dependent or reduced cAMP-dependent increase of intracellular Ca^{2+} [111].

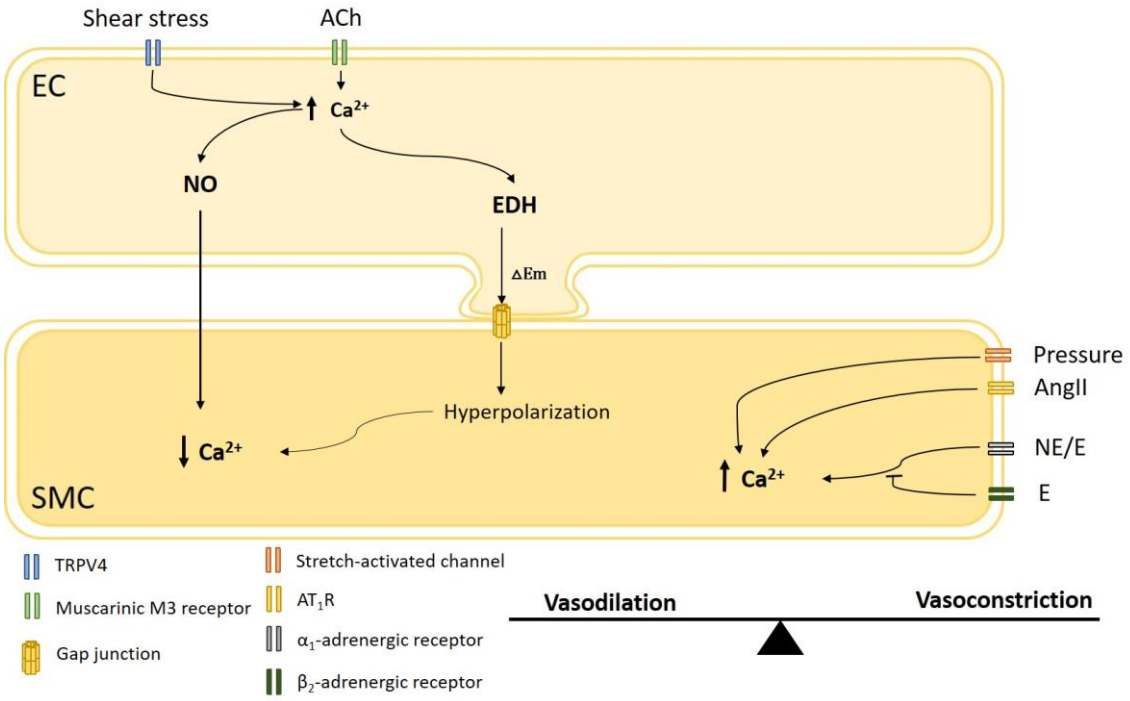

Fig. 7: Cellular effects of extrinsic and intrinsic factors on vascular tone
Extrinsic factors such as acetylcholine (ACh), norepinephrine (NE), epinephrine (E) and angiotensin II (AngII) and intrinsic factors (shear stress and intraluminal pressure) can affect vascular tone by influencing intracellular SMC Ca^{2+} levels. While shear stress and acetylcholine are sensed by receptors on ECs, all other factors activate SMC receptors.
Shear stress is sensed by ECs, most likely by TRPV4 and induces an increase of EC Ca^{2+}. Similarly, ACh binds to endothelial muscarinic M3 receptors which also increases endothelial intracellular Ca^{2+}. The increase of endothelial intracellular Ca^{2+} in turn leads to generation of NO and EDH which decrease SMC Ca^{2+} and induce vasodilation. In contrast, increased intraluminal pressure is sensed by stretch-activated channels (SAC) on SMCs which induces membrane depolarization and subsequent increase of SMC Ca^{2+}. Also, AngII-dependent activation of the GPCR AT_1R leads to activation of primarily coupled $G_{q/11}$ heterotrimeric proteins which induce increases of SMC Ca^{2+}. While NE mainly activates alpha$_1$- (α_1-) adrenergic receptors leading to increases of SMC Ca^{2+}, E has dose-dependent effect on SMC Ca^{2+}. At low concentrations E activates beta$_2$- (β_2-) adrenergic receptors which induce vasodilation by decreasing SMC Ca^{2+} thus antagonizing effects of NE. However, if concentrations of E are higher, they active α_1- adrenergic receptors thereby further enhancing NE-induced increases of SMC Ca^{2+} and shutting of its antagonizing effects on SMC contraction.

3.5.2 Intrinsic factors in regulation of vascular tone

While extrinsic factors are important to adapt vascular tone to systemic effects, intrinsic regulation of myogenic tone allows adaptation in response to local changes e.g. changes in intraluminal pressure or blood flow. The effects of pressure-induced myogenic tone have been extensively described in 3.3.2.. Briefly, if the intraluminal pressure changes, myogenic tone is adapted to allow a constant blood flow. Usually, a decrease of intraluminal pressure reduces myogenic tone while an increase of pressure also leads to an increase in myogenic tone.

Conversely, blood flow also influences myogenic tone. Increases in blood flow lead to a proportional increase of shear stress at the vessel wall. This shear stress is sensed by ECs

and increases in shear stress induce vasodilation which in turn leads to a decrease in shear stress (and respective blood flow). As ECs are in contact to the blood, it is assumed that a mechanosensor, most likely endothelial TRPV4, can "sense" the shear stress leading to increases of endothelial Ca^{2+} levels [112, 113]. This in turn induces flow-dependent vasodilation by Ca^{2+}-dependent activation of eNOS and EDH [113, 114]. The obligatory function of ECs in mediation of this process was demonstrated as EC removal inhibits shear-stress dependent vasodilation [115]. Thus, sensing of shear stress by ECs allows to adapt myogenic tone for maintaining a constant blood flow within resistance arteries [116].

In conclusion, regulation of vascular tone is influenced by intrinsic and extrinsic factors which allow adaptation of vascular tone depending on both local and systemic demands. This complex regulation is of high importance in maintaining a physiological vascular resistance and blood pressure regulation, respectively. Any changes in expression levels of factors influencing vascular tone can lead to pathological alterations in vascular resistance and blood pressure.

3.6 Obesity-dependent pathological changes in the cardiovascular system

Obesity and its associated comorbidities are known risk factors for CVDs including coronary heart disease, myocardial infarction or stroke with dramatically increasing prevalence [117-119]. Worldwide, the incidence of obesity has more than doubled since 1980 with 52% of adults being either overweighted or obese and the number is still increasing [117, 120]. Similarly, also the number of CVDs is growing, although they already represent the leading cause of death worldwide accounting for 17.3 million deaths per year [117]. Therefore, it is of particular importance to decrease the number of cardiovascular deaths by better understanding obesity-dependent pathological changes in CVDs to find a putative therapy.

Both obesity and being overweighted are defined by an abnormal fat accumulation which presents a health risk. To assess the level of obesity, the most commonly used tool is determining the relative weight of a person by the body mass index (BMI). The BMI is equal to the ratio of total body weight (in kg) over the squared height (in m^2) of the person. While a BMI between 18.5 and 24.9 kg/m^2 is defined as normal or acceptable weight, a BMI between 25 and 29.9 kg/m^2 is accounted to overweight. BMIs higher than 30 kg/m^2

are defined as obese [120]. Although the BMI does not take fat to lean mass ratio into account, it is a population-wide guide to estimate if a person is overweight or obese.

3.6.1 Risk factors for obesity

The prevalence of obesity is increasing worldwide and its primary cause is an increased consumption of high-caloric food in combination with decreased physical activity [120, 121]. This leads to an imbalance between consumed calories and energy expenditure and the excess calories are stored as fat deposits causing increased body weight. Additionally, this balance is influenced by other factors such as age, lifestyle (e.g. insufficient sleep, smoking) and genetic factors revealing an interaction between environment and genetics [122]. Special interest was set to genetic contributions to obesity since the opportunity of genome wide association studies (GWAS). GWAS allow to identify correlations of genetic variations with a trait (e.g. obesity) and enabled to identify more than 100 genetic variations to be correlated with obesity [123, 124].

3.6.2 Obesity as a metabolic cardiovascular disease risk factor

Obesity itself is a known risk factor for CVDs as it effects various metabolic pathways. These pathological changes favor the development of comorbidities such as type II diabetes, hypertension and subsequent CVDs [125]. To understand how obesity affects metabolic processes, it is important to first explain the physiological regulation of blood glucose levels and insulin regulation in normal-weighted subjects.

In healthy subjects, blood glucose levels are accurately regulated by insulin. Insulin is a hormone produced in beta-cells of the pancreas in response to increased blood glucose levels. Insulin in turn helps to decrease blood glucose by mediating insulin-dependent glucose-uptake to different organs (e.g. fat and skeletal muscle) [126]. However, some organs (e.g. the liver) take up glucose insulin-independent [127]. After glucose is uptaken by the tissue, it is converted to glucagon (in the skeletal muscle) or fat (in adipose tissue) or both (in the liver) for storing. Independent of mediating glucose uptake, insulin also affects other processes. In the liver, insulin inhibits the generation of new glucose (gluconeogenesis) and stimulates triglyceride synthesis in the liver [128]. These triglycerides are released to the blood and are known to decrease high density lipoprotein cholesterol (HDL) levels [129]. Furthermore, insulin also affects vascular tone as it can adapt blood flow to support transportation of glucose to organs. This is mediated by regulating both NO and ET-1 release [130].

In contrast to healthy subjects, obese subjects are more likely to develop elevated blood glucose levels (hyperglycemia), elevated blood lipid levels (dyslipidemia), insulin resistance and an impairment of endothelial function. These obesity-induced pathological changes are primarily depending on two initial factors: an increase of adipose tissue mass and permanently hyperglycemic glucose levels in the blood caused by increased caloric intake. Both factors can induce cellular cascades in different tissues leading to insulin resistance and obesity-induced metabolic comorbidities.

In obesity, the pancreas tries to produce more insulin by expanding islets to decrease hyperglycemic blood glucose levels [131]. Although the exact mechanisms are still unknown, this situation leads to decreased or inhibited response of tissues to insulin which is defined as insulin resistance. Insulin resistance favors hyperglycemia as the insulin-dependent glucose uptake is abolished. Furthermore, insulin resistance in the liver increases gluconeogenesis which additionally supports hyperglycemia and leads to increased fat accumulation in the liver. This in turn favors the release of triglycerides into the blood, which subsequently reduces HDL-levels [132]. In addition to its effect on the liver, insulin resistance also supports endothelial dysfunction which is defined by an imbalance of vasodilators and vasoconstrictors. Insulin-resistant ECs have impaired insulin-dependent NO generation, but maintained ET-1 levels leading to a shift to more vasoconstriction [130]. In addition to decreased vasodilation, the impairment of insulin-induced NO-dependent vasodilation was shown to inhibit insulin-dependent glucose uptake in the skeletal muscle [133]. This suggests that endothelial insulin resistance might be detrimental for the progress of insulin resistance and hyperglycemia.

In addition to hyperglycemia, the increase of adipose tissue itself also induces pathological changes in metabolism. As fat is an endocrine organ, it releases substances which are called adipokines. Among these, the most important ones are adiponectin, tumor necrosis factor alpha (TNF- α) and interleukin-6 (IL-6) [134]. While the adiponectin level is reduced in obesity, IL-6 and TNF- α levels are increased [135, 136]. These changes in adipokines are known to support the development of hyperglycemia, dyslipidemia and endothelial dysfunction. Increased TNF- α levels can induce insulin resistance in different organs and also increased IL-6 levels are correlating with reduced insulin sensitivity [136, 137]. Additionally, increased IL-6 serum levels are known to impair NO-dependent endothelial vasodilation and could induce hypertension in rats [138]. Also, low adiponectin levels have been shown to correlate with dyslipidemia, insulin resistance and endothelial dysfunction [139, 140]. These data reveal that increases

in fat mass itself are promoting metabolic changes in obesity by affecting adipokine release. Additionally, as obese persons have increased adipose tissue masses, they also have increased free fatty acid (FFA) levels in the blood as they are derived from adipose tissue by lipolysis [141]. FFAs are known to support the development of hyperglycemia, dyslipidemia and endothelial dysfunction by different mechanisms. First, increased influx of FFA into skeletal muscle favors insulin resistance [142]. Second, increased influx of FFA into the liver leads to fat accumulation which supports insulin resistance [129]. Lastly, increased FFA levels also support the development of endothelial dysfunction [143].

Collectively, these data show that obesity favors an inflammatory pathological state which can lead to dyslipidemia, insulin resistance, type II diabetes, endothelial dysfunction and hypertension. Interestingly, all these factors have been shown to further increase the risk for CVDs [125, 144-148].

3.6.3 Metabolic syndrome

Obesity favors the development of metabolic comorbidities by hyperglycemia, dyslipidemia, endothelial dysfunction and insulin resistance. Therefore, a common complication of obesity is the metabolic syndrome (MetS) affecting approximately (approx.) 34% of all adults in the USA and around 20-22% in Germany [149, 150]. Although the exact definition of the MetS is controversially discussed, the most broadly used definition was published in 2009 in agreement of the International Diabetes Foundation and the American Heart Association [151]. According to this definition, a person has the MetS if three of the following five criteria are fulfilled: Elevated waist circumference, elevated serum triglycerides, reduced serum HDL levels, elevated blood pressure and elevated fasting glucose level or diabetes (see Table (Tab.) 1 for details). Compared to other definitions, there is no obligatory criteria which has to be fulfilled for diagnosis of the MetS. Also, insulin resistance is not included in this definition although it was obligatory for diagnosis of the MetS according to the initial definition by the WHO in 1998 [152]. However, type II diabetic patients mainly have the MetS [151].

Criteria for diagnosis of the MetS	Threshold
Elevated waist circumference	Population-specific, for EU: ≥94 cm in males ≥94 cm in females
Elevated serum triglycerides	>150 mg/dL
Reduced serum HDL	<40 mg/dL in males <50 mg/dL in females
Elevated blood pressure	≥130 mmHg systolic and/or ≥85 mmHg diastolic
Elevated fasting glucose level or diabetes	≥100 mg/dL

Tab. 1: Unified criteria for diagnosis of the metabolic syndrome (MetS)
For diagnosis of the MetS, 3 of the described 5 criteria have to be fulfilled: Elevated waist circumference with population-specific differences, elevated serum triglycerides, reduced serum HDL, elevated blood pressure and elevated fasting glucose level (or diabetes) [151].

In concern to CVDs, the influence of the MetS is very striking as it doubles the risk compared to persons without the MetS [151]. Although less is known about the exact time line of events, hypertension is thought to be a main risk factor for the development of subsequent CVDs in subjects with the MetS. Furthermore, endothelial dysfunction is thought to be of particular importance in the development of obesity-induced hypertension revealing the importance of ECs in the development of the MetS and subsequent CVDs [153].

3.6.4 Obesity-dependent endothelial dysfunction

A key role in the development of metabolic changes in obesity and following CVDs plays the endothelium. ECs are not only important in regulation of vascular tone, but also in glucose homeostasis and inflammatory processes. Pathological changes in ECs lead to endothelial dysfunction which is known to affect insulin response, vascular tone and blood pressure [126]. However, endothelial dysfunction is heterogeneous and can vary depending on vessel type and cause. It is defined by an imbalance between endothelial vasodilators and vasoconstrictors which no longer allow proper physiological functioning (Fig. 8) [154].

Obesity was shown to impair EC function by various factors such as hyperglycemia, dyslipidemia and increased insulin levels (hyperinsulinemia) mainly by the generation of reactive oxygen species (ROS) [143, 155-157]. During the progression of obesity and

obesity-induced comorbidities, EC dysfunction is thought to develop in the early stages and to further support the development of obesity-dependent hypertension and following CVDs [158].

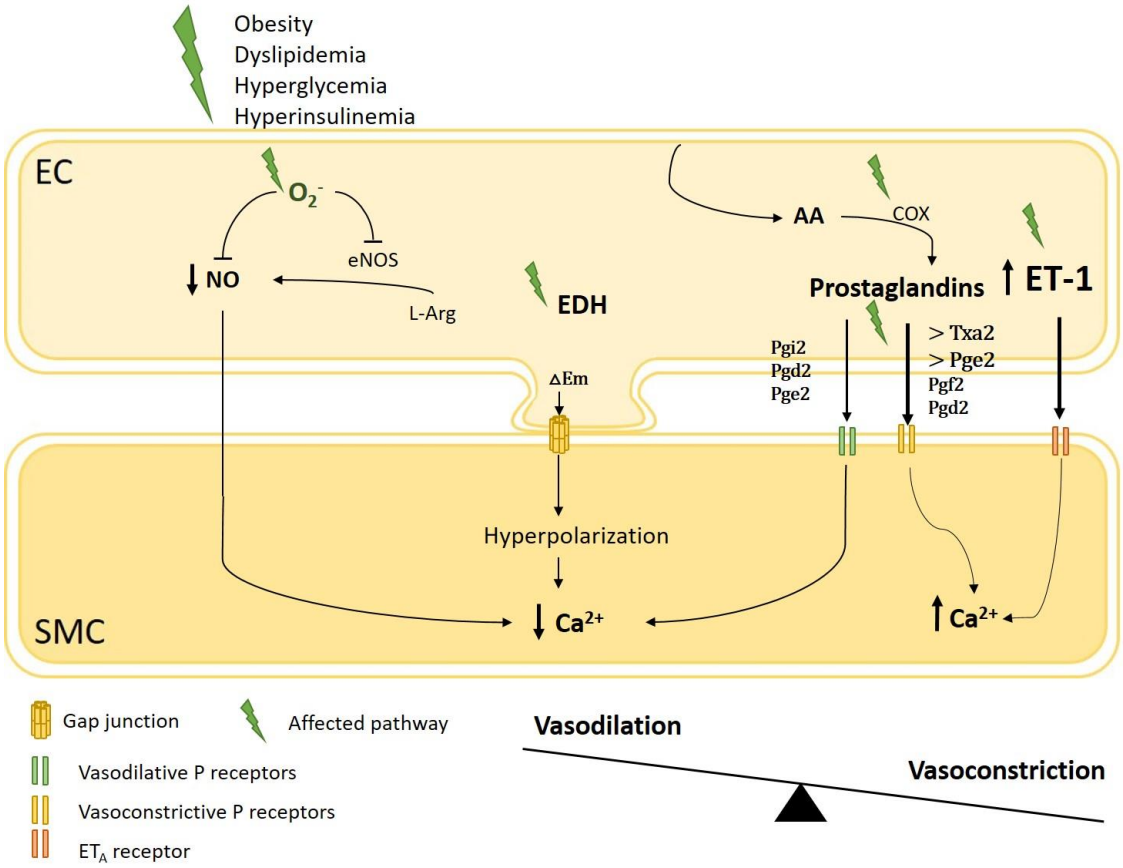

Fig. 8: Cellular pathways affected in endothelial dysfunction
Schematic and simplified illustration of endothelium-dependent effects on vascular tone which have been shown to be affected in endothelial dysfunction. The risk factors obesity, dyslipidemia, hyperglycemia, hyperinsulinemia can influence generation of NO, EDH, prostaglandins and ET-1 by different mechanisms (marked with a green flash). The risk factors can lead to increased generation of superoxide (O_2^-) which inhibits eNOS-dependent synthesis of NO and interferes with NO directly, thus decreasing bioavailability of NO. They can also influence the generation of EDH and affect the balance of different prostaglandins. Thus, some prostaglandins (Txa2, Pge2) have been shown to be increased in endothelial dysfunction. In parallel, ET-1 is gaining importance in EC dysfunction, most likely by increased ET_A receptor expression. Collectively, the changes in endothelial mediators of vascular tone result in an imbalance of vasodilation and vasoconstriction, the characteristic of EC dysfunction.

As already described, EC dysfunction is a heterogeneous pathological state. In obesity, it is known that different risk factors contribute to reduced NO bioavailability leading to decreased ACh-mediated vasodilation [159-161]. This is mainly caused by an increased generation of ROS which reduces the bioavailability of NO by different pathways [155, 162]. For example, hyperglycemia increases mitochondria-dependent generation of the ROS superoxide (O_{2^-}) which reduces NO levels by interacting with NO leading to the

formation of peroxynitrate [156, 163, 164]. Second, O_{2}^{-} can uncouple eNOS leading to the generation of O_{2}^{-} instead of NO thereby further decreasing NO bioavailability [165, 166].

Interestingly, reduced NO bioavailability in endothelial dysfunction has been shown to induce activation of compensatory vasodilative pathways, similar to *eNOS* negative mice. In *eNOS*$^{-/-}$ mice, ACh-induced vasodilation was reduced compared to wildtypic mice and was completely dependent on EDH [167]. Also, in endothelial dysfunction ACh-mediated vasodilation is reduced and EDH was shown to have an increased importance [168].

But endothelial dysfunction does not only affect vasodilators, it also influences vasoconstrictors. ET-1 has been shown to gain importance in endothelial dysfunction. In diabetic rats, the vasoconstriction to ET-1 is enhanced most likely by increased ET-A receptor expression [169]. Additionally, it could be revealed that insulin resistance specifically decreases insulin-dependent eNOS activation without influencing insulin-dependent ET1 generation in spontaneously hypertensive rats [170]. Thus, insulin resistance favors an imbalance towards ET-1 mediated vasoconstriction.

Further studies could reveal that also prostaglandin expression levels can be affected in endothelial dysfunction. In insulin resistant mice, increased FFA levels reduced prostacyclin synthase expression by increased generation of O_{2}^{-} [171]. Others revealed an increased expression of the EP1 receptor in diabetic mice pointing to an increased importance of Pge2 in endothelial dysfunction [172]. Additionally, it could be shown that ACh-induced vasodilation in spontaneously hypertensive rats led to an increased release of Pgi2 and Pgh2 which favored vasoconstriction rather than vasodilation [173].

In conclusion, obesity induces endothelial dysfunction mainly by an increased generation of ROS which affects various endothelial mediators of vascular tone, leading to an imbalance between vasodilation and vasoconstriction.

3.6.5 Effects of obesity-dependent endothelial dysfunction on vascular tone

As endothelial mediators are known to affect vascular tone and subsequently blood pressure, endothelial dysfunction is important in the development of hypertension. However, similar to endothelial dysfunction itself, the reports about obesity-dependent changes in vascular tone are diverse. While some papers reported increases in pressure-induced myogenic tone, others reported respective decreases [172, 174, 175]. Increased myogenic tone and hypertension was reported in a diabetic mouse model. They could show that 12-16 week old diabetic mice had enhanced myogenic tone and blood pressure

which was reversed by inhibition of COX-activity or by blocking TP receptors. In respective non-diabetic mice, neither inhibition of COX-activity nor TP-receptor blocking affected myogenic tone suggesting a pathological effect of prostaglandins in diabetic alterations of myogenic tone [174, 176]. Similarly, another group also reported increased myogenic tone and blood pressure in 12 week old diabetic mice. However, they showed that EP1 receptor expression was increased in diabetic mice and that inhibition of EP1 receptor activation could reduce myogenic tone and blood pressure in diabetic, but not control mice [172]. These data suggest that diabetes may alter prostaglandin expression leading to increased myogenic tone and hypertension. However, the identified prostaglandin to be causative for this effect were different. Interestingly, another publication showed that inhibition of one prostaglandin synthase affected also the expression level of other prostaglandins and thereby altered myogenic tone suggesting a complex interaction between the different prostaglandins [177-179]. Collectively, these data suggest that interfering with the physiological balance between the different prostaglandins affects myogenic tone which may be a reason for obesity-dependent changes in myogenic tone.

In contrast to these studies, other publications reported decreased myogenic tone induced by diabetes. Schofield et al. compared resistance vessels of hypertensive type 2 diabetic patients to control subjects and saw decreased myogenic tone simultaneously to endothelial dysfunction [175]. Similarly, a study using high fat diet- (HFD-) fed rats also reported decreased myogenic tone and endothelial dysfunction in mesenteric arteries compared to normal chow- (NC-) fed rats [180]. Ito et al. could confirm reduced myogenic tone in type II diabetic rats compared to control rats and were suggesting that increased glucose levels caused this effect [181].

In conclusion, obesity-induced endothelial dysfunction is associated with divergent effects on myogenic tone. As endothelial dysfunction is a heterogeneous adaptation, a putative explanation might be that EC function was differentially impaired between the studies. Additionally, the vessel type and species may also affect the results. Therefore, although endothelial dysfunction is a known risk factor for hypertension, its contribution to effects on myogenic tone and hypertension is still not clear.

3.7 Fat mass and obesity associated gene

The first gene identified in human GWAS to be linked to obesity is the gene called *Fat mass and obesity associated* (*FTO*). This study could reveal that risk allele carriers of the single nucleotide polymorphism (SNP) rs9939609 within the *FTO* locus weight in average 3 kg more and have an increased risk of being obese compared to non-risk allele carriers [182]. Highlighting the significance of this association, the correlation could be confirmed in different populations and ages pointing to a global validity [183-185]. Although GWASs unravel correlations, they do not allow conclusion about the cause. For this, murine loss or gain of function analysis can help understanding the functional role of a protein.

For *Fto* the first mouse mutant was described already 8 years earlier in 1999 as part of a deletion in the murine *Fused toes (Ft)* mutant. To this time, *Fto* was called *Fatso* due to having the largest size of all genes being affected in this mutation [186]. Peters et al. could show that homozygous *Ft* mutants died *in utero* having drastic embryonic developmental defects such as polydactyly of fore- and hindlimbs and defects in establishing left-right asymmetry. Heterozygous *Ft mutant* mice had fused toes on the forelimbs and thymic hyperplasia, but body weight was not analyzed [186]. Only after the first GWAS was published, a *Fto*-specific inactivation was generated. Mice having a global deletion of *Fto* showed significantly reduced body weight and body length and confirmed also a functional role of Fto in obesity [187]. However, the cellular mechanism revealing how Fto affects obesity, remains unknown.

3.7.1 Fto is a m6A-specific RNA demethylase

Later studies aimed to investigate the molecular function of Fto. Therefore, different studies analyzed protein structure, cellular localization and tissue expression of Fto. These studies could show that the gene *Fto* is highly conserved in vertebrates and algae and is ubiquitously expressed in various tissues during embryogenesis and adolescence in both, human and mice [182, 186, 188]. Further structural analysis revealed that the protein Fto has a size of 58 kilodalton (kDa) and has a N-terminal nuclear localization sequence (NLS) which allows Fto to shuttle between nucleus and cytosol [189]. Furthermore, Fto was identified to be a family member of the alpha-ketoglutarate dependent dioxygenase (AlkB) family which has been identified to be important in DNA repair [189-191]. In 2011, Jia et al. could finally reveal that Fto is an efficient demethylase of a RNA-modification on nitrogen-6 of adenosines (m6A) [192]. The importance of

m6A was emphasized by a study revealing that m6A is one of the most abundant RNA modifications present in eukaryotic mRNA with around 0.1-0.4% methylated adenosines of total adenosine residues in cellular RNA [193]. Moreover, m6A was shown to be highly conserved throughout mammals, yeast, bacteria and viruses strengthening its biological importance [194-196]. Although m6A methylation had been discovered already in the 1970s, for a long time little was known about its biological function in mRNA regulation because of missing detection strategies [197, 198]. First in 2012, two groups published a protocol which allowed transcriptome-wide mapping of m6A-sides by RNA immunoprecipitation using an m6A-specific antibody combined with RNA sequencing (MeRIP-sequencing). These studies revealed that approximately 7000 mRNAs were methylated with 2-3 m6A-methylation sites per gene on average and suggesting a high physiological role of m6A [199, 200].

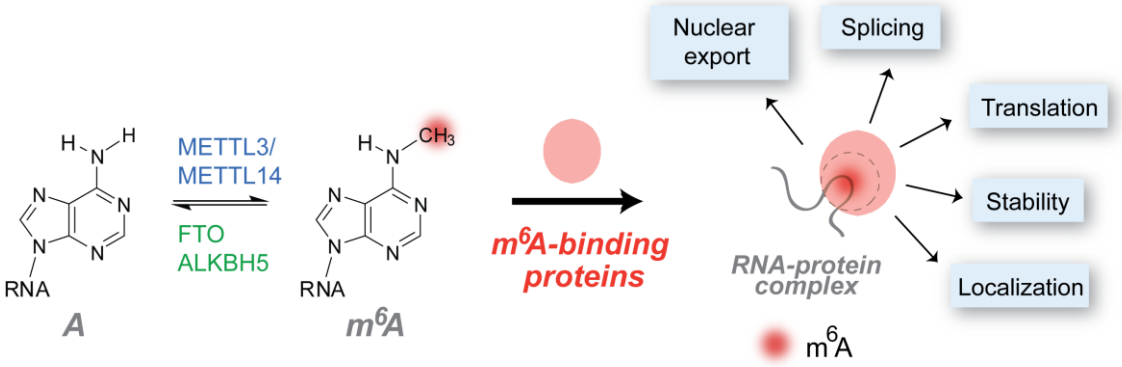

Fig. 9: Regulation of m6A methylation and its putative role in mRNA regulation
Adenosine (A) can be reversible methylated by the Mettl3/Mettl14 complex on nitrogen 6 to m6A. Fto and Alkbh5 can both reverse the process by removing the methylation. The cellular function of m6A is most likely mediated by m6A binding proteins and affect the nuclear export, splicing, translation, stability and localization of the RNA [201].

As m6A methylation is a reversible process, different proteins next to Fto have been identified to affect m6A methylation: a "writer" complex which methylate respective adenosines in RNA, "readers" which can bind and recognize m6A and "erasers" such as Fto which can remove the methylation making the process reversible (Fig. 9). To understand the physiological role of Fto, it is therefore important to understand the regulation of m6A methylation as well as its biological importance.

In contrast to the "erasers", only one "writer" complex exists consisting of different proteins [202]. Until now 3 proteins have been identified being part of this complex: Methyltransferase-like 3 (Mettl3), methyltransferase-like 14 (Mettl14) and Wilms tumour 1-associated protein (WTAP) [203-206]. For detection of m6A, one "reader" named YTH

domain family 2 protein (YTHDF2) have been identified and its binding to m6A has been shown to induce mRNA translocation to processing bodies thereby inducing mRNA decay [207]. To remove the methylation, two different erasers have been identified which are both members of the alpha-ketoglutarate-dependent deoxygenase family: Fto and AlkB Homolog 5 (AlkBH5) [192, 208-211]. These erasers have been shown to have gene- and tissue-specific preferences pointing to different functions [187, 209, 212].

As m6A-methylation is a highly regulated process, different studies analyzed its biological importance. Until now, m6A-methylation could be shown to influence mRNA stability, nuclear export, translation and alternative splicing [199, 200, 213, 214]. Furthermore, m6A has been revealed to be also present in microRNAs (miRNA) and to regulate miRNA processing [215]. Also, m6A methylation could be revealed to be an influencing factor in biological processes such as cell differentiation, regulation of circadian rhythm and heat shock responses revealing its broad biological importance in various processes [213, 216-218]. Also, some *Fto*-specific effects on m6A-methylation could be revealed. First, comparative analysis of transcriptome wide m6A analysis comparing "methylomes" of midbrains from *Fto* wildtypic and *Fto* deficient mice revealed that 1514 transcripts were differently m6A-methlyated. This altered m6A methylation was shown to affect transcript expression and thus was suggested to be the physiological effect of *Fto* on influencing dopaminergic signaling [219]. Second, *Fto* deficiency increased m6A methylation of the transcript coding for the transcription factor *runt-related transcription factor 1* (*Runx1*) in adipose tissue leading to the inclusion of an alternatively spliced exon and thus impeding adipogenesis [217]. Therefore, the data on m6A regulation suggest that Fto exerts its cellular function by influencing m6A methylation of different transcripts and thereby affecting transcript expression and splicing. It remains to be determined if RNA demethylation by Fto also regulates the effects of Fto in the development of obesity.

3.7.2 Role of Fto in obesity

After the discovery that Fto regulates body weight, further studies analyzed how Fto affects obesity and if Fto might be associated with other obesity-dependent comorbidities. Therefore, different murine loss- and gain of function analyses were performed to understand how Fto affects obesity. Additionally, as Fto has been shown to be ubiquitously expressed, the effect of tissue-specific *Fto* deficiency on obesity was investigated [182].

First it was analyzed if Fto affects body weight and body composition. In four different global *Fto* deficient mouse models body weight was reduced, while *Fto* overexpression increased body weight [187, 220-222]. Also, neuronal-specific loss of *Fto* reduced body weight indicating that *Fto* expression in the central nervous system (CNS) is important in regulation of obesity [223]. However, further analysis of body composition in these mouse strains revealed differences. While the fat mass was reduced in all global *Fto* deficient mice and increased in *Fto* overexpressing mice, neuronal loss of *Fto* increased fat mass [187, 220-223]. This suggests that either 1) Fto has divergent effects on obesity in different cell types or 2) that strain-specific differences are causing differences in adipose tissue accumulation. Similarly, also the effect of loss of *Fto* on lean mass was different. While neuronal loss of *Fto* and two global *Fto*-deficient mouse strains showed reduced lean mass, lean mass was unchanged in *Fto* overexpressing mice and in one global *Fto* deficient mouse model [187, 220-223]. Most likely, these differing effects are caused by strain-specific differences or variances in experimental design and make it more difficult to understand the effect of Fto on body composition.

Furthermore, as obesity is principally the result of an imbalance between food intake and energy expenditure, these parameters were also analyzed in the different mouse models and did not show congruent results. In two global *Fto*-deficient mouse models and in neural-specific *Fto*-deficient mice, energy expenditure was increased [187, 221, 223]. In contrast, neither in mice overexpressing *Fto* nor in another global *Fto*-deficient mouse model these results could be confirmed, as energy expenditure was unchanged [220, 222]. Further analysis of food intake revealed that contrary to expectations, *Fto* deficiency did not reduce food intake in any mouse model. In two global *Fto*-deficient mouse models and in mice overexpressing *Fto*, food intake was unchanged [220-222]. In one global *Fto*-deficient mouse model and in the neuronal-specific *Fto*-deficient mouse model, food intake was increased suggesting that *Fto* deficiency does not induce effects on body weight by reducing food intake [187, 223].

Collectively, these data confirm that murine loss of *Fto* reduces body weight most likely by reducing fat mass and possibly lean mass. Additionally, loss of *Fto* also protected from HFD- induced obesity underlining that loss of Fto has a protective role in the development of obesity [187]. However, which cell types other than neurons are important in mediating *Fto*-dependent effects on body weight has to be determined in the future.

Similar to murine studies, also GWAS analyzed correlation of *FTO* SNPs with food intake and energy expenditure. In contrast to expectations, these data revealed that the

risk allele of the *FTO* SNPs correlated with increased food intake and unchanged energy expenditure, in contrast to the murine studies [224-226]. This suggests that the effect of genetic variations in human *FTO* might be different to the effects observed in *Fto* mouse models. Furthermore, there is an ongoing discussion about whether human *FTO* SNPs regulate *FTO* expression, or the expression of the *Iroquois-class homeodomain protein 3* (*IRX 3*) or *RPGRIP1L*, two genes located close to the *FTO* gene [227, 228]. Further studies are necessary to answer this question.

In conclusion, murine loss of *Fto* reduces body weight although the effect on fat and lean mass vary among the different mouse models. Similarly, effects on energy expenditure and food intake are inconsistent between the mouse models making it difficult to analyze the cellular effects of Fto during the development of obesity. Similar to the murine data, human GWAS show a correlation of risk allele *FTO* SNPs with obesity. However, whether the effect seen in murine *Fto*-deficient mouse models explains the correlation of human *FTO* SNPs with obesity remains to be determined in further studies.

3.7.3 Role of Fto in obesity-dependent comorbidities

As obesity is a risk factor for metabolic comorbidities and CVDs, numerous studies have investigated the role of Fto in these pathological changes. The first indication was a human GWAS showing that *FTO* SNPs correlate with increased risk for type 2 diabetes which was in turn also investigated in murine mouse models [182]. In mice, *Fto* overexpression was shown to not affect glucose tolerance in NC-fed mice, but to worsen glucose tolerance in HFD-fed mice [220]. This indicates that Fto may affect the regulation of glucose homeostasis and insulin signaling in obesity. Interestingly, Ikels et al. could confirm a role of Fto in glucose homeostasis. They could show that loss of *Fto* significantly improved glucose tolerance in Leptin-resistant $Lep^{ob/ob}$ mice, a mouse model for the metabolic syndrome [229]. Additionally, they analyzed whether *Fto* may exert its effect on improving glucose homeostasis by affecting insulin sensitivity in these mice, but there was no significant difference. This suggests that Fto affects glucose homeostasis most likely by influencing insulin-independent glucose uptake. Furthermore, Ikels et al. analyzed if loss of *Fto* affects $Lep^{ob/ob}$ mice from other signs of the MetS. Interestingly, they could show that *Fto*-deficiency protected $Lep^{ob/ob}$ mice from increases in body weight gain, fat accumulation in the liver and pancreatic islet size. These data suggest that Fto has a role in the development of the MetS and that global loss of *Fto* appears to be protective to most signs of obesity-dependent comorbidities [229]. Surprisingly, as

obesity and the MetS are known risk factors for hypertension, it is unknown if Fto may protect from obesity-dependent hypertension. Until now, only different GWAS analyzed a putative correlation between *FTO* SNPs and hypertension with divergent results. While five studies could reveal a significant correlation of *FTO* SNPs with hypertension, two other publications could not confirm these results [230-236]. He et al. claimed that these divergent results might be depending on an obesity-dependent effect of Fto on blood pressure. Therefore, they performed a meta-analysis using these seven publications and could show that *FTO* SNPs correlate with hypertension in obese subjects, but not in non-obese subjects [237]. These data suggest that *FTO* may play a role in the development of hypertension depending on body weight, as genetic variations within *FTO* are a known risk factors for both, hypertension and subsequent CVDs [238, 239].

3.8 Aim of the project

Although Fto is known to affect obesity and obesity-dependent comorbidities, a role of Fto in blood pressure regulation has not yet been explored. A meta-analysis of multiple human GWASs showed a correlation between *FTO* SNPs and obesity-dependent hypertension indicating that *FTO* is important in blood pressure regulation. As unpublished data from our lab revealed that loss of *Fto* affected ACh-induced vasodilation in aortic ring assays, we hypothesized that vascular Fto influences blood pressure by altering vascular tone (Stefanie Seehaus, unpublished data). Therefore, we started with microarray analysis to see whether Fto affects cellular signaling in the vasculature to mediate blood pressure. As both cell types can influence vascular tone, EC- and SMC-specific *Fto* deficient mice were generated to analyze cell-type specific effects of Fto in regulation of myogenic tone and blood pressure. Furthermore, as ECs are known to be important in obesity-dependent comorbidities and hypertension, the role of EC-specific *Fto*-deficiency should be analyzed in HFD-fed mice to understand the role of endothelial *Fto* in obesity-dependent comorbidities and hypertension.

4 Material and methods

4.1 Material

4.1.1 Animals

Animal species	Genetic background
Global *Fto*$^{-/-}$	C57BL6J/NMRI background
VeCadherin-Cre^{ERT2} *Fto*$^{flox/flox}$	C57BL6
SMMHC CreER^{T2} *Fto*$^{flox/flox}$	C57BL6

Tab. 2: Animal species used

4.1.2 Human primary cell donors

Cell type	Catalogue number	Company
Human coronary smooth muscle cells (HCoSMC)	CC-2583	Lonza
Human aortic endothelial cells (HAoEC)	C-12271	Promocell

Tab. 3: Human donor for primary cell culture

4.1.3 Equipment and expendable material

Equipment	Type	Company
Accuracy weighing machine	EW 6000-M	Kern& Sohn GmbH
Agarose gel chamber	Not applicable (n.a).	Manufactured at the University of Düsseldorf
Blood glucose meter	Ascensia Contour	Bayer
Blood glucose test strips	Ascensia Contour	Bayer
Cell culture dishes	10 cm	VWR
Cell culture flasks	25 cm^2; 75 cm^2; 175 cm^2	VWR
Cell culture plate	6 well, 12 well, 24 well	VWR
Centrifuge	Centrifuge 5424 R Megafuge 1.0	Eppendorf Heraeus Instruments
Collecting tubes	15 mL, 50 mL	Becton Dickson
Confocal microscope	Fluoview 1000	Olympus
Cover slips	Menzel cover slips, 12 mm	ThermoFisher

Gel electrophoresis chamber	n.a.	Manufactured at University of Düsseldorf
Heating block	Thermomixer compact	Eppendorf
Imaging system (agarose gel electrophoresis)	Phase 312 nm, professional system	Phase
Incubator	HeraCell	Heraeus Instruments
Micropipette puller	Model P-2000	Sutter instrument Co.
Microplate reader	FLUOstar Omega	BMG Labtech
Microscope Microscope camera	Axio Imager A.2 AxioCam TRm	Zeiss
Microscope slide	SuperFrost ROSA, cut edges	Roth
PCR machine	T3000 Thermocycler Sensoquest	Biometra Labcycler
PCR tubes	0.2ml, 8-stripes	Sarstedt
pH-meter	MP220	Mettler TOLEDO
Power supply	E83T Consort	Welabo
Precellys	Precellys 24 homogenizer+ CryoLys	PeqLab
Pressure myograph	Culture Myograph System, model 202CM	Danish Myo Technologies (DMT)
Reaction tubes	1.5/2.0 mL	Sarstedt
Real-time PCR machine	CFX96 Real time System	Bio-Rad
Shaking device	VortexGenie 2	Scientific Industries
Spectrophotometer 1000	BioPhotometer	Eppendorf
Sterile bench	HeraSafe	Hereaus Instruments
Tissue embedding	OCT compound	Tissue Tek
Water bath	Type 1003	GFL

Tab. 4: Equipment and expendable materials

4.1.4 Chemicals

All chemicals were analytically pure ordered from the companies AppliChem, Merck, Roth and Sigma Aldrich.

4.1.5 Fine chemicals and reagents

Fine chemical	Company
Acetylcholine	Sigma Aldrich
Agarose	BioBudget Technologies GmbH
Bariumchloride	Sigma Aldrich
DNA-ladder, 100 bp plus DNA	New England BioLabs
dNTP	ThermoFisher
Donkey Serum	Millipore
Fibronectin, human	Millipore
Insulin (Human insulin 100 U/mL)	Novolin R
L-Pgds inhibitor (AT 56)	Tocris Bioscience
Mounting media for cells	Roche
Mounting media for tissue: ProLong Gold	Invitrogen
NS309	Tocris
Peanut oil	Sigma Aldrich
Phenylephrine	Sigma Aldrich
Prostaglandin D2	Cayman Chemicals
Proteinase K, recombinant, PCR grade	Roche
Sodium nitroprusside	Sigma Aldrich
Tamoxifen	Sigma Aldrich

Tab. 5: Fine chemicals and substrates

4.1.6 Cell culture media, buffers and substances

Cell culture substance	Company
PBS without $Ca^{2+}$and Mg^{2}	Millipore
Non-essential amino acids (NEAA)	Thermo Fisher
DMEM : F-12, Glutamax, without HEPES, with pyruvates	Thermo Fisher
DMEM Glutamax, 1 g/L glucose, with pyruvates	Thermo Fisher
Fetal bovine serum (FBS)	Thermo Fisher
Penicillin-streptomycin liquid (P/S) (100x) 10000 U/ mL penicillin,	Thermo Fisher

10000 µg / mL streptomycin	
Trypsin (for cell preparation)	Thermo Fisher
Trypsin-EDTA 0.05%	Thermo Fisher
Collagenase Type II, CLS II	BioChrom
Hanks balanced salt solution (HBSS) with $Ca^{2+}$and Mg^{2+}	Thermo Fisher
EBM-2 Basal Medium	Lonza
EGM-2 MV Single Quot Kit Supplement and Growth Factors	Lonza
SmBM Basal Medium	Lonza
SmGM-2 Single Quot Kit Supplements and Growth Factors	Lonza
Lipofectamine RNAiMAX transfection reagent	Thermo Fisher

Tab. 6: Cell culture media, buffers and substances

4.1.7 Buffer and culture medium

4.1.7.1 Buffer for pressure myography

Krebs-HEPES-buffer:
118.4 mM NaCl
4.7 mM KCl
1.2 mM $MgSO_4$
4 mM $NaHCO_3$
1.2 mM KH_2PO_4
10 mM Hepes
6 mM Glucose
pH 7.38-7.42

Ca^{2+}-containing HEPES buffer:
Krebs-HEPES buffer
2 mM $CaCl_2$

Ca^{2+}-containing HEPES buffer with BSA:
Krebs-HEPES buffer
2 mM $CaCl_2$
1% BSA (w/v)

Ca^{2+}-free HEPES buffer:	Krebs-HEPES buffer
	1 mM EGTA
	10 µM Sodium nitroprusside (*SNP*)

4.1.7.2 Buffer for molecular biological methods

50x TAE buffer	2 M Tris
	6% acetic acid (v/v)
	50 mM EDTA
	pH 8- 8.5
Genotyping-buffer	100 mM NaCl
	50 mM Tris-HCl pH 8
	100 mM EDTA
	1% SDS (w/v)

4.1.7.3 Buffer for histochemical analysis

Blocking solution for IF on tissue slides:	0.5% BSA (w/v)
	5% goat serum (v/v)
	0.25% Tritox X-100 (v/v)
	PBS

4.1.7.4 Buffer for cell preparation

Collagenase II -solution	HBSS
	100 U/ mL collagenase II
	0.1% trypsin (w/v)

4.1.7.5 Cell culture media

Murine cell culture:

Growing medium:	DMEM/ F-12 + Glutamax
	10% FBS (v/v)
	1 x P/S
	0.1% non-essential amino acid (w/v)

Serum-starved medium:	DMEM, low glucose 0.4% fetal calf serum (v/v) 1 x P/S
HAoEC cell culture:	
Growing medium:	EBM- Basal Medium EGM-2 MV Single Quot Kit Supplement and Growth Factors with 5% fetal bovine serum (FBS) (v/v)
Transfection medium:	EBM- Basal Medium EGM-2 MV Single Quot Kit Supplement and Growth Factors with 0.5% FBS (v/v) without gentamycin
Growing medium for transfected cells:	EBM- Basal Medium EGM-2 MV Single Quot Kit Supplement and Growth Factors with 5% FBS (v/v) without gentamycin
HCoSMC cell culture:	
Growing medium:	SmBM- Basal Medium SmGM-2 Single Quot Kit Supplement and Growth Factors with 5% FBS (v/v)
Transfection medium:	SmBM- Basal Medium SmGM-2 Single Quot Kit Supplement and Growth Factors with 1% FBS (v/v) without gentamycin

Growing medium for transfected cells:	SmBM- Basal Medium SmGM-2 Single Quot Kit Supplement and Growth Factors with 0.5% FBS (v/v) without gentamycin

4.1.8 Antibodies

4.1.8.1 Primary antibodies for immunofluorescence analysis

All primary antibody incubations were performed overnight at 4°C while constantly shaking.

Primary antibody target	Protein size	Dilution IF	Species	Company
Alpha-smooth muscle actin	42 kDa	1:200	Rabbit	Abcam
Fto	58 kDa	1:1500	Guinea Pig	Produced by EMT

Tab. 7: Primary antibodies for immunofluorescence (IF)

4.1.8.2 Secondary antibodies and fluorescently-labeled toxin for immunofluorescence analysis

Secondary antibody target	Dilution	Produced in	Clone/ company
Anti rabbit IgG AlexaFluor 488	1:200	Donkey	Jackson ImmunoResearch
Anti guinea pig IgG Alexa Fluor 568	1:400	Goat	Thermo Fisher

Tab. 8: Fluorescently-labeled secondary antibody for immunofluorescence analysis

Fluorescently-labeled toxin	Target	Dilution	Company
TRITC-phalloidin	F-actin	1:500	P 1951 Sigma Aldrich

Tab. 9: Fluorescently-coupled toxin for immunofluorescence analysis

4.1.9 Enzymes and kits

RNA isolation from tissue

RNeasy Lipid Tissue kit	Qiagen (Cat. No.: 74804)

RNA isolation from cells

RNeasy Mini Kit	Qiagen (Cat. No.: 74104)

DNaseI- digestion

RNase-Free DNase Set	Qiagen (Cat. No.: 79254)

cDNA synthesis:

SuperScript III First strand synthesis system	ThermoFisher (Cat. No.: 18080051)

qRT-PCR master mix:

Power Up SYBR Green master mix	ThermoFisher (Cat. No.: A25742)

Endpoint-PCR master mix:

5x GoTaq Green Master Mix	Promega (Cat. No: 7911)

Endpoint-PCR polymerase:

Taq polymerase	Produced at the EMT, University of Düsseldorf as described previously [240].

4.1.10 siRNA

The following siRNAs were ordered from Origene, Cat. No.: SR312322

Name	**Species**	**Sequence**	**Company**
FTO siRNA A	Human	GCAGCUGAAAUAUCCUAAACUAATT	Origene
FTO siRNA B	Human	AGACAGAACUUAGAGACAUCCCAGT	Origene
FTO siRNA C	Human	AGCGUGUGACAAAGCCUAACCUACT	Origene

Scrambled siRNA	Human	Not listed	Origene

Tab. 10: siRNA sequences used for siRNA-mediated transcript knockdown

4.1.11 Gene-specific primers

Name	Species	Sequence (5'3' direction)
FTO For	Human	AAG AGG AAA GTG AGG ATG AC
FTO Rev	Human	TCA AGC ATG AAA TAG CAG TC
GAPDH For	Human	ACA GTT GCC ATG TAG ACC
GAPDH Rev	Human	TTT TTG GTT GAG CAC AGG

Tab. 11: Gene-specific primer sequences used for quantitative real time PCR

Mouse genotype	PCR name	Primer name	Sequence (5'3' direction)
VeCadherin-Cre^{ERT2} *Fto$^{flox/flox}$*	Cre PCR	EC-Cre FOR	TTAATCCATATTGGCAGAACGAAAACG
		EC-Cre REV	CAGGCTAAGTGCCTTCTCTACA
	Flox PCR	Fto flox FOR	GAGCAGAGAGCTGGAGCTT
		Fto flox REV	ACAGAAACGAGAGCAGGAAAAGAC
SMMHC-Cre^{ERT2} *Fto$^{flox/flox}$*	Cre PCR	SMC-Cre FOR	TCCTGGGCATTGCCTACAAC
		SMC-Cre REV	CTTCACTCTGATTCTGGCAATTTCG
	Flox PCR	Fto flox FOR	GAGCAGAGAGCTGGAGCTT
		Fto flox REV	ACAGAAACGAGAGCAGGAAAAGAC
Global *Fto$^{-/-}$*	Fto WT	Fto wt FOR	CGCCTCTCCCCCATCTAAATCCT
		Fto wt REV	AAGCCAAGAACAAGTCCATACCTG

	Neo PCR	Neo FOR	CTGTGCTCGACGTTGTCACTG
		Neo REV	GATCCCCTCAGAAGAACTCGT

Tab. 12: Gene-specific primer sequences for genotyping

4.1.12 Mouse laboratory diet

Mice	Company	Product number
High fat diet, 60% fat calories	BioServ	F3282

4.1.13 Software and statistical analysis

For statistical analysis, Microsoft Office Excel 2016 and GraphPad Prism 7 were used. Depending on experimental design, unpaired t-test, 1-way or 2-way ANOVA were performed as indicated in the respective figure description.

4.2 Methods

4.2.1 Mouse housing

For animal care, all guidelines of the National Institutes of Health were complied. Mice were kept in standard cages at 12 h light/ 12 h dark cycle at 22-24°C. Mice had access to water and food (either normal rodent chow or high fat diet) *ad libitum*.

4.2.2 Generation of cell type-specific *Fto* deficient mice

To create cell-type specific *Fto*-deficient mice, the Cre- loxP system was used. As previously published, a Cre recombinase is under the control of a tissue-specific promotor while the target gene sequence is flanked by two loxP sites. If the Cre recombinase is expressed, it cuts at the respective *loxP* sites thus inducing a tissue-specific gene knockout [241].

In this study, a previously published mouse having exon 3 of the gene *Fto* flanked by loxP sites ($Fto^{floxed/floxed}$) was used [219]. This mouse was crossed to Cre-recombinase expressing (Cre+) mice to allow Cre-loxP mediated generation of tissue-specific *Fto* deficient mice. In detail, Cre-;$Fto^{floxed/floxed}$ (Cre-;$Fto^{fl/fl}$) mice were crossed with Cre+;$Fto^{+/+}$ mice resulting in offspring being either Cre-;$Fto^{fl/+}$ or Cre-;$Fto^{fl/+}$. Mating of Cre+;$Fto^{fl/+}$ litters allowed to obtain Cre+;$Fto^{fl/fl}$ mice.

For breeding, Cre+;*Fto*$^{fl/fl}$ and Cre-;*Fto*$^{fl/fl}$ mice were used to get litters being either Cre+;*Fto*$^{fl/fl}$ or Cre-;*Fto*$^{fl/fl}$.

4.2.2.1 Generation of endothelial cell-specific *Fto*-deficient mice

To generate endothelial cell-specific *Fto* deficient mice, a tamoxifen-inducible Cre-recombinase (Cre-ER^{T2}) under the regulatory control of the vascular endothelial Cadherin (VeCadherin) promoter was used. The endothelial cell-type specificity of the VeCadherin-Cre^{ERT2} has been proved before and was a kind gift from R. Adams (Max Planck Institute, Germany) [242].

To induce Cre-recombinase expression, 6 week old VeCadherin-Cre^{ERT2}+; Fto$^{fl/fl}$ mice were intraperitoneally injected with tamoxifen dissolved in peanut oil (1 mg Tmx in 100 µL peanut oil per day) for 10 days. Control groups (VeCadherin-Cre^{ERT2}+; *Fto*$^{fl/fl}$ and VeCadherin-Cre^{ERT2} -; *Fto*$^{fl/fl}$) were injected with either peanut oil (Po) with or without tamoxifen (Tmx) for 10 days, respectively.

4.2.2.2 Generation of smooth muscle cell-specific *Fto*-deficient mice

To induce SMC-specific depletion of *Fto*, mice expressing Cre-recombinase under the regulatory control of the smooth muscle myosin, heavy polypeptide 11, smooth muscle (*Myh11,* also called *SMMHC*) promoter/enhancer were used. The mice were a kind gift of S. Offermann and their tissue specificity has been proven before [243, 244].

To induce Cre- recombinase expression, 6 week old SMMHC CreER^{T2}+; *Fto*$^{fl/fl}$ mice were intraperitoneally injected for 10 days with Tmx (1 mg Tmx in 100 µL Po) per day). Control groups (SMMHC CreER^{T2}+; *Fto*$^{fl/fl}$ and SMMHC CreER^{T2}-; *Fto*$^{fl/fl}$*)* were injected with either Po with or without Tmx for 10 days, respectively.

4.2.2.3 High fat diet feeding

To analyze obesity-dependent effects, a subgroup of tamoxifen- injected VeCadherin-Cre^{ERT2}+; *Fto*$^{fl/fl}$ mice, peanut oil- injected VeCadherin-Cre^{ERT2}+; *Fto*$^{fl/fl}$ mice and tamoxifen- injected VeCadherin-Cre^{ERT2}-; *Fto*$^{fl/fl}$ mice were set on HFD. HFD-feeding *ad libitum* started with an age of 8 weeks for a time period of 12 weeks until mice were sacrificed.

4.2.3 *In vivo* methods

4.2.3.1 Measurement of body weight

To obtain data for body weight curves over time, mice were weighted weekly on the same day. Therefore, a single mouse was removed from the cage, put in a container on a scale

and body weight was measured. Body weight measurements started with an age of 7 weeks until an age of 20 weeks.

4.2.3.2 Measurement of blood glucose levels

To measure blood glucose levels, the tail of the mouse was cleaned with 70% ethanol before cutting the end of the tail with sterile scissors. Using a blood glucose meter, a blood droplet was put onto a blood glucose strip and blood glucose level were measured. After successful measurement, the mouse was placed back into the mouse cage.

4.2.3.3 Glucose tolerance test

Glucose tolerance tests (GTTs) are used to assess the glucose tolerance of mice. Therefore, mice are challenged with an exogenously administered glucose amount and blood glucose clearance is analyzed. In healthy subjects increases in blood glucose induce insulin secretion and a quick glucose uptake from the blood. However, if glucose homeostasis is impaired (e.g. by insulin resistance or diabetes), glucose clearance from blood is diminished resulting in prolonged higher blood glucose levels.

For measuring glucose tolerance, mice were fasted over night for 16 h without food, but with water *ad libitum*. A sterile-filtered prewarmed D-glucose solution (400 mg/ml in physiological saline) was prepared and mice were weighted. Each mouse was challenged with 2 mg glucose per g body weight which was injected i.p.. Blood glucose level were measured 0, 15, 30, 45, 60 and 120 min after glucose injection as described in 4.2.3.2. Afterwards, mice were returned to housing colony cages.

4.2.3.4 Insulin tolerance test

To measure if mice have impaired insulin sensitivity, mice were challenged with an exogenously administered amount of insulin. In healthy subjects, insulin induces a decrease in blood glucose levels. However, if insulin sensitivity is impaired (e.g. insulin resistance, diabetes), blood glucose levels are either unchanged or decrease less compared to healthy subjects.

To measure insulin sensitivity, mice were fasted for 5 h without food, but with water *ad libitum*. After determining fasting glucose levels, mice were weighted and 0.75 U insulin per kg body weight i.p. injected (insulin solution: 0.0001 U/µl in physiological saline). Blood glucose was measured after 15, 30, 45, 60 and 90 min and the relative blood glucose level quantified as percentage to fasted glucose level.

4.2.4 *Ex vivo* methods

4.2.4.1 Measurement of body weight, body length and epigonadal fat weight

After cervical dislocation, 20 week old mice were weighted and body length measured (from nose to anus). Afterwards, epigonadal fat was isolated and weighted.

4.2.4.2 Analysis of serum lipids in murine blood samples

For measuring serum lipids, blood was isolated by cardiac puncture using a 1 ml syringe with 27-gauge needle. 600 µl whole blood was transferred into BD Vacutainer blood collection tubes (light green lid) which contain lithium heparin and gel for plasma separation. The samples were inverted several times and stored on ice until further processing. Lipid panel analyses were performed by the University of Virginia Health System, clinical pathology laboratory to determine triglyceride, cholesterol, HDL and low-density lipoprotein (LDL) levels as well as ratios of LDL to HDL and cholesterol to HDL.

4.2.4.3 Isolation of living 3rd order mesenteric arteries

For isolation of living 3rd order mesenteric arteries, mice were euthanized using carbon dioxide (CO_2) and cervical dislocation. Afterwards, the abdominal cavity was opened and sutures tightened around the beginning (after the stomach) and the end of the intestine. The intestine was then quickly isolated and washed in ice-cold Krebs-HEPES buffer with Ca^{2+}. The intestine was spread on a silicon-covered 10 cm dish to see the mesenteric tree. Here, 3rd order mesenteric arteries (lumen diameter approx. between 80-100 µm at 20 mmHg) were isolated by carefully using a microscissor and fine forceps. After successful removal of the surrounding perivascular fat tissue, a segment of the vessel was cut out and transferred into a 1.5 mL reaction tube containing Krebs-HEPES buffer with Ca^{2+}. The vessel could be stored in the tube for up to two to three hours on ice. In general, for isolation of living mesenteric arteries it should be avoided to touch or overstretch the part of the vessel which is used for further analysis.

4.2.4.4 Pressure myograph analysis of isolated mesenteric arteries

Pressure myography allows to analyze vasoactive properties of small vessels with a lumen diameter between 60- 600 µm. For example, response to vasodilators or vasoconstrictors as well as myogenic tone can be assessed.

To allow these analyses, the setup of the pressure myograph contains a pressure myograph chamber in which two micropipettes are inserted on opposing sites (Fig, 10 A). These

micropipettes are connected with tubes to a pressure regulator and optionally a flow meter (Fig. 10 B). The pressure myograph chamber is placed on an inverted microscope which is connected to a computer with data acquisition software to allow recording and analysis of lumen diameter of the vessel. For experiments the myo interface allows the regulation of intraluminal pressure and flow while the data acquisition software records inner lumen diameter, wall thickness and outer lumen diameter.

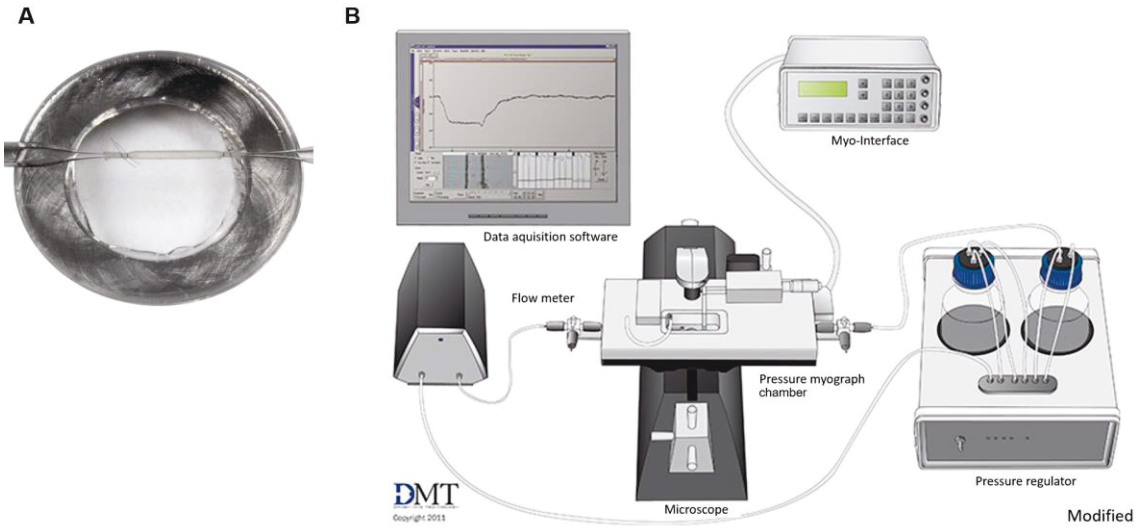

Fig. 10: Cannulation of a resistance artery (A) and setup of a pressure myograph (B)
(A) A resistance artery is cannulated at both sides from micropipettes and tied with sutures. (B) A pressure myograph setup consists of a pressure myograph chamber which has two micropipettes at opposing ends of the chamber. These are connected with tubes to the pressure regulator and flow meter. Lumen diameter can be monitored as the pressure myograph chamber is placed on an inverted microscope. This is connected to a computer with data acquisition software which allows monitoring and recording of inner lumen diameter and wall thickness of the vessel. The myo-interface allows regulation of pressure or flow depending on the experimental procedure (Modified, (A) [245] and (B) [246]).

4.2.4.4.1 *Micropipette preparation*

As for pressure myography micropipettes with a specific size have to be used for cannulating vessels, they have to be pulled from glass capillaries. To get micropipettes usable for cannulation of small vessels with a lumen diameter of approx. 100 µm, a micropipette puller was used with 800 Ω and 40 velocity. All micropipettes were analyzed on impurity before being used for pressure myography.

4.2.4.4.2 *Cannulation and equilibration of the mesenteric artery*

Freshly isolated 3rd order mesenteric arteries can be used for vasoactive analyses (for isolation see: 4.2.4.3). For preparation of the pressure myograph, the pressure myograph chamber is filled with Krebs-HEPES buffer with Ca^{2+}. The micropipettes are carefully opened using forceps, connected to the tubes and filled with Krebs-HEPES buffer with Ca^{2+} and 1% BSA by using a syringe. After the chamber is successfully prepared, the

isolated vessel is tied to one micropipette using sutures and remaining blood is flushed out of the vessel. Then, the vessel is tied on the second micropipette and stretched to approx. *in vivo* length. The chamber is transferred to the pressure myograph setup and the tubes connected to the pressure regulator. For mimicking physiological conditions, the temperature of the chamber is constantly kept at 37°C and the buffer is exchanged by a peristaltic pump.

Before starting an experiment, the vessel has to be equilibrated to pressure. Therefore, the intraluminal pressure is set to 80 mmHg for approx. 30-45 min until the mesenteric artery develops myogenic tone. After myogenic tone plateaued, endothelial survival has to be proven using either 1 µM NS309 or 10 µM ACh. Only vessels showing more than 85% vasodilation of tone have been used.

4.2.4.4.3 *Myogenic tone curves*

To allow the calculation of myogenic tone, two pressure curves have to be measured. First, a pressure curve in Ca^{2+}- containing buffer and second a pressure curve in Ca^{2+}-free buffer. For each curve, the pressure is decreased to 20 mmHg and increased in 20 mmHg increments to 120 mmHg. For the Ca^{2+}- containing curve (active curve), pressure is kept constant for at least 5 min or until myogenic tone plateaued. After the active curve was measured, the buffer was exchanged to Ca^{2+}- free buffer and after equilibration for 30 min the second pressure curve (passive curve) was measured. In the passive curve, the pressure was increased every 5 min.

For calculation of myogenic tone, the inner lumen diameter (LD) from the active curve and passive curve were measured at each pressure and myogenic tone calculated as:

$$Myogenic\ tone\ (in\ \%) = \frac{passive\ LD\ (in\ \mu m) - active\ \mathrm{LD}\ (in\ \mu m)}{passive\ LD\ (in\ \mu m)} \times 100$$

4.2.4.4.4 *Myogenic tone curves with pharmacological reagents*

Myogenic tone was measured either with the addition of 100 µM Pgds inhibitor AT 56 or with exogenously added 10 µM Pgd2.

To assess the effect of Pgd2 on myogenic tone, three pressure curves were performed on one mesenteric artery after equilibration of the vessel. First, the bath solution was exchanged to Krebs Ca^{2+} buffer with 0.01% DMSO and after equilibration of 30 min, pressure was increased in 20 mmHg increments up to 120 mmHg. Afterwards, the bath solution was exchanged to 10 µM Pgd2 (dissolved in DMSO) in Krebs Ca^{2+} buffer and

after 30 min equilibration a second pressure curve was performed. Afterwards, the bath solution was exchanged to Ca^{2+} free Krebs buffer and after 30 min equilibration, the passive pressure curve was performed. Myogenic tone was calculated for both 0.01% DMSO and 10 µM Pgd2 using the respective active curve and the same passive curve.
For assessing the influence of Pgds inhibition of myogenic tone, the water bath was exchanged to 100 µM Pgds inhibitor (dissolved in DMSO, final concentration 0.1%) in Krebs Ca^{2+} buffer. After 30 min preincubation, myogenic tone was measured as described in 4.2.4.4.3.

4.2.4.4.5 *Analysis of pharmacological reagents on vasoreactivity of mesenteric arteries*
For analyzing vasoactive properties of mesenteric arteries, different pharmacological reagents have been used. After successful isolation and hanging of a mesenteric artery, the vessel was equilibrated until it developed myogenic tone. Afterwards, the pharmacological agent was added to the bath and changes in lumen diameter analyzed.
Vasoconstriction was assessed to 40 mM KCl, 1 µM phenylephrine (PE) or 30 µM bariumchloride ($BaCl_2$). Vasodilation in response to 1 µM NS309 was measured as percentage of myogenic tone. For ACh dose-dependent vasodilation curves, vessels were pre-constricted with 1 µM PE and after a stable LD was achieved, 1 µM ACh was added to the vessel. If maximal vasodilation was reached, the next dose was added to the vessel. In the following the calculations for vasoconstriction and vasodilation are listed:

Vasoconstrictors:
KCl, PE or $BaCl_2$

$$\%\ constriction = \frac{LD\ (in\ \mu m)\ after\ reagent\ added - LD\ (in\ \mu m)\ before\ reagent}{LD\ (in\ \mu m) before\ reagent} \times 100$$

Vasodilators:
Vasodilation as % of tone for NS309

$$\%\ vasodilation = \frac{LD\ (in\ \mu m)\ after\ reagent\ added - LD\ (in\ \mu m)\ before\ reagent}{passive\ LD\ (in\ \mu m) - LD\ (in\ \mu m)\ before\ reagent} \times 100$$

Vasodilation as % of precontraction with 1 µM phenylephrine for acetylcholine

$$\%\ vasodilation = \frac{LD\ (in\ \mu m)\ after\ ACh - LD\ (in\ \mu m)\ after\ PE}{Active\ \ (in\ \mu m)\ before\ PE - LD\ (in\ \mu m)\ after\ PE} \times 100$$

4.2.5 Cell biological methods

4.2.5.1 Preparation of adult mouse smooth muscle cells from the thoracic aorta

For isolation of primary smooth muscle cells from the thoracic aorta, 3-4 22 week old mice per genotype (global *Fto*$^{+/+}$ and *Fto*$^{-/-}$) were sacrificed. After perfusion of the mouse with ice-cold PBS, the thoracic aorta was removed by cutting at the aortic arch and in proximity to the diaphragm. Then, the thoracic aorta was washed in ice-cold PBS and put in a 10 cm dish with ice-cold PBS to remove the adventitia. Afterwards, the aorta was cut longitudinally, remaining blood clots were removed and endothelial cells scrapped off with forceps. In the next step, all vessels of one genotype were pooled together, cut into small 2 mm long rings, transferred into a collagenase solution and kept at 37°C for 20 min to allow successful digestion. Then, collagenase solution was removed, growing medium added to the tissue and transferred to a 25 cm^2 cell culture flask. The volume of the media was adjusted to allow that the tissue was attached to the bottom to allow outgrowth of SMCs. After 48 h, medium was exchanged and after additional 5-7 days, the tissue was removed. After cells reached confluence of approx. 80%, cells were passaged. For experiments, passages 1-4 were used.

4.2.5.2 Cultivation and passaging of cells

All cells were kept in growing medium at 37°C with 5% CO_2 in a humidified atmosphere. Before reaching confluency, cells were passaged as follows. The medium was removed and cells once washed with PBS. After incubation with 0.05% trypsin for 5 min at 37°C and cell detachment occurred, an equivalent amount of growing medium was added and transferred into a 50 mL falcon. To remove trypsin, cells were centrifuged for 5 min at 200 *g*, cells resuspended in an appropriate growing media volume and seeded in cell culture plates or flasks depending on need.

For murine primary smooth muscle cells passages 1-4 and for HAoECs and HCoSMCs passages 4-10 were used.

4.2.5.3 siRNA-mediated knockdown of *FTO* in HAoECs and HCoSMCs

For siRNA-mediated knockdown of *FTO* in HAoECs and HCoSMCs, forward transfection was performed. Therefore, cells were seeded in 6 and 96 well dishes one day before transfection allowing to have a cell confluency of 30-70% to the time of transfection. To prepare transfection, the needed amount of siRNA was first mixed with transfection media (mix 1) and in parallel the appropriate amount of transfection reagent (2 µl per mL) was mixed with transfection media (mix 2). Both solutions (mix 1 and 2)

were then combined (mix 3), several times inverted and incubated for 10 min at RT. For transfection, the media was removed from the cells, cells washed one time with PBS and either 2 mL or 0.5 mL of the prepared mix 3 added per 6 well or 96 well. To decrease cell death, medium was exchanged to growing media for transfected cells after 18 h.

For transfection of both HCoSMCs and HAoECs siRNA-mediated knockdown was revealed to be most efficient using a combination of 1 nM of each siRNA A, B and C; scrambled siRNA was used as a respective control.

4.2.5.4 Seahorse assay of transfected HAoECs and HCoSMCs

For analyzing the metabolic activity of both HAoECs and HCoSMCs after siRNA-mediated knockdown of *FTO*, seahorse assays were performed.

The seahorse assay analyzes the oxygen consumption rate (OCR) and by specifically modulating components of the electron transport chain, the metabolic function can be assessed (see Fig. 11). Briefly, first basal respiration is measured and then the compounds oligomycin, FCCP, and a mixture of antimycin A and rotenone are serially added to the cells to inhibit ATP-dependent respiration, maximal respiration and non-mitochondrial respiration, respectively. Additionally, this allows the calculation of proton leakage and spare capacity.

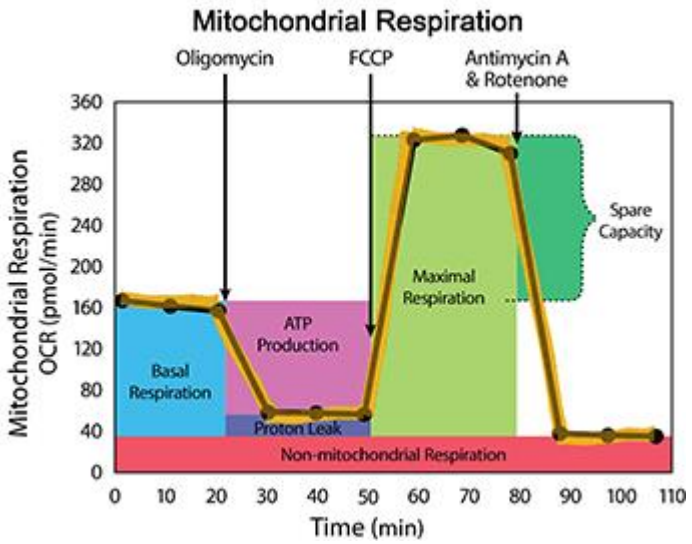

Fig. 11: Measurement of oxygen consumption rate in a seahorse assay
Oxygen consumption rate (OCR) is measured over time while different components of the respiratory chain are specifically inhibited. After measuring basal respiration, oligomycin addition inhibits ATP production leading to a decreased OCR. After washout, FCCP is added to the cells allowing to analyze maximal respiration by disrupting ATP synthesis. In the last step, FCCP is washed out and antimycin A and rotenone added to the cells allowing to analyze non-mitochondrial respiration by inhibiting the respiratory chain. Differences between OCR after oligomycin-addition to OCR after antimycin A and rotenone addition allow calculation of the proton leak. Similarly, difference between OCR after FCCP addition to basal respiration allows to determine spare capacity [247].

For measuring *FTO*-dependent effects on metabolic function, 5000 HCoSMCs or HAoECs were seeded per well in Seahorse XF24 cell culture microplates. One day later, transfection was performed as explained in 4.2.5.3. Measurement of metabolic function was assessed 48 hours after transfection using a Seahorse XF-24 Flux analyzer in collaboration with Vlad Serbulea in the lab of Norbert Leitinger, University of Virginia as previously published [248, 249].

4.2.5.5 Indirect immunofluorescence analysis and actin staining of cells

To analyze cellular localization of proteins, indirect immunofluorescence was used. Therefore, glass coverslips were placed in 24 well plates. To allow cell detachment on glass, coverslips were precoated with 2.5 µg/cm^2 fibronectin for 30 min at 37°C. After washing with PBS twice, 15000 cells per well were seeded. 24 h later, cells were set serum-free for 48 h. Cells were once washed with PBS and fixed for 15 min at RT using 4% paraformaldehyde (PFA) in PBS. After two washing steps with PBS, cells were permeabilized using 0.5% Triton X-100 in PBS for 5 min. Cells were three times washed with PBS before blocking with 10% (v/v) donkey serum in 0.2% Triton X-100 in PBS (PBS-T) for 1 h at RT was performed. To allow binding of protein-specific antibodies, cells were incubated with primary antibodies diluted in 1% (v/v) donkey serum in PBS-T overnight at 4°C (see Tab. 7 for dilution factor). On the next day, cells were washed three times with PBS-T. Fluorescence-coupled secondary antibody incubation with additional nuclei staining using 1 µg/mL 4′,6-Diamidin-2-phenylindol (DAPI) was performed at RT for 1 h in the dark (see Tab. 8 for dilution factor). In case of additional actin cytoskeleton staining, 1 µg/mL TRITC-Phalloidin (Tab. 9) was added to the secondary-antibody solution. Finally, cells were washed with PBS-T for three times, before glass coverslips were mounted using mounting media.

4.2.6 Molecular biological methods

4.2.6.1 Total RNA isolation

To isolate total RNA from the thoracic aorta or cells the RNeasy Lipid Tissue Kit or the RNeasy Mini Kit (Qiagen) were used according to manufacturer's instruction.

Briefly, for RNA isolation from the thoracic aorta homogenization was performed using the Precellis system. Therefore, up to 30 mg tissue was transferred into an 0.5 mL Precellis tube containing 1.4 mm ceramic beads (CK14 0.5 mL) and 500 µl QIAzol lysis buffer. Homogenization was performed for 30 seconds with 5000 rpm at 4°C using the

Precellis system. Afterwards, the tissue homogenate was transferred into a 1.5 mL reaction tube, chloroform was added and mixed. After incubation for 2 min and centrifugation, the upper aqueous phase was transferred into a new tube, the equal volume of 70% ethanol added and transferred on a RNeasy spin column. After centrifugation, the membrane of the column was washed once with RW1 buffer until DNase digestion was performed. Afterwards, the column was washed once with RW1 and twice with RPE buffer. To elute the RNA, the column was transferred into a new collection tube and 20 µl RNase-free water added. RNA concentration was determined using the NanoDrop system and RNA stored at -80°C until further use.

For RNA isolation from cells, cells were grown until reaching confluency of approx. 80%. Cells were washed twice with PBS before adding RLT buffer to lyse cells. The equal volume of 70% ethanol was added, mixed by pipetting and transferred on an RNeasy spin column. All further steps were performed as described for RNA isolation from tissue.

4.2.6.2 cDNA synthesis

For cDNA synthesis, 1 µg total RNA was used as a template for reverse transcribing mRNA into cDNA using the SuperScript III first strand synthesis system according to manufacturer's instruction.

Table 13 and 14 show pipetting schemes:

Substrate	**Volume**
Total RNA (1 µg)	x µL
Random hexamers	1 µL
10 mM dNTP	1 µL
RNase-free water	Ad 10 µL

Tab. 13: Pre-reaction mixture for cDNA synthesis

After heating for 5 min at 65°C (lid temperature 95°C), following reagents were added:

Substrate	Volume
Pre-reaction mixture	10 µL
35 mM $MgCl_2$	4 µL
100 mM DTT	2 µL
RNase Out	1 µL
SuperScript III reverse transcriptase	1 µL

Tab. 14: Reaction mixture for cDNA synthesis

Samples were heated for 10 min at 25°C to allow binding of primers and were then reverse transcribed into copy DNA (cDNA) for 50 min at 50°C. At the end, reaction was terminated for 5 min at 85°C. Samples were stored at -20°C until further use with a final concentration was 50 ng/µl.

4.2.6.3 Quantitative real-time polymerase chain reaction (qRT-PCR)

For quantitative analysis of transcript expression, cDNA was used as a template for qRT-PCR using the Power Up SYBR Green master mix. All data were measured in duplicates and relative transcript expression was determined using the housekeeping gene Glyceraldehyde 3-phosphate dehydrogenase (GAPDH). For statistical analysis, delta delta Ct method was performed using the CFX Manager Software (Biorad).

The following tables show the pipetting scheme and amplification protocol for all samples, gene-specific primer sequences are listed in Tab. 11:

Reagent	Volume
Primer FOR (10 µM)	1 µL
Primer REV (10 µM)	1 µL
25 ng cDNA	4 µL
2x Power Up SYBR Green Master Mix	10 µL
RNase-free water	4 µL
Total volume	20 µL

Tab. 15: Reagent mixture for qRT-PCR

Amplification was performed as indicated below and fluorescence detection was performed after elongation of every cycle.

Cycle	Temperature	Time	Number of cycles
UDG activation	50°C	2 min	1
Ampli Taq Fast DNA polymerase, UP activation	95°C	2 min	1
Denaturation	95°C	15 s	42
Annealing/elongation	60°C	1 min	
Melting curve to determine primer specificity	60°C to 95°C increment	0.5°C each 10 sec	1

Tab. 16: Protocol for gene-specific amplification using qRT-PCR

4.2.6.4 Isolation and purification of genomic DNA from tail biopsies

To allow genotyping of mice, tail biopsies of 3 week old mice were used to extract genomic DNA. Therefore, tail biopsies were incubated with 750 µl genotyping-buffer with additional 30 µl proteinase K over night at 56°C while constantly shaking. In the next step, 250 µl saturated NaCl solution (> 6M) was added, the sample shaken and centrifuged at 13000 *g* for 10 min. The supernatant was then transferred into a new reaction tube, 500 µl isopropanol added and centrifuged at 13000 *g* for 10 min to precipitate the DNA. After discarding the supernatant, the pellet was washed with 500 µl 70% ethanol and was a last time centrifuged at 13000 *g* for 10 min. In the last step, supernatant was removed and the DNA pellet dried at RT for 30 min before getting dissolved in 150 µl dd H_2O at 56°C for 10 min.

Until further use for genotyping, the DNA was stored at 4°C.

4.2.6.5 Genotyping of mice

For genotyping of mice, genomic DNA was isolated from tail biopsies and used as a template for PCR amplification. For every sample, two PCR reactions were performed. For global *Fto*-deficient mice, one PCR using Fto wt primers and another PCR using Neo primers was performed (see Tab. 12 for primer sequences). If the Fto PCR did amplify a product, the mouse had at least one wildtype *Fto* allele. Vice versa, Neo primers could just bind to the genomic DNA, if the mouse had at least one mutant allele.

For VeCadherinCre^{ERT2} and SMMHCCre^{ERT2} mouse strains, also two PCRs were performed. First one PCR using Fto floxed primers and a second PCR using either EC-Cre for the VeCadherinCre^{ERT2} mouse strain or SMC-Cre primers for the

SMMHCCre^{ERT2} mouse strain (see Tab. 12 for primer sequences). Successful amplification of a product using the Fto floxed primers was possible if the mouse had at least one wildtype allele. EC-Cre or SMC-Cre primers could bind to the DNA if the respective VeCadherin- or SM MHC Cre was successfully integrated to the genome.
For cell-type specific *Fto*-deficient mice, genotyping was performed by Transnetyx using real time PCR as previously published [250]. For global *Fto*$^{+/+}$ and *Fto*$^{-/-}$ mice, the following pipetting scheme was used:

Substrate	**Volume in µl**
Primer FOR (10 µM)	1
Primer REV (10 µM)	1
Endpoint PCR buffer (5x)	4
Taq-polymerase (5 U/µl)	0.2
dNTPs (10 mM)	0.4
Genomic DNA	1
dd H_2O	12.4

Tab. 17: PCR reaction mix for genotyping

The PCR reaction mix for genotyping was pipetted on ice and transferred to a PCR machine using the following program:

Cycle	**Temperature**	**Time**	**Number of cycles**
Lid heating	95°C	continously	
Initial denaturation	95°C	5 min	1
Denaturation	94°C	1 min	35 cycles
Annealing	56°C	1 min	
Elongation	72°C	1 min	
Final elongation	72°C	5 min	1
Cooling	20°C	forever	1

Tab. 18: PCR program for genotyping

4.2.6.6 Agarose gel electrophoresis

To analyze PCR products, agarose gel electrophoresis was performed using gels containing 1.5% agarose and GelRed Nucleic acid stain (5 µl/100 mL) in 1x TAE buffer.

Electrophoresis was performed at 120 V in 1x TAE buffer and DNA detected using the Imager Phase 312 with UV-light.

4.2.6.7 Microarray

Microarrays were performed at the Biologisch-Medizinisches Forschungszentrum (BMFZ) of the University of Düsseldorf by Dr. René Deenen.

After successful isolation of RNA from thoracic aortae of global *Fto*$^{+/+}$ and *Fto*$^{-/-}$ mice (n=4), RNA quality was assessed using a RNA 6000 Pico Chip (Agilent). Only samples with an RNA integrity number (RIN) >8 were used for further experiments.

Following cRNA synthesis was performed according to manufactory's instruction (One-Color Microarray-Based Gene Expression Analysis / Low Input Quick Amp Labeling, Agilent Technologies). First, 100 ng of respective sample RNA were reverse transcribed in cDNA. cDNA was then used as a template for *in vitro* transcription into cRNA using Cy3-dCTP to allow photometric determination of cRNA yield. Successful labeled cRNA was fragmented according to manufactory's instruction, hybridized for 17 h at 65°C to an Agilent SurePrint G3 Mouse GE 8x60K Microarray and scanned. Using 20bit tiff-pictures of the scan, fluorescence-signal intensities for each oligonucleotide-probe for each array were extracted using the feature Extraction Software (Vers. 11.0.1.1; Agilent Technologies).

For data analysis, GeneSpring GX Software (Vers. 12.5; Agilent Technologies) was used. Raw signal intensities of every single oligonucleotide-probes were first quantile-normalized across all arrays. Afterwards, normalized signal intensities were baseline-transformed by dividing every probe from every array with the respective median of signal intensities. After each biological replicate was assigned to its respective genotype (wt vs. ko), transcripts which were not detected in all replicates of at least one genotype were excluded from further analysis as being "not transcribed" (Feature Extraction Software). To asses significantly different expressed transcripts, moderated unpaired t-test was used. Significance threshold was set to $p<0.01$.

4.2.6.8 Database for Annotation, Visualization and Integrated Discovery (DAVID)-based bioinformatical analysis of microarray data

To bioinformatically analyze microarray data, the Database for Annotation, Visualization and Integrated Discovery (DAVID) was used. This online program allows identification of significantly enriched pathways and gene ontology (GO) by functional chart analysis. Respective functional chart analysis were performed as previously published [251].

For data analysis, microarray lists with significantly altered transcripts was uploaded, the species selected and transcripts identified using the official gene symbol nomenclature. Functional chart analysis was performed and Kyoto Encyclopedia of Genes and Genomes (KEGG) pathways analyzed.

4.2.6.9 Ingenuity pathway analysis- (IPA-) based analysis of microarray data

IPA-based upstream analysis of microarray data allows to identify significantly altered signaling cascades. It identifies upstream regulators (e.g. transcription factor) together with their known target genes to more easily identify affected pathways.

For data analysis, lists of significantly altered transcripts identified by microarray analysis were uploaded into the IPA software (Qiagen). Afterwards, core analysis was performed using presettings and revealed significantly altered upstream regulators as well as their target genes.

4.2.7 Histochemical analysis

4.2.7.1 Removal of mesenteric arteries and paraffin embedding

For histochemical analysis of mesenteric arteries, the vessels were quickly isolated after sacrificing the mouse. After washing with PBS, samples were fixed in 4% PFA over night at 4°C. Mesenteric arteries were then embedded in 3% agarose to allow a better detection of the vessel and transferred into 70% ethanol until further use.

To allow dehydration of the vessel, ethanol series were performed. The vessel was transferred first into 80% ethanol and then 90% ethanol for 30 min each. Afterwards, the tissue was stored in 96% ethanol for 1 h and twice in 100% ethanol for 1 h or 30 min, respectively. The vessel was then transferred into a 1:1 mixture of toluol and ethanol for 15 min and then moved to toluol for 1 h. At the end, new toluol was added for 30 min and the vessel transferred into warm paraffin and stored at 55°C overnight.

The mesenteric artery was then embedded in paraffin longitudinally to allow cross-sectional cutting. Until further use, the embedded tissues were kept at RT.

4.2.7.2 Sectioning and deparaffinization of paraffin-embedded tissues

After tissues were embedded in paraffin, 6 µm thick slices were cut and transferred to a cover slide. To allow immunofluorescence staining of the tissues, deparaffinization and antigen retrieval had to be performed. Briefly, slides were incubated twice in xylene for 4 min each. Afterwards, the slides were transferred to 100% ethanol for two times 3 min. Ethanol series was performed by first washing slides twice in 95% ethanol for 3 min

before being incubated in 70% ethanol for 3 min. Before antigen retrieval was started, slides were washed 20 min in 100% H_2O.

4.2.7.3 Indirect immunofluorescence analysis of tissue

Before indirect immunofluorescence could be performed, deparaffinized sections were prepared for antigen retrieval by heat activation. Therefore, 2.34 mL of antigen retrieval solution were dissolved in 250 mL water. Afterwards, the slides were placed in a slide rack in a container and antigen retrieval solution added. For heating the container was put into a microwave and heated for a total of 11 min. After 4, 7 and 10 min, the container was filled back up with antigen retrieval solution. Then the container was removed from the microwave, antigen retrieval solution filled up a last time and the container stored at 4°C for 30 min. After successful antigen retrieval, slides were stored in PBS until further use.

Before staining was performed, slides were incubated in blocking solution for 30 min at RT. Afterwards, blocking solution was removed, the diluted primary antibody (dissolved in blocking solution, see Tab.7) added to the slide and incubated over night at 4°C. On the next day, the slides were washed three times for 5 min in PBS. Afterwards, the diluted secondary antibody (diluted in blocking solution, see Tab. 8) was added to the slide and incubated at RT for 1 h in the dark. Afterwards, slides were washed one time for 5 min in PBS before slides were mounted using mounting media (with DAPI). The cover glass was sealed with nail polish and stainings analyzed using a confocal microscope.

5 Results

5.1 Microarray analysis of thoracic aortae of *Fto*$^{+/+}$ *and Fto*$^{-/-}$ mice

Previous work in our laboratory could show that Fto is expressed in ECs and SMCs of the vasculature. Furthermore, thoracic aortae of *Fto*-deficient mice showed reduced ACh-induced vasodilation in aortic rings suggesting that Fto is functionally important in the vasculature (Stefanie Seehaus, unpublished data). To identify cellular pathways which are regulated by vascular Fto expression, microarray analysis of thoracic aortae of global *Fto*$^{+/+}$ and *Fto*$^{-/-}$ mice were performed.

Interestingly, microarray analysis identified that 1997 transcripts were significantly altered in expression between thoracic aortae of *Fto*$^{+/+}$ and *Fto*$^{-/-}$ mice ($p<0.01$). In order to identify cellular pathways which are affected by *Fto* depletion, the Database for Annotation, Visualization and Integrated Discovery (DAVID) was used. This online program allows identification of significantly enriched pathways and gene ontology (GO) classes by functional chart analysis. Respective functional chart analyses of thoracic aortae microarray data revealed that 344 GO terms were significantly different between both genotypes including 22 pathways. Strikingly, the pathway with the lowest p-value was vascular smooth muscle cell contraction, as 21 different transcripts in this pathway were altered in expression levels (see Tab. 19). Furthermore, also regulation of actin cytoskeleton and insulin signaling were among the identified pathways which are both known to be important in regulation of myogenic tone ($p=0.0099$ and $p=0.028$) [130, 252].

As these data indicated a functional role of vascular Fto in smooth muscle cell contraction, we wanted to analyze the role of endothelial and smooth muscle Fto in regulation of myogenic tone.

Pathway	Count	P value
mmu04270: Vascular smooth muscle contraction	21	5,46E-05
mmu05410: Hypertrophic cardiomyopathy (HCM)	17	5,90E-05
mmu04120: Ubiquitin mediated proteolysis	21	3,21E-04
mmu04310: Wnt signaling pathway	22	4,14E-04
mmu05412: Arrhythmogenic right ventricular cardiomyopathy	14	7,52E-04
mmu00565: Ether lipid metabolism	9	1,25E-03
mmu05414: Dilated cardiomyopathy	15	1,79E-03
mmu04510: Focal adhesion	24	0,003278
mmu05222: Small cell lung cancer	13	0,006914
mmu04144: Endocytosis	23	0,008553
mmu04810: Regulation of actin cytoskeleton	24	0,009979
mmu04730: Long-term depression	11	0,014676
mmu00240: Pyrimidine metabolism	13	0,017572
mmu05200: Pathways in cancer	31	0,021211
mmu04916: Melanogenesis	13	0,023565
mmu00564: Glycerophospholipid metabolism	10	0,02454
mmu03020: RNA polymerase	6	0,025352
mmu04910: Insulin signaling pathway	16	0,027723
mmu04010: MAPK signaling pathway	26	0,028508
mmu00230: Purine metabolism	17	0,039628
mmu05210: Colorectal cancer	11	0,044455
mmu04350: TGF-beta signaling pathway	11	0,047525

Tab. 19: Identified affected pathways in microarray data of thoracic aortae of *Fto*$^{+/+}$ and *Fto*$^{-/-}$ mice

5.2 Characterization of EC Cre+/- ;*Fto*$^{fl/fl}$ mice

For investigating cell-type specific functions of vascular Fto, EC-specific *Fto*-deficient mice were generated using a tamoxifen-inducible VeCadherin-CreER^{T2} lox P system.

For inducing EC-specific *Fto*-deficient mice, 6 week old VeCadherin CreER^{T2}+ *Fto*$^{floxed/floxed}$ mice were injected for 10 days with tamoxifen dissolved in peanut oil (abbreviated EC Cre+ ;*Fto*$^{fl/fl}$ +Tmx). Additionally, two control groups were used to rule out leakiness of the Cre loxP system or of tamoxifen itself. Therefore, VeCadherin-CreER^{T2}+ ;*Fto*$^{floxed/floxed}$ mice were injected with peanut oil (abbreviated EC Cre+ ;*Fto*$^{fl/fl}$ +Po) and VeCadherin-CreER^{T2}- ;*Fto*$^{floxed/floxed}$ were injected with tamoxifen dissolved in peanut oil (abbreviated EC Cre- ;*Fto*$^{fl/fl}$ +Tmx), respectively (see Fig. 12). The successful endothelial depletion of Fto was verified by immunofluorescent analysis of mesenteric arteries of EC Cre+ ;*Fto*$^{fl/fl}$ +Po and EC Cre+ ;*Fto*$^{fl/fl}$ +Tmx mice showing a reduced Fto staining in ECs (see suppl. Fig. 1).

Furthermore, as *Fto* is known to be associated with obesity, the three different groups were analyzed after feeding of NC and compared to mice being fed a HFD for 12 weeks.

Thus, a total of six groups were compared in the following analyses to investigate the cell-type specific function of *Fto* in ECs in both basal and HFD conditions (Fig. 12).

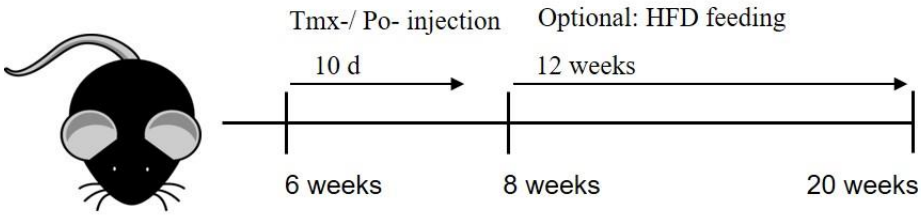

Normal chow	High fat diet
EC Cre-; *Fto*$^{fl/fl}$ + Tmx	EC Cre-; *Fto*$^{fl/fl}$ + Tmx
EC Cre+; *Fto*$^{fl/fl}$ + Po	EC Cre+; *Fto*$^{fl/fl}$ + Po
EC Cre+; *Fto*$^{fl/fl}$ + Tmx	EC Cre+; *Fto*$^{fl/fl}$ + Tmx

Fig. 12: Overview about experimental groups in EC Cre+/- ;*Fto*$^{fl/fl}$ mice
For analyzing the function role of Fto in ECs, three different groups of mice were compared: EC Cre+ ;*Fto*$^{fl/fl}$ +Po, EC Cre+ ;*Fto*$^{fl/fl}$ +Tmx and EC Cre- ;*Fto*$^{fl/fl}$ +Tmx mice. For generation of these groups, six week old EC Cre+ ;*Fto*$^{fl/fl}$ were injected with either peanut oil (EC Cre+ ;*Fto*$^{fl/fl}$ +Po) or tamoxifen dissolved in peanut oil (EC Cre- ;*Fto*$^{fl/fl}$ +Tmx) for 10 days. In parallel, EC Cre- ;*Fto*$^{fl/fl}$ were only injected with tamoxifen (EC Cre- ;*Fto*$^{fl/fl}$ +Tmx), respectively. To analyze obesity-dependent effects, mice from all three groups were divided into two groups which were either fed a NC or a HFD for 12 weeks. Mice from all six groups were then analyzed with an age of 20 weeks.

5.2.1 Phenotypic characterization of NC- and HFD-fed EC Cre+/- ;*Fto*$^{fl/fl}$ mice

As *Fto* is known to affect obesity, we wanted to investigate if endothelial-specific loss of *Fto* also influences body weight. Therefore, different parameters which are known to be affected in global *Fto*$^{-/-}$ mice were analyzed [187]. First, body weight was measured weekly during week 7 and week 20 in NC- or HFD-fed EC Cre+; *Fto*$^{fl/fl}$ +Tmx, EC Cre+; *Fto*$^{fl/fl}$ +Po and EC Cre-; *Fto*$^{fl/fl}$ +Tmx mice. And second, 20 week old mice were analyzed for epigonadal fat weight and body length.

As visualized in Fig. 13 A, weight gain over time was not affected by EC-specific *Fto* deficiency in both NC-fed (left column) and HFD-fed (right column) mice. All NC-fed EC Cre+; *Fto*$^{fl/fl}$ +Tmx, EC Cre+; *Fto*$^{fl/fl}$ +Po and EC Cre-; *Fto*$^{fl/fl}$ +Tmx mice gained approx. 40% body weight over time, while respective HFD-fed mice increased body weight about 120%. In line with body weight gain over time, also body weight was not significantly different between the analyzed groups in both NC-fed and HFD-fed mice (Fig. 13 B). While all NC-fed mice weighted around 30 g, HFD-fed mice weighted significantly more with a mean of approx. 45 g. Further analysis of epigonadal fat weight

and body length also revealed no significant differences between the genotypes (Fig. 13 C-D). All three groups of NC-fed mice had a mean epigonadal fat weight of approx. 0.5 g which was significantly increased in all groups of HFD-fed mice to a mean of 3 g. In line, analysis of body length revealed a mean body length of 9 cm in all NC-fed and 10 cm in all HFD-fed mice, respectively.

Collectively, these data reveal that EC-specific *Fto* deficiency did not affect body weight, epigonadal fat accumulation or body length in both NC- and HFD-fed mice.

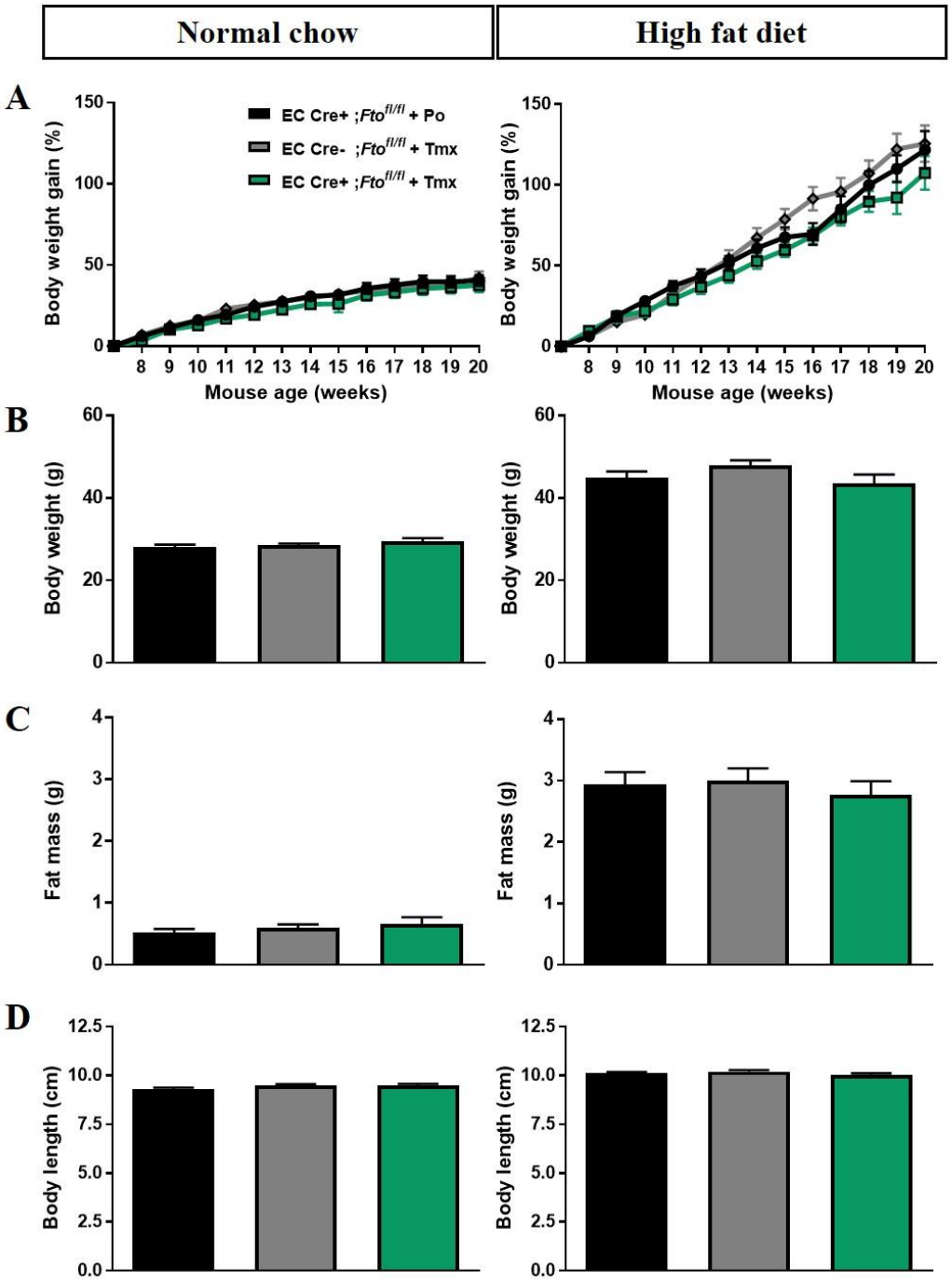

Fig. 13: Phenotypic characterization of NC- and HFD-fed EC Cre+; *Fto*$^{fl/fl}$ +Tmx, EC Cre+; *Fto*$^{fl/fl}$ +Po and EC Cre-; *Fto*$^{fl/fl}$ +Tmx mice

EC Cre+; *Fto*$^{fl/fl}$ +Tmx mice were phenotypically compared to both control EC Cre+; *Fto*$^{fl/fl}$ +Po and EC Cre-; *Fto*$^{fl/fl}$ +Tmx mice in both NC-fed (left column) and HFD-fed (right column) male mice. In (A) percentage body weight gain from week 7 to week 20 is shown. HFD-fed mice gained more weight over time compared to NC-fed mice, but endothelial-specific *Fto* deficiency did not affect body weight gain in both NC-fed (n=9, 13, 11) and HFD-fed (n=7, 15, 11) mice. (B) Body weight measurement in 20 week old mice also revealed no influence of endothelial *Fto*-deficiency in both NC-fed (n=11, 19, 12) and HFD-fed (n=11, 16, 14) mice. (C) Epigonadal fat weight in 20 week old mice did not show significant differences between all analyzed genotypes in both NC-fed (n=10, 14, 9) and HFD-fed (n=10, 10, 10) mice. (D) Measurement of body length of 20 week old mice was not affected by endothelial Fto-deficiency in both NC-fed (n=11, 19, 12) and HFD-fed (n=11, 14, 13) mice.

Data represent mean ± SEM, for statistical analysis one-way ANOVA with Tukey's post-hoc test was performed; $p<0.05$ was defined as significant.

5.2.2 Vasoactive analyses in mesenteric arteries of EC Cre+/- ;*Fto*$^{fl/fl}$ mice

As human GWAS point to a role of Fto in the development of hypertension, resistance arteries are of particular importance as they are the main contributor to vascular resistance and thus influence blood pressure. To investigate if endothelial Fto may be important in regulation of vascular resistance, 3rd order mesenteric arteries were isolated from 20 week old NC-fed and HFD-fed EC Cre+; *Fto*$^{fl/fl}$ +Tmx, EC Cre+; *Fto*$^{fl/fl}$ +Po and EC Cre-; *Fto*$^{fl/fl}$ +Tmx mice. These vessels were then analyzed for their vasoactive properties using pressure myography.

5.2.2.1 Myogenic tone analysis

To analyze if endothelial Fto influences myogenic tone, lumen diameter of 3rd order mesenteric arteries were recorded at different intraluminal pressures either in the presence of Ca^{2+} (active curve) or in the absence of Ca^{2+} (passive curve) using pressure myography. With respective lumen diameter of the active and passive curve, myogenic tone was calculated for each pressure.

As shown in Fig. 14 A, left column, EC-specific loss of *Fto* did not affect myogenic tone in mesenteric arteries of NC-fed mice. In each group, mesenteric arteries started to develop myogenic tone at 40– 60 mmHg and reached its maximum of approx. 38% at a pressure of 100- 120 mmHg. However, in contrast to mesenteric arteries of NC-fed mice myogenic tone of mesenteric arteries from HFD-fed EC Cre+; *Fto*$^{fl/fl}$ +Tmx mice was significantly different to mesenteric arteries of both HFD-fed control groups (Fig. 14 A, right column). While mesenteric arteries of HFD-fed EC Cre+; *Fto*$^{fl/fl}$ +Po and EC Cre-; *Fto*$^{fl/fl}$ +Tmx mice developed maximal myogenic tone of approx. 32% at 120 mmHg, mesenteric arteries of endothelial-specific *Fto* deficient mice developed myogenic tone of approx. 38% at 120 mmHg which was comparable to maximal myogenic tone of mesenteric arteries of all NC-fed mice.

As myogenic tone is depending on both active and passive lumen diameter, respective changes in relative lumen diameter were analyzed for both active and passive curve. Analysis of relative lumen diameter in active curves revealed no significant differences in mesenteric arteries of all NC-fed mice (Fig. 14 B, left column). With increasing pressure, the relative lumen diameter increased first to 140-150% of initial lumen diameter at 40- 60 mmHg and then decreased to 120% of initial lumen diameter for pressures between 80 and 120 mmHg. In contrast to mesenteric arteries of NC-fed mice, respective vessels of HFD-fed mice showed significant differences in relative lumen

diameter of the active curves between the groups (Fig. 14 B, right column). In mesenteric arteries of both control groups, the relative lumen diameter first increased to approx. 140% of initial lumen diameter at 40- 60 mmHg and then further decreased to approx. 130% of initial lumen diameter at 120 mmHg. In comparison, mesenteric arteries of HFD-fed EC Cre+; *Fto*$^{fl/fl}$ +Tmx mice also first increased to approx. 140% of initial lumen diameter at 40 mmHg, but had a significantly reduced lumen diameter compared to both controls between 80 and 120 mmHg. Respective analysis of relative lumen diameter of the passive curve revealed no significant differences between mesenteric arteries of all groups in both NC-fed and HFD-fed mice (Fig. 14 C, left and right column). All analyzed mesenteric arteries showed incremental increase of relative lumen diameter with increasing pressure reaching a maximal relative lumen diameter of 160- 170% at 120 mmHg.

In summary, the data revealed that loss of endothelial *Fto* did not affect myogenic tone in mesenteric arteries of NC-fed mice, but significantly increased myogenic tone in mesenteric arteries of HFD-fed mice. While mesenteric arteries of both control groups had a decreased myogenic tone after HFD compared to NC, this was not present in mesenteric arteries of EC Cre+; *Fto*$^{fl/fl}$ +Tmx mice. In line with these data, loss of endothelial *Fto* did not affect relative lumen diameter of active and passive curves in mesenteric arteries in NC-fed mice. Only in mesenteric arteries of HFD-fed mice, loss of endothelial *Fto* significantly reduced relative lumen diameter in active curves compared to mesenteric arteries of control mice.

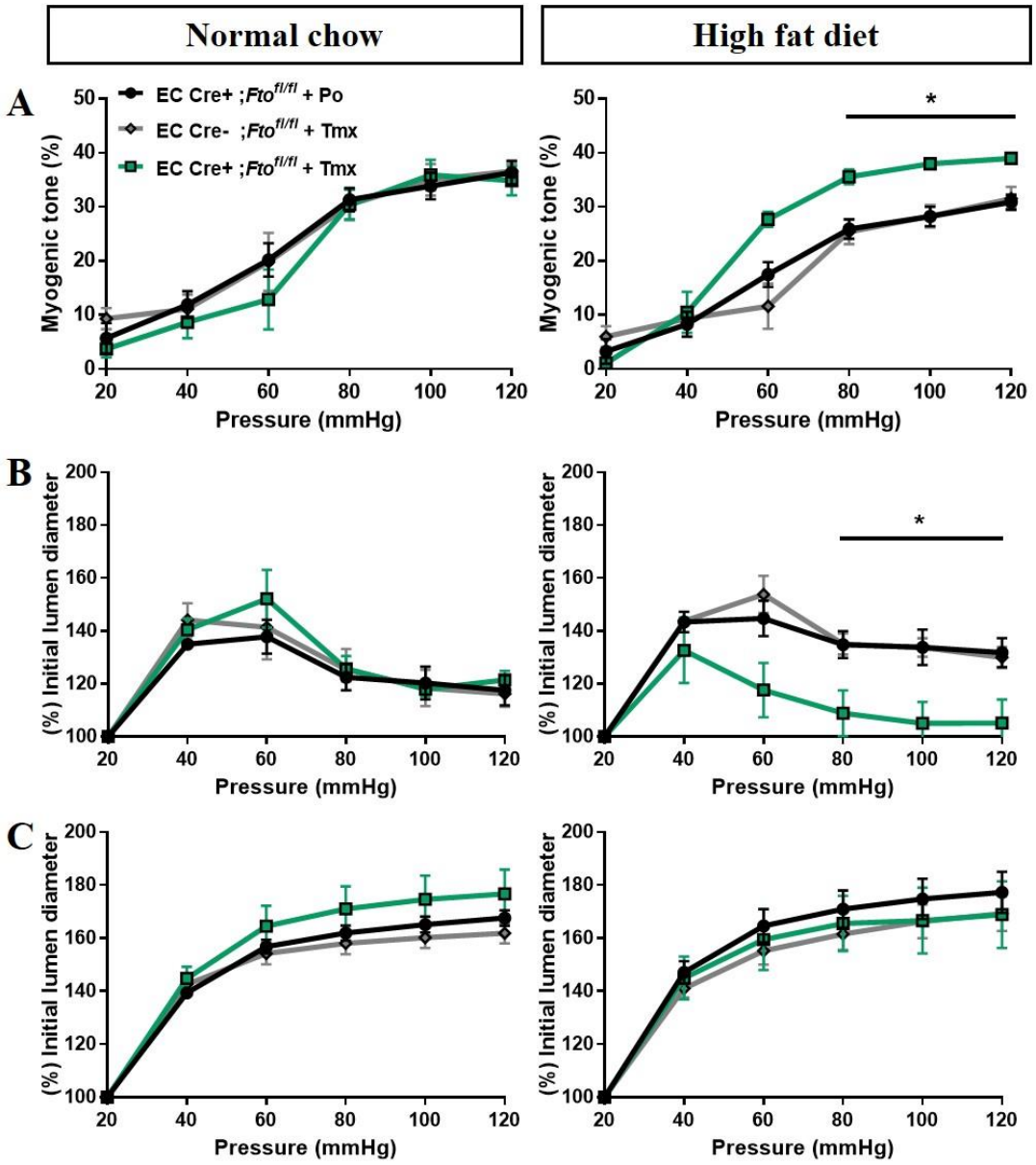

Fig. 14: Analysis of myogenic tone in mesenteric arteries of NC- or HFD-fed EC Cre+; *Fto*$^{fl/fl}$ +Tmx, EC Cre+; *Fto*$^{fl/fl}$ +Po and EC Cre-; *Fto*$^{fl/fl}$ +Tmx mice

3rd order mesenteric arteries were isolated from NC-fed (left column) and HFD-fed (right column) EC Cre+; *Fto*$^{fl/fl}$ +Tmx, EC Cre+; *Fto*$^{fl/fl}$ +Po and EC Cre-; *Fto*$^{fl/fl}$ +Tmx male mice and pressure curves were performed. (A) Myogenic tone curves showed no significant differences between all genotypes in NC-fed mice (n=4, 5, 6). In HFD-fed mice, mesenteric arteries of EC Cre+ *Fto*$^{fl/fl}$ +Po and EC Cre-; *Fto*$^{fl/fl}$ +Tmx mice had significantly reduced myogenic tone compared to mesenteric arteries of EC Cre+; *Fto*$^{fl/fl}$ +Tmx mice (n=6, 6, 4) between 80 and 120 mmHg. (B) Pressure curves were performed in Ca^{2+}-containing buffer allowing SMC contraction (active curve). Lumen diameter at different pressures were plotted as percentage of initial lumen diameter at 20 mmHg. While active curves showed no significant differences in NC-fed mice (n=4, 5, 6), active curves of HFD-fed mice (n=6, 6, 4) revealed significant differences. Lumen diameter of mesenteric arteries from EC Cre+; *Fto*$^{fl/fl}$ +Tmx was significantly reduced between 80 and 120 mmHg compared to both controls. (C) Pressure curves were performed in Ca^{2+}-free buffer (passive curve) to measure stiffness of mesenteric arteries of NC-fed mice (n=4, 5, 6) and HFD-fed mice (n=6, 6, 4). Lumen diameter at different pressures were plotted as percentage of initial lumen diameter at 20 mmHg. Passive curves showed no significant differences independent of genotype and chow between all analyzed groups. Data represent mean ± SEM, for statistical analysis one-way ANOVA with Tukey's post-hoc test was performed; $p<0.05$ was defined as significant.

5.2.2.2 Agonist-induced vasoactive analysis

Within mesenteric arteries, the endothelial ion channels IK_{Ca}, SK_{Ca} and K_{ir} are known to be important regulators of myogenic tone. Also, general SMC contractility is known to affect vascular tone. To identify if loss of endothelial *Fto* may exert its effect on myogenic tone in mesenteric arteries of HFD-mice by affecting ion channel properties, lumen diameter changes to pharmacological activators or inhibitors of these channels were analyzed. Therefore, mesenteric arteries from NC-fed and HFD-fed EC Cre+; $Fto^{fl/fl}$ +Tmx, EC Cre+; $Fto^{fl/fl}$ +Po and EC Cre-; $Fto^{fl/fl}$ +Tmx mice were pressurized at 80 mmHg until myogenic tone developed and vasodilation or vasoconstriction to 1µM NS309, 30 µM $BaCl_2$ and 40 mM KCl were assessed. While NS309 is a known activator of IK_{Ca} and SK_{Ca} channels which leads to EC and subsequent SMC hyperpolarization, $BaCl_2$ inhibits endothelial K_{ir} channels leading to EC depolarization and subsequent vasoconstriction of SMCs. KCl in contrast induces non-agonist induced depolarization-dependent SMC contraction.

Interestingly, analysis of NS309-induced vasodilation showed no significant differences between mesenteric arteries of EC Cre+; $Fto^{fl/fl}$ +Tmx, EC Cre+; $Fto^{fl/fl}$ +Po and EC Cre-; $Fto^{fl/fl}$ +Tmx mice after both NC-feeding and HFD-feeding (Fig. 15 A, left and right column). In all vessels, addition of 1 µM NS309 induced a mean vasodilation of around 90% of myogenic tone. Similarly, also $BaCl_2$- induced vasoconstriction was similar in mesenteric arteries of all NC-fed and HFD-fed mice (Fig. 15 B, left and right column). Ba^{2+}-induced vasoconstriction was in mean approx. 9% of initial lumen diameter in mesenteric arteries of NC-fed mice, while it was slightly decreased in mesenteric arteries of HFD-fed mice to a mean of approx. 7.5%. Also, KCl-induced vasoconstriction was not affected by EC-specific *Fto* deficiency (Fig. 15 C, left and right column) as mean percentage of constriction was between 22 and 28% in mesenteric arteries of all NC-fed and HFD-fed mice.

Thus, loss of endothelial *Fto* seems to affect myogenic tone in HFD-fed mice without affecting endothelial IK_{Ca}, SK_{Ca} and K_{ir} channel function or general SMC contractility.

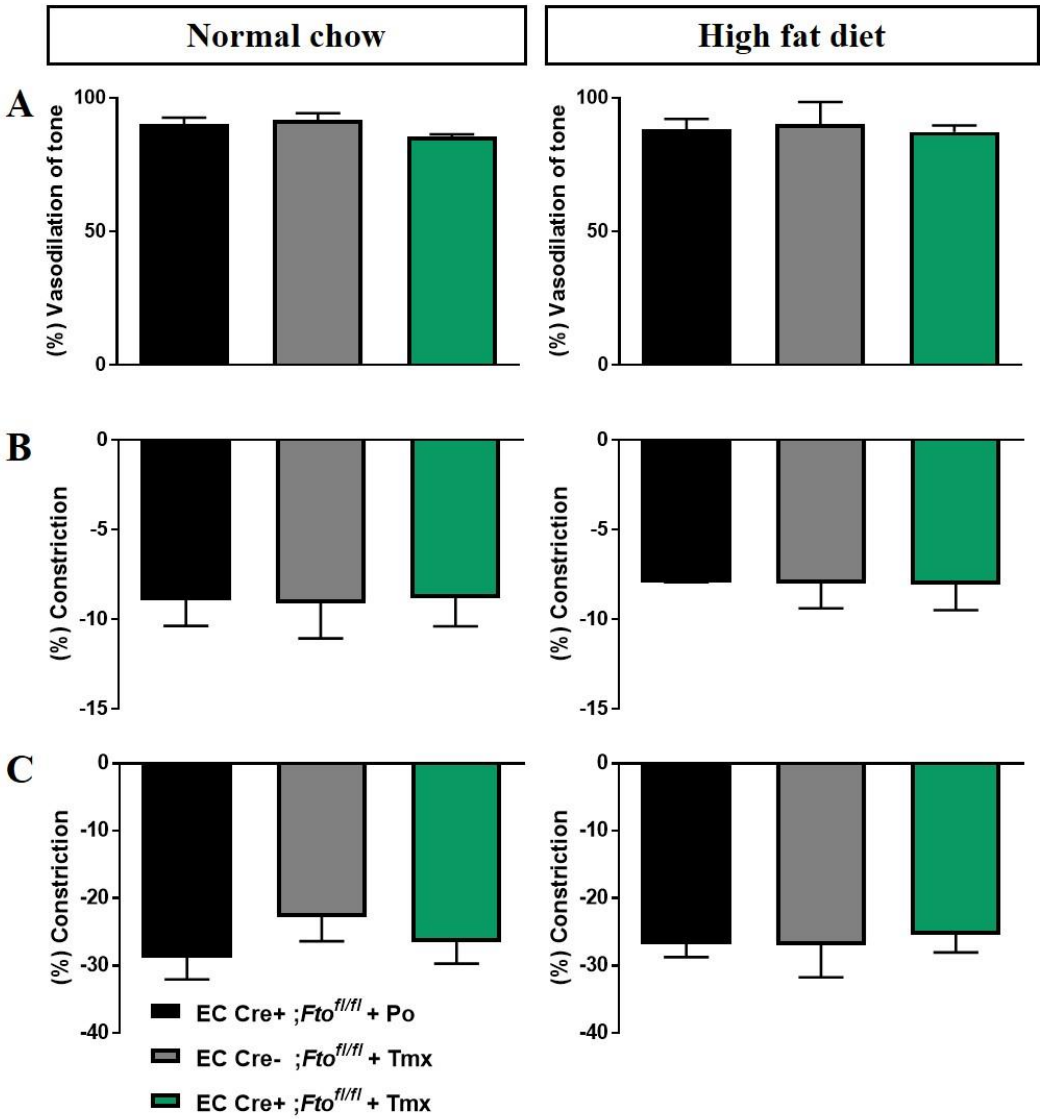

Fig. 15: Analysis of vasoactive response to different pharmacological compounds in mesenteric arteries of NC- or HFD-fed EC Cre+; *Fto*$^{fl/fl}$ +Tmx, EC Cre+; *Fto*$^{fl/fl}$ +Po and EC Cre-; *Fto*$^{fl/fl}$ +Tmx mice

3rd order mesenteric arteries were isolated from 20 week old NC-fed (left column) and HFD-fed (right column) EC Cre+; *Fto*$^{fl/fl}$ +Tmx, EC Cre+; *Fto*$^{fl/fl}$ +Po and EC Cre-; *Fto*$^{fl/fl}$ +Tmx male mice and equilibrated at 80 mmHg until myogenic tone developed. (A) 1 µM of the IK_{Ca}- and SK_{Ca}- channel activator NS309 was added to mesenteric arteries and vasodilation analyzed. In both NC-fed (n=3, 3, 7) and HFD-fed (n=4, 3, 3) mice, vasodilation in response to NS309 accounted to approx. 90% vasodilation which was unaltered between all genotypes. (B) 30 µM $BaCl_2$ was added to mesenteric arteries to inhibit endothelial K_{ir} channels. Ba^{2+}- induced contraction was in mean approx. 9% or 7.5% in mesenteric arteries of NC-fed (n=3, 3, 4) and HFD-fed (3, 3, 4) mice, respectively and revealed no differences between the genotypes. (C) 40 mM KCl was added to induce depolarization and subsequent contraction of SMCs in mesenteric arteries. Mean contraction was approx. 25% in mesenteric arteries of both NC-fed (n=4, 7, 6) and HFD-fed (n=8, 6, 5) mice with no significant differences between the genotypes.

Data represent mean ± SEM, for statistical analysis one-way ANOVA with Tukey's post-hoc test was performed; $p<0.05$ was defined as significant.

5.2.2.3 Acetylcholine-induced vasodilation in mesenteric arteries of HFD-fed EC Cre+/- ;*Fto*$^{fl/fl}$ mice

ACh-induced vasodilation, which is mainly NO-dependent, is known to be reduced in HFD-fed mice and to influence vascular tone. In order to analyze if endothelial *Fto* deficiency exerts its effect on myogenic tone in mesenteric arteries of HFD-fed mice by influencing NO bioavailability, dose-dependent ACh-induced vasodilation was measured in mesenteric arteries of HFD-fed EC Cre+; *Fto*$^{fl/fl}$ +Tmx, EC Cre+; *Fto*$^{fl/fl}$ +Po and EC Cre-; *Fto*$^{fl/fl}$ +Tmx mice. As a comparison, mesenteric arteries of NC-fed EC Cre+; *Fto*$^{fl/fl}$ +Po were measured in parallel. To allow measurement of ACh-induced vasodilation, mesenteric arteries were isolated, pressurized at 80 mmHg until myogenic tone developed and pre-constricted using 1 µM PE. After a stable contraction was achieved, dose-dependent ACh-induced vasodilation was measured.

PE-induced vasocontraction revealed no significant differences between mesenteric arteries of all analyzed groups (data not shown). Also, the following ACh-induced vasodilation was not affected by loss of endothelial *Fto* (Fig. 16). Mesenteric arteries from all HFD-fed mice showed a significantly decreased vasodilation in response to 4 and 10 µM ACh compared to mesenteric arteries of NC-fed EC Cre+; *Fto*$^{fl/fl}$ +Po mice. While mesenteric arteries of all HFD-fed mice showed nearly no increased vasodilation with increasing doses of ACh, mesenteric arteries of NC-fed EC Cre+; *Fto*$^{fl/fl}$ +Po mice further vasodilated with increasing doses of ACh. 1 µM to 10 µM ACh-induced vasodilation was between 10 and 30% in mesenteric arteries of HFD-fed mice while it induced vasodilation up to 70% in mesenteric arteries of NC-fed EC Cre+; *Fto*$^{fl/fl}$ +Po mice.

Collectively, these data show that loss of endothelial *Fto* did not affect HFD-induced reduction of ACh-dependent vasodilation. Thus, effects of endothelial-specific *Fto*-deficiency on myogenic tone in HFD-fed mice seem to be independent of HFD-induced effects on ACh-dependent vasodilation.

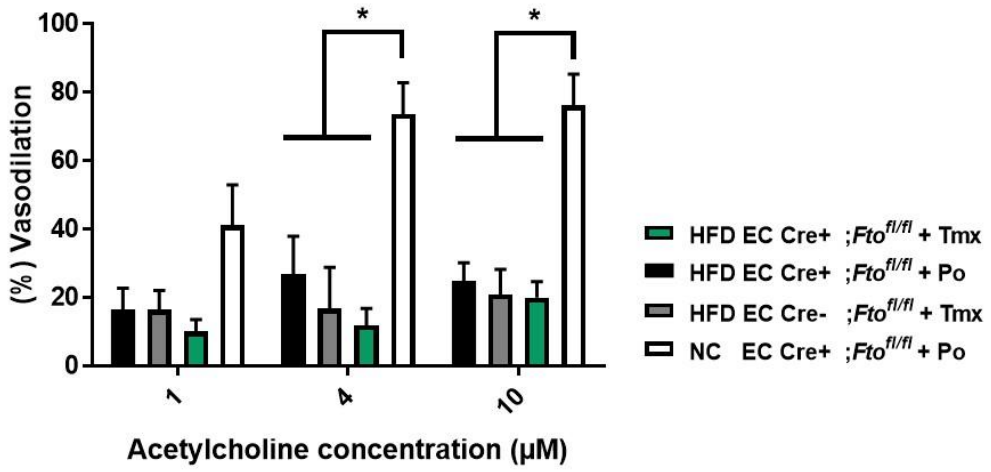

Fig. 16: Analysis of endothelial loss of *Fto* on acetylcholine-induced vasodilation in mesenteric arteries of HFD-fed mice
3rd order mesenteric arteries were isolated from 20 week old HFD-fed EC Cre+; *Fto*$^{fl/fl}$ +Tmx, EC Cre+; *Fto*$^{fl/fl}$ +Po and EC Cre-; *Fto*$^{fl/fl}$ +Tmx mice (n=3, 4, 3) and compared to 3rd order mesenteric arteries from 20 week NC-fed EC Cre+; *Fto*$^{fl/fl}$ +Po mice (n=3). Vessels were equilibrated at 80 mmHg until myogenic tone developed and were then preconstricted with 1 µM phenylephrine. After stable contraction was achieved, ACh was dose-dependently added and maximal vasodilation measured.
1 µM ACh induced vasodilation was not significantly different between mesenteric arteries of NC-fed EC Cre+; *Fto*$^{fl/fl}$ +Po mice compared to mesenteric arteries of all HFD-fed mice. However, ACh-induced vasodilation was significantly reduced in all mesenteric arteries of HFD-fed mice compared to mesenteric arteries of NC-fed EC Cre+; *Fto*$^{fl/fl}$ +Po mice at both 4 µM and 10 µM.
Data represent mean ± SEM, for statistical analysis 2-way repeated measurement (RM) ANOVA with Tukey's post-hoc test was performed; $p<0.05$ was defined as significant.

5.2.3 Analysis of obesity-induced metabolic changes in HFD-fed EC Cre+/- ;*Fto*$^{fl/fl}$ mice

As loss of endothelial *Fto* protected from HFD-induced effects on myogenic tone, analysis should identify if endothelial-specific *Fto*-deficiency also influenced other obesity-dependent metabolic changes such as dyslipidemia or hyperglycemia. Therefore, blood lipid levels as well as glucose homeostasis should be analyzed in HFD-fed EC Cre+; *Fto*$^{fl/fl}$ +Tmx and EC Cre+; *Fto*$^{fl/fl}$ +Po mice. For investigating glucose homeostasis, glucose and insulin tolerance as well as blood glucose levels were measured.

5.2.3.1 Analysis of blood serum lipids in HFD-fed EC Cre+/- ;*Fto*$^{fl/fl}$ mice

For analyzing blood serum lipids, 20 week old HFD-fed EC Cre+; *Fto*$^{fl/fl}$ +Tmx and EC Cre+; *Fto*$^{fl/fl}$ +Po mice were sacrificed and blood isolated by cardiac puncture. After centrifugation of the blood, serum was analyzed for concentration of triglycerides, total cholesterol and HDL- as well as LDL- cholesterol levels.

Interestingly, serum analysis of different lipids did not reveal differences between HFD-fed EC Cre+; *Fto*$^{fl/fl}$ +Tmx and EC Cre+; *Fto*$^{fl/fl}$ +Po mice. Mean serum cholesterol (Fig. 17 A) and triglyceride levels (Fig. 17 B) showed no significant differences between both analyzed groups with mean values of approx. 200 mg/dL in both groups. Also, respective analysis of HDL-cholesterol (Fig. 17 C) and LDL-cholesterol (Fig. 17 D) concentrations were similar between HFD-fed EC Cre+; *Fto*$^{fl/fl}$ +Tmx and EC Cre+; *Fto*$^{fl/fl}$ +Po mice. In line, also analysis of ratios of total cholesterol to HDL (Fig. 17 E) and LDL to HDL (Fig. 17 F) revealed no differences. While ratios of total cholesterol to HDL were approx. 2-2.5 in both groups, respective LDL to HDL ratio were approx. 1:1.
Collectively, these data revealed that loss of endothelial *Fto* did not affect blood lipid levels in HFD-fed mice.

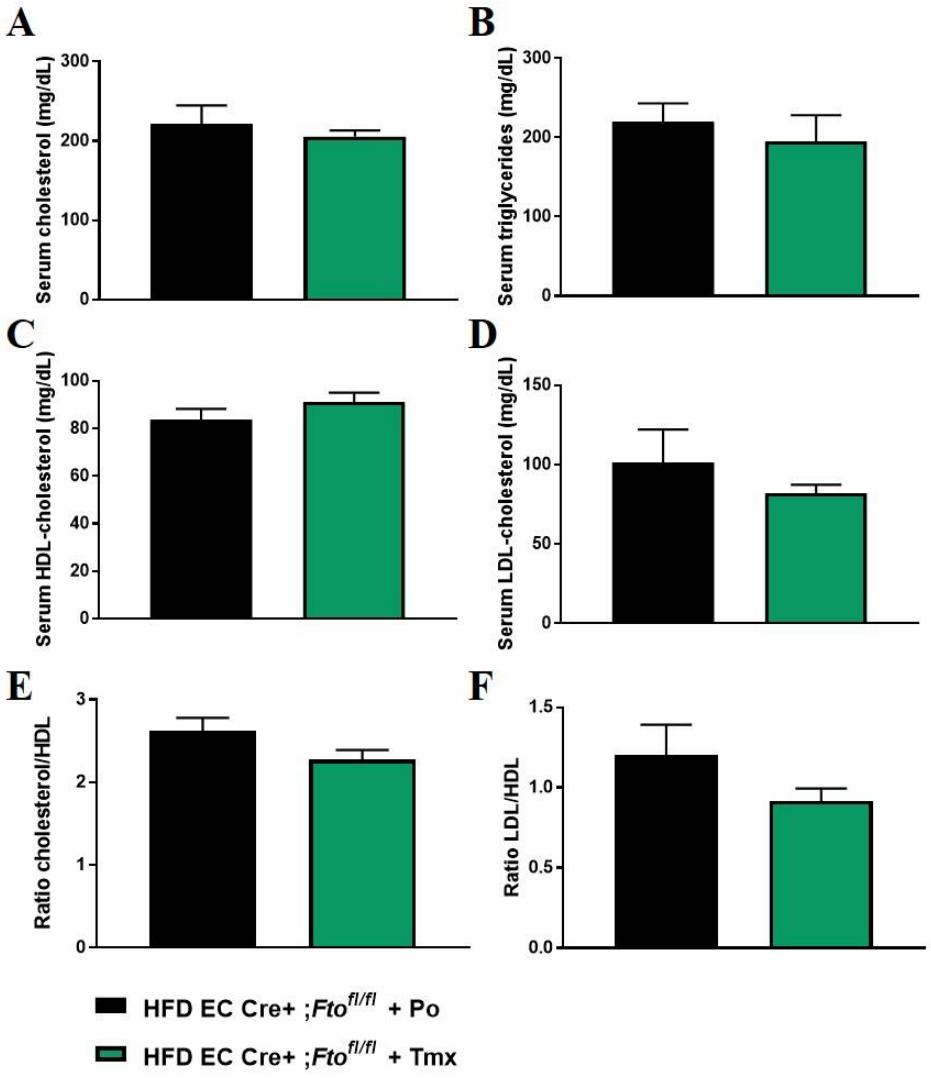

Fig. 17: Serum lipid analysis of HFD-fed EC Cre+; *Fto*$^{fl/fl}$ +Po and EC Cre+; *Fto*$^{fl/fl}$ +Tmx mice
20 week old HFD-fed EC Cre+; *Fto*$^{fl/fl}$ +Po and EC Cre+; *Fto*$^{fl/fl}$ +Tmx male mice were sacrificed and blood isolated by cardiac puncture (n=5, 7). Serum was analyzed for triglyceride, total cholesterol and HDL- and

LDL- cholesterol levels. Also, ratios of total cholesterol to HDL and ratios of LDL to HDL were calculated. (A) Total cholesterol levels were in mean 200 mg/dL and showed no significant differences between both genotypes. (B) Also total triglyceride levels with approx. means of 200 mg/dL for both HFD-fed EC Cre+; $Fto^{fl/fl}$ +Po and EC Cre+; $Fto^{fl/fl}$ +Tmx mice was unaffected by endothelial *Fto*-deficiency. Measurement of HDL-cholesterol levels (C) and LDL-cholesterol levels (D) also revealed no difference between both genotypes. Similarly, also ratios of total cholesterol to HDL (E) and LDL to HDL (F) was not influenced by endothelial *Fto*-deficiency.
Data represent mean ± SEM, for statistical analysis unpaired, two-tailed t-test was performed; $p<0.05$ was defined as significant.

5.2.3.2 Analysis of glucose metabolism in HFD-fed EC Cre+/- ;$Fto^{fl/fl}$ mice

In addition to blood lipid levels, also glucose metabolism was investigated in 20-23 week old HFD-fed EC Cre+; $Fto^{fl/fl}$ +Tmx and EC Cre+; $Fto^{fl/fl}$ +Po mice. As HFD is known to induce hyperglycemia and hyperinsulinemia in mice which is characterized by increased blood glucose levels as well as decreased insulin and glucose tolerance.

For assessing if HFD-fed EC Cre+; $Fto^{fl/fl}$ +Tmx and EC Cre+; $Fto^{fl/fl}$ +Po mice had an impaired glucose metabolism, fasted and unfasted blood glucose levels were measured. In addition, also glucose and insulin tolerance were analyzed.

Analysis of glucose tolerance revealed that blood glucose levels were significantly reduced in HFD-fed EC Cre+; $Fto^{fl/fl}$ +Tmx compared respective Po-injected mice 15, 30 and 45 min after glucose administration (Fig. 18 A). Also, respective analysis of area under curve values from the GTT measurement tended to be decreased in endothelial-specific *Fto* deficient HFD-fed mice compared to EC Cre+; $Fto^{fl/fl}$ +Po mice ($p=0.065$) (Fig. 18 B). In addition to improved glucose tolerance, also insulin tolerance was significantly better in HFD-fed EC Cre+; $Fto^{fl/fl}$ +Tmx compared to control mice (Fig. 18 C). Blood glucose levels were significantly reduced in HFD-fed EC Cre+; $Fto^{fl/fl}$ +Tmx mice 30 and 45 min after insulin administration and tended to stay improved after 60 and 90 min, respectively ($p=0.08$ and $p=0.06$).

In addition to glucose tolerance, blood glucose levels were measured in unfasted mice and after 5 and 17 h fasting. Interestingly, while unfasted blood glucose levels (Suppl. Fig. 2 A) and blood glucose levels after 5 h (Suppl. Fig. 2 B) were unchanged between both groups, fasted blood glucose levels after 17 h were significantly reduced in HFD-fed EC Cre+; $Fto^{fl/fl}$ +Tmx mice compared to respective Po-injected litters (Fig.18 D).

These data revealed that loss of endothelial *Fto* significantly improved glucose and insulin tolerance as well as fasted glucose levels in HFD-fed mice, although unfasted blood glucose levels were not affected.

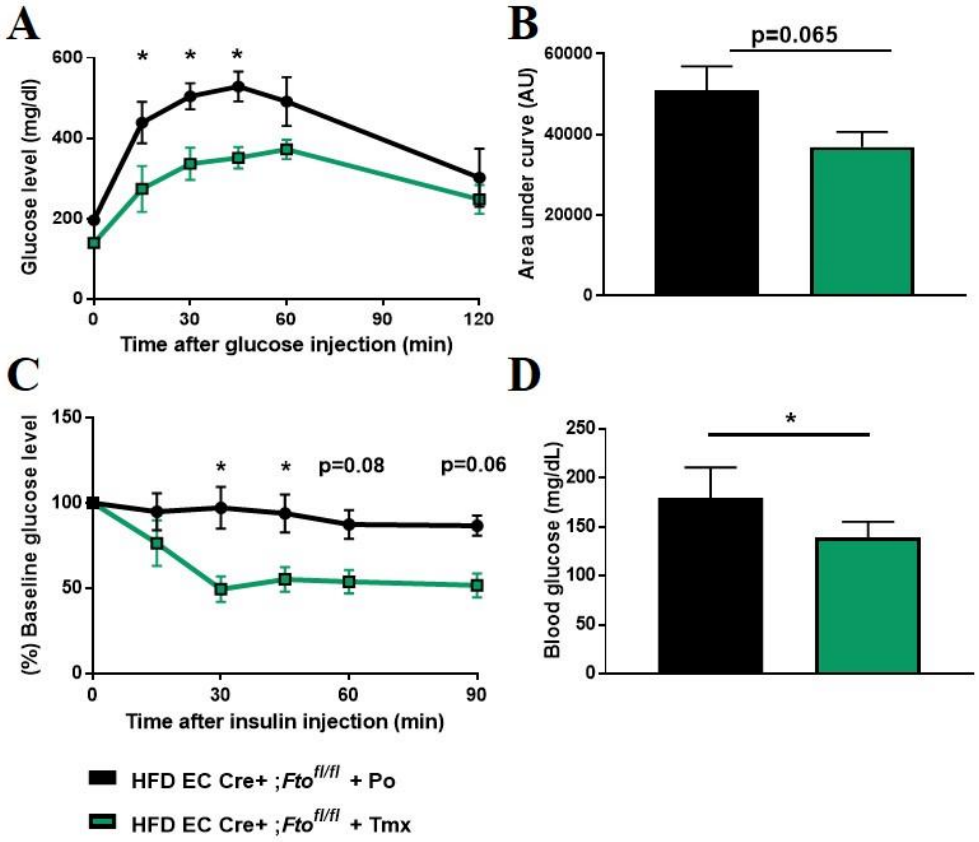

Fig. 18: Analysis of glucose and insulin tolerance in HFD-fed EC Cre+; *Fto*$^{fl/fl}$ +Po and EC Cre+; *Fto*$^{fl/fl}$ +Tmx mice

20-23 week old HFD-fed EC Cre+; *Fto*$^{fl/fl}$ +Po and EC Cre+; *Fto*$^{fl/fl}$ +Tmx male mice were fasted and either challenged with i.p. injected glucose or insulin. (A) After 17 h fasting, glucose was i.p. injected and blood glucose level measured at different time points. Blood glucose level were significantly reduced in EC Cre+; *Fto*$^{fl/fl}$ +Tmx mice (n=6) compared to EC Cre+; *Fto*$^{fl/fl}$ +Po mice (n=4) after 15, 30 and 45 min. (B) Area under curve (AUC) was calculated from performed GTTs and showed a trend to reduced AUC in EC Cre+; *Fto*$^{fl/fl}$ +Tmx mice (n=6) compared to EC Cre+; *Fto*$^{fl/fl}$ +Po mice (n=4) (p=0.065). (C) After fasting, insulin was i.p. injected into HFD-fed EC Cre+; *Fto*$^{fl/fl}$ +Po and EC Cre+; *Fto*$^{fl/fl}$ +Tmx male mice (n=6, 3) and blood glucose levels measured at different time points. Analysis of blood glucose level as percentage of baseline glucose level revealed significantly reduced levels in EC Cre+; *Fto*$^{fl/fl}$ +Tmx mice compared to EC Cre+; *Fto*$^{fl/fl}$ +Po mice after 30 and 45 min and a trend to reduced glucose levels after 60 and 90 min (p=0.08 and 0.06, respectively). (D) Blood glucose levels were measured after 17 h fasting in HFD-fed EC Cre+; *Fto*$^{fl/fl}$ +Po and EC Cre+; *Fto*$^{fl/fl}$ +Tmx mice (n=4, 6). Blood glucose levels were significantly reduced in EC Cre+; *Fto*$^{fl/fl}$ +Tmx mice compared to EC Cre+; *Fto*$^{fl/fl}$ +Po mice.

Data represent mean ± SEM, calculation of area under curve was performed using GraphPad Prism, and statistical analysis were performed using either 2-way RM ANOVA (A and C) or unpaired, two-tailed t-test (B and D); $p<0.05$ was defined as significant.

5.2.4 Measurement of cellular metabolism in human aortic endothelial cells after siRNA-mediated *FTO* knockdown

As loss of endothelial *Fto* in HFD-fed mice protected from HFD-induced changes on myogenic tone and significantly improved glucose and insulin tolerance in HFD-fed mice, analysis should investigate if endothelial Fto affected ROS production and subsequently mitochondrial respiration. To allow analyzing the role of *FTO* in respiration

of endothelial cells, human aortic endothelial cells (HAoECs) were transfected using either *FTO* or scrambled siRNA and seahorse assays were performed.

First, successful downregulation of *FTO* transcript expression was verified using qRT-PCR. In comparison to scrambled siRNA transfected cells, relative transcript expression of *FTO* was significantly downregulated to approx. 10% in *FTO* siRNA-transfected HAoECs (Fig.19 A). Respective *FTO* and scrambled siRNA transfected HAoECs were then used for seahorse assay analysis. This analysis revealed that downregulation of *FTO* in HAoECs did not affect respiration. Neither basal respiration, ATP-dependent respiration, maximal respiration nor non-mitochondrial respiration was significantly different between *FTO* and scrambled siRNA transfected HAoECs (Fig.19 B). These data reveal that endothelial *FTO* did not affect mitochondrial respiration in ECs and is thus unlikely to be the cellular pathway causing EC-specific effects of *Fto* on myogenic tone in HFD-fed mice.

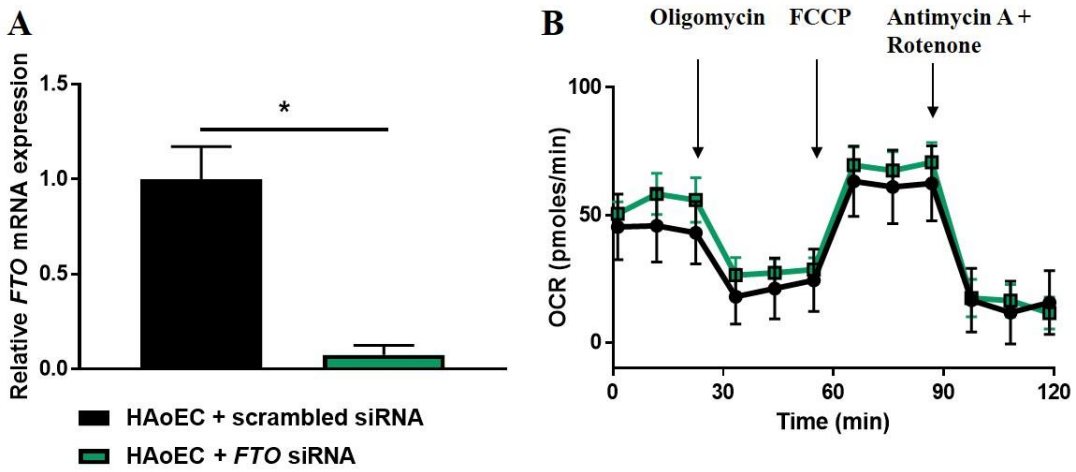

Fig. 19: Analysis of *FTO* knockdown on mitochondrial function in siRNA-transfected HAoECs
HAoECs were either transfected with *FTO* or scrambled siRNA. After 48 h, *FTO* knockdown efficiency was quantified and mitochondrial function assessed by performing seahorse assays. (A) Transcript expression of *FTO* was quantified in *FTO* and scrambled siRNA transfected HAoECs (n=3, 3) by qRT-PCR and normalized to GAPDH transcript expression levels. Delta-delta Ct analysis revealed that relative *FTO* transcript expression was significantly reduced in *FTO* siRNA transfected cells compared to scrambled siRNA transfected cells. (B) Seahorse assay was performed in *FTO* and scrambled siRNA transfected HAoECs (n=4, 4) and oxygen consumption rate (OCR) was measured. Analyses revealed no significant differences in basal respiration. Also, ATP-dependent respiration (inhibited by oligomycin), maximal respiration (induced by FCCP) and non-mitochondrial respiration (Antimycin A + rotenone inhibit mitochondrial-dependent respiration) were not different between *FTO* and scrambled siRNA transfected HAoECs.
Data represent mean ± SEM, for statistical analysis either unpaired, two-tailed t-test (A) or 2-way RM ANOVA (B) was performed; $p<0.05$ was defined as significant.

5.2.5 Influence of Pgd2 levels on myogenic tone in mesenteric arteries of HFD-fed EC Cre+/- *Fto*$^{fl/fl}$ mice

To analyze putative pathways being affected in ECs by *Fto* deficiency in the vasculature, further bioinformatical analysis of microarray data from thoracic aortae of *Fto*$^{+/+}$ and *Fto*$^{-/-}$ mice were performed. Interestingly, the transcript of *Pgds* was shown to be 4.4-fold upregulated in thoracic aortae of *Fto*$^{-/-}$ mice compared to those of *Fto*$^{+/+}$mice (Fig. 20 A). As prostaglandins, such as Pgd2 which is synthesized by Pgds are known to affect myogenic tone, it should be analyzed if altered Pgd2 levels may be causative for increased myogenic tone in mesenteric arteries of HFD-fed EC-specific *Fto* deficient mice.

To allow analysis of vasoactive effects of Pgd2 on myogenic tone, 3rd order mesenteric arteries of HFD-fed mice were isolated and myogenic tone measured after either adding Pgd2 to vessels of EC Cre+; *Fto*$^{fl/fl}$ +Po mice, or AT56, a Pgds inhibitor, to vessels of respective EC Cre+; *Fto*$^{fl/fl}$ +Tmx mice.

Interestingly, in mesenteric arteries of HFD-fed EC Cre+; *Fto*$^{fl/fl}$ +Po mice external supply of 10 µM Pgd2 significantly increased myogenic tone curves in comparison to respective DMSO-treated vessels (Fig. 20 B). While DMSO-treated vessels of HFD-fed EC Cre+; *Fto*$^{fl/fl}$ +Po mice maximally reached myogenic tone of approx. 25- 30% between 80 and 120 mmHg, Pgd2-treated vessels developed myogenic tone up to 38% at 100 mmHg which was comparable to mesenteric arteries of HFD-fed EC Cre+; *Fto*$^{fl/fl}$ +Tmx mice. In line, respective analyses of active and passive curves revealed that in the active curve, relative lumen diameter was significantly reduced between 60 and 100 mmHg in vessels with Pgd2 addition compared to DMSO-treated vessels (Suppl. Fig. 3 A) while relative lumen diameter of passive curves were not altered (Suppl. Fig. 3 C).

In comparison, myogenic tone was measured in mesenteric arteries of HFD-fed EC Cre+; *Fto*$^{fl/fl}$ +Tmx mice after addition of the Pgds inhibitor AT56. These data could reveal that myogenic tone in mesenteric arteries of HFD-fed EC Cre+; *Fto*$^{fl/fl}$ +Tmx mice tended to be decreased after addition of AT56 compared to respective non-treated vessels (Fig. 20 C). While non-treated vessels of EC Cre+; *Fto*$^{fl/fl}$ +Tmx mice developed myogenic tone of approx. 38% and 120 mmHg, myogenic tone was significantly reduced after AT56 addition to approx. 25%. Also at 100 mmHg, a trend to decreased myogenic tone was observed in AT56-treated vessels in comparison to non-treated vessels ($p=0.08$) which was similar to myogenic tone of vessels from HFD-fed EC Cre+; *Fto*$^{fl/fl}$ +Po mice. However, respective analyses of relative lumen diameter of active and passive curves

showed that AT56 only significant affected respective relative lumen diameter at 40 mmHg. In both, the active and passive curves lumen diameter was significantly reduced in AT-56 treated vessels compared to respective non-treated vessels (Suppl. Fig. 3 B and D).

Collectively, these data show that influencing Pgd2 levels or Pgds activity affected myogenic tone. While external addition of Pgd2 could increase myogenic tone curves in mesenteric arteries of HFD- EC Cre+; *Fto*$^{fl/fl}$ +Po mice to myogenic tone curves of vessels from HFD-fed EC Cre+; *Fto*$^{fl/fl}$ +Tmx mice, Pgds inhibition could decrease myogenic tone at higher intraluminal pressure in vessels of HFD-fed EC Cre+; *Fto*$^{fl/fl}$ +Tmx mice. However, Pgds inhibition had less effect on myogenic tone development compared to respective Pgd2 addition.

A

GeneSymbol	p-value	Absolute fold-change ko / wt
Pgds	1,51E-04	4,42 up

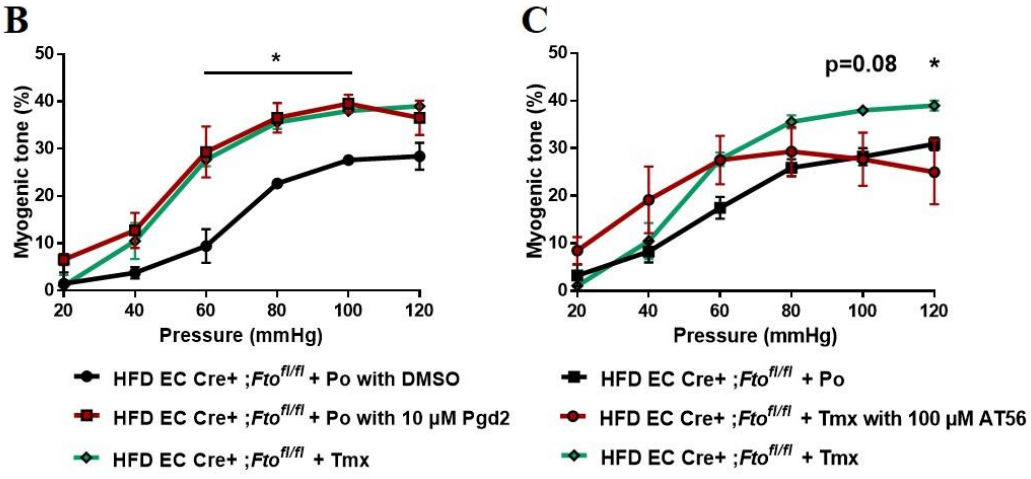

Fig. 20: A putative role of Pgd2 in Fto-dependent effects on myogenic tone in mesenteric arteries
(A) Microarray analysis of thoracic aortae of global *Fto*$^{+/+}$ and *Fto*$^{-/-}$ mice (n=4, 4) were screened for altered expression levels of transcripts which are known to influence myogenic tone. *Pgds* transcript expression was shown to be 4.4-fold upregulated in thoracic aortae of global *Fto*$^{-/-}$ mice compared to *Fto*$^{+/+}$ mice. (B) Myogenic tone was analyzed in 3rd order mesenteric arteries of 20 week old HFD-fed EC Cre+; *Fto*$^{fl/fl}$ +Po mice in the presence of 10 µM Pgd2 (dissolved in DMSO) or DMSO alone. Curves were compared to myogenic tone of mesenteric arteries from HFD-fed EC Cre+; *Fto*$^{fl/fl}$ +Tmx mice (n=3, 3, 3). Myogenic tone was significantly increased between 60 and 100 mmHg in mesenteric arteries of HFD-fed EC Cre+; *Fto*$^{fl/fl}$ +Po mice in the presence of 10 µM Pgd2 compared to mesenteric arteries respective DMSO-treated vessels. Furthermore, myogenic tone in mesenteric arteries of HFD-fed EC Cre+; *Fto*$^{fl/fl}$ +Po mice in the presence of 10 µM Pgd2 was similar to myogenic tone in mesenteric arteries of HFD-fed EC Cre+; *Fto*$^{fl/fl}$ +Tmx mice. (C) Myogenic tone was analyzed in 3rd order mesenteric arteries of 20 week old HFD-fed EC Cre+; *Fto*$^{fl/fl}$ +Tmx mice in the presence of 100 µM AT56, a specific Pgds inhibitor and compared to myogenic tone of mesenteric arteries from HFD-fed EC Cre+; *Fto*$^{fl/fl}$ +Tmx and EC Cre+; *Fto*$^{fl/fl}$ +Po mice (n=3, 3, 6). Data analysis revealed that myogenic tone of HFD-fed EC Cre+; *Fto*$^{fl/fl}$ +Tmx mice in the

presence of 100 µM AT56 was significantly reduced to respective vessels without Pgds inhibition at 120 mmHg and showed a trend to reduced myogenic tone already at 100 mmHg (p=0.08).
Data represent mean ± SEM, for statistical analysis either ordinary 2-way ANOVA (A) or 1-way ANOVA (B) was performed; $p<0.05$ was defined as significant.

5.3 Characterization of SMC Cre+/- ;*Fto*$^{fl/fl}$ mice

To induce SMC-specific depletion of *Fto*, a tamoxifen-inducible SmMHC-CreER^{T2} system was used. For activation of Cre expression, 6 week old SmMHC-CreER^{T2}+ ;*Fto*$^{floxed/floxed}$ mice were injected with Tmx dissolved in Po for 10 days (abbreviated: SMC Cre+ ;*Fto*$^{fl/fl}$ +Tmx). As respective control groups, SmMHC-CreER^{T2}+ ;*Fto*$^{floxed/floxed}$ mice were injected with Po without Tmx (abbreviated: SMC Cre+ ;*Fto*$^{fl/fl}$ +Po) and SmMHC-CreER^{T2}+ ;*Fto*$^{floxed/floxed}$ mice with Tmx dissolved in Po (abbreviated: SMC Cre- ;*Fto*$^{fl/fl}$ +Tmx). For all experiments, mice with an age of 20 weeks were used to get comparable results to VeCadherin-CreER^{T2}+ ;*Fto*$^{floxed/floxed}$ mice (Fig. 21).

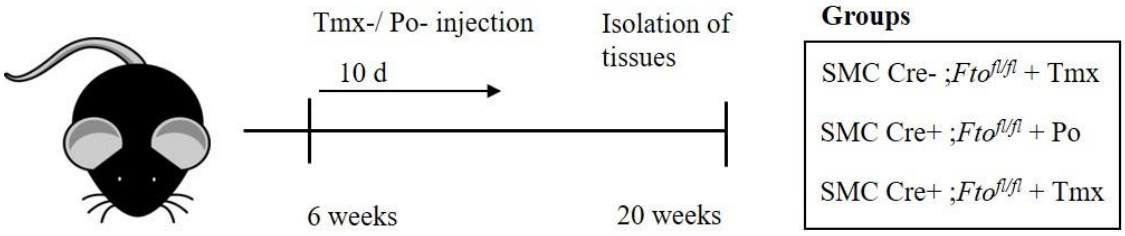

Fig. 21: Overview about experimental groups in SMC Cre+/- ;*Fto*$^{fl/fl}$ mice
6 week old mice were i.p. injected for 10 days with Po or Tmx dissolved in Po. With an age of 20 weeks, mice were sacrificed and tissues isolated. For verifying specificity of effects, three different groups were analyzed: The two control groups SMC Cre- ;*Fto*$^{fl/fl}$ +Tmx and SMC Cre+ ;*Fto*$^{fl/fl}$ +Po and SMC-specific *Fto*-deficient mice (SMC Cre+ ;*Fto*$^{fl/fl}$ +Tmx).

To verify that *Fto* was successfully depleted in SMCs of SMC Cre+ ;*Fto*$^{fl/fl}$ +Tmx mice, mesenteric arteries were isolated from SMC Cre+ ;*Fto*$^{fl/fl}$ +Po and SMC Cre+ ;*Fto*$^{fl/fl}$ +Tmx mice, paraffin embedded, cross-sectioned and fluorescently stained for Fto.
Immunofluorescence analysis revealed Fto expression in adventitia (A), smooth muscle layer (S) and endothelial layer (E) of mesenteric arteries from SMC Cre+ ;*Fto*$^{fl/fl}$ +Po mice (Fig. 22). In comparison, respective Tmx-injected mice showed Fto expression in E and A, but not in respective SMCs. Thus, Fto expression was successfully depleted in SMCs of SMC Cre+ ;*Fto*$^{fl/fl}$ +Tmx mice and allowed analysis of the function of smooth muscle *Fto* expression *in vivo*.

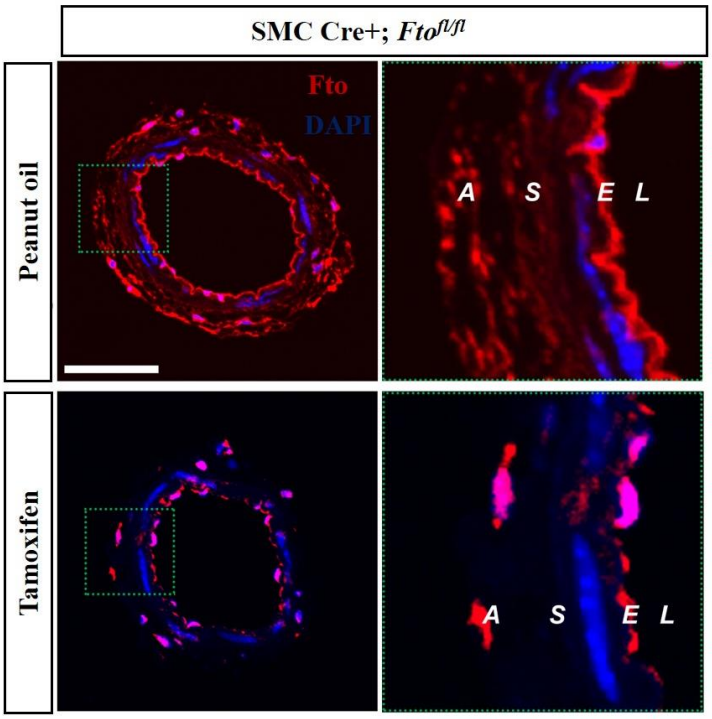

Fig. 22: Immunofluorescence analysis of smooth muscle Fto expression in mesenteric arteries of SMC Cre+ ;*Fto*$^{fl/fl}$ +Po and SMC Cre+ ;*Fto*$^{fl/fl}$ +Tmx mice

3rd order mesenteric arteries were isolated from 20 week old SMC Cre+ ;*Fto*$^{fl/fl}$ +Po and SMC Cre+ ;*Fto*$^{fl/fl}$ +Tmx mice, paraffin-embedded and sectioned. Fto expression was fluorescently analyzed and cell nuclei stained using DAPI. Mesenteric arteries of SMC Cre+ ;*Fto*$^{fl/fl}$ +Po (upper panel) show Fto staining in endothelial cells (E), smooth muscle cells (S) and in the adventitia (A) in both overview (left panel) and close-up (right panel). In comparison, mesenteric arteries of SMC Cre+ ;*Fto*$^{fl/fl}$ +Tmx mice show Fto staining in endothelial cells (E) and the adventitia (A), but not in respective smooth muscle cells (S). Scale bar represents 50 µm.

5.3.1 Phenotypic characterization of SMC Cre+/- ;*Fto*$^{fl/fl}$ mice

As global *Fto*-deficient mice have a reduced body weight, body length and reduced white adipose tissue accumulation, a putative influence of smooth muscle Fto on body weight should be investigated [187].

For analyzing body weight gain, SMC Cre+ ;*Fto*$^{fl/fl}$ +Tmx, SMC Cre+ ;*Fto*$^{fl/fl}$ +Po and SMC Cre- ;*Fto*$^{fl/fl}$ +Tmx mice were weighted once weekly between an age of 7 and 20 weeks to assess body weight gain over time. With an age of 20 weeks, body length was determined in all three groups and after sacrificing the mice, epigonadal fat was removed and weighted.

Analysis of body weight gain revealed no significant differences between the three groups (Fig. 23 A) as all mice gained approx. 40% of initial weight gain during measurement time. Similarly, also mean body weight was similar between 20 week old SMC Cre+ ;*Fto*$^{fl/fl}$ +Tmx, SMC Cre+ ;*Fto*$^{fl/fl}$ +Po and SMC Cre- ;*Fto*$^{fl/fl}$ +Tmx mice with approx. 28 g in mean (Fig. 23 B). Also, mean epigonadal fat weight showed no significant differences

between the analyzed groups with mean values of approx. 0.5 g (Fig. 23 C). Lastly, also analyzed body length revealed no significant differences between the three groups with mean body lengths of approx. 9 cm (Fig. 23 D).

Collectively, these data demonstrate that loss of smooth muscle *Fto* did not affect body weight or fat accumulation as well as body length in mice.

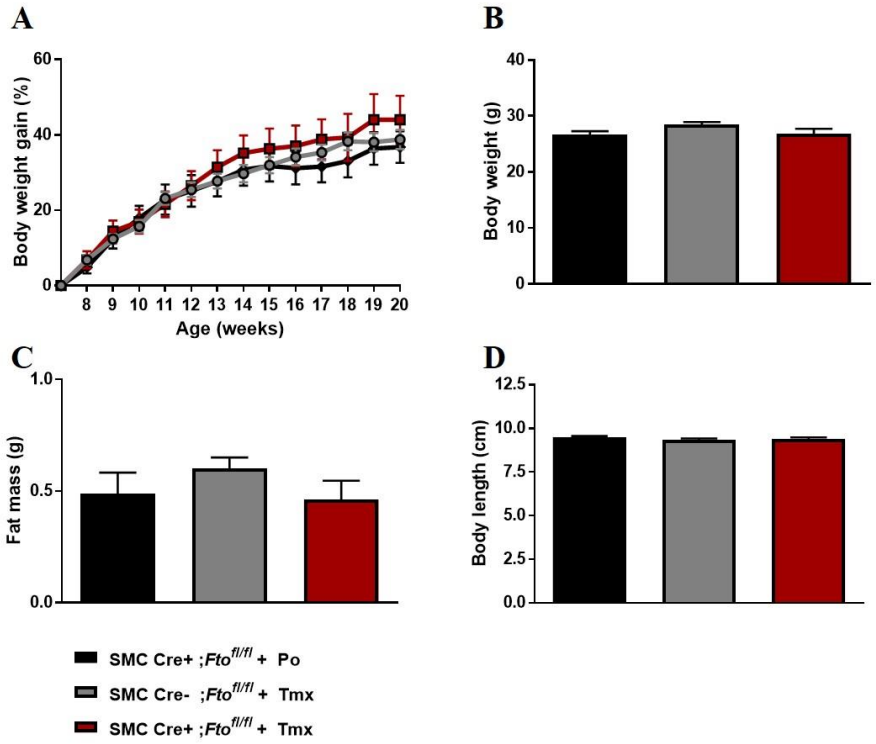

Fig. 23: Phenotypic characterization of SMC Cre+/- ;*Fto*$^{fl/fl}$ mice
SMC Cre+ ;*Fto*$^{fl/fl}$ +Po, SMC Cre- ;*Fto*$^{fl/fl}$ +Tmx and SMC Cre+ ;*Fto*$^{fl/fl}$ +Tmx mice were phenotypically analyzed. (A) Percentage body weight gain was analyzed in all three genotypes between an age of 7 to 20 weeks (n=8, 13, 8) and revealed no differences. In all three groups mice gained approx. 40% of initial body weight. (B) 20 week old SMC Cre+ ;*Fto*$^{fl/fl}$ +Po, SMC Cre- ;*Fto*$^{fl/fl}$ +Tmx and SMC Cre+ ;*Fto*$^{fl/fl}$ +Tmx mice were weighted and body weight determined (n=7, 19, 8). Comparable to (A), mean body weight was similar in all analyzed genotypes. (C) 20 week old SMC Cre+ ;*Fto*$^{fl/fl}$ +Po, SMC Cre- ;*Fto*$^{fl/fl}$ +Tmx and SMC Cre+ ;*Fto*$^{fl/fl}$ +Tmx mice were sacrificed, epigonadal fat isolated and weighted. Also, mean epigonadal fat weight showed no significant differences between all three groups (n=7, 14, 5). (D) Body length was determined in 20 week old SMC Cre+ ;*Fto*$^{fl/fl}$ +Po, SMC Cre- ;*Fto*$^{fl/fl}$ +Tmx and SMC Cre+ ;*Fto*$^{fl/fl}$ +Tmx mice and revealed that SMC-specific *Fto* deficiency did not affect body length (n=7, 19, 8).
Data represent mean ± SEM for statistical analysis one-way ANOVA with Tukey's post-hoc test was performed; $p<0.05$ was defined as significant.

5.3.2 Vasoactive analyses in mesenteric arteries of SMC Cre+/-; *Fto*$^{fl/fl}$ mice

Similar to analysis in endothelial *Fto* deficient mice, a putative role of smooth muscle Fto in regulation of vasoactive properties of mesenteric arteries should be analyzed. Therefore, 3rd order mesenteric arteries were isolated from 20 week old SMC Cre+ ;*Fto*$^{fl/fl}$

+Tmx, SMC Cre+ ;*Fto*$^{fl/fl}$ +Po and SMC Cre- ;*Fto*$^{fl/fl}$ +Tmx mice and used for vasoactive analyses using pressure myography.

5.3.2.1 Myogenic tone analysis

To assess pressure-induced contraction of mesenteric arteries, 3rd order mesenteric arteries were isolated, equilibrated at 80 mmHg until myogenic tone developed and pressure curves performed. Relative lumen diameter was measured at different intraluminal pressures either in presence of Ca^{2+} (active curve) or in the absence of Ca^{2+} (passive curve). With respective lumen diameter values, myogenic tone was calculated for each pressure.

Fig. 24 A shows myogenic tone curves of all analyzed groups. Mesenteric arteries from both control groups (SMC Cre+ ;*Fto*$^{fl/fl}$ +Po and SMC Cre- ;*Fto*$^{fl/fl}$ +Tmx) developed similar myogenic tone with increasing pressure which was significantly impaired in vessels of SMC-specific *Fto* deficient mice between 80 and 120 mmHg. While myogenic tone in both control groups increased from 10% at 40 mmHg up to 35% at 100-120 mmHg, vessels of SMC Cre+ ;*Fto*$^{fl/fl}$ +Tmx mice maintained myogenic tone levels of approx. 10% throughout all pressures. Furthermore, mesenteric arteries of SMC Cre+ ;*Fto*$^{fl/fl}$ +Tmx mice also needed longer time until myogenic tone developed (data not shown).

Respective analysis of relative lumen diameter of active and passive pressure curves revealed that SMC-specific *Fto* deficiency affected respective active and not passive curves (Fig.24 B and C). While relative lumen diameter of active curves from vessels of both control groups decreased with increasing pressure to approx. 80% of initial diameter at 120 mmHg, relative lumen diameter of vessels of SMC Cre+ ;*Fto*$^{fl/fl}$ +Tmx mice did not decrease with increasing pressure resulting in a relative lumen diameter of approx. 100% at 120 mmHg. Thus, in presence of Ca^{2+} relative lumen diameter was significantly increased between 80 and 120 mmHg in mesenteric arteries of SMC Cre+ ;*Fto*$^{fl/fl}$ +Tmx mice. In contrast, relative lumen diameter of passive curves showed no differences between all groups as all vessels had a relative lumen diameter of approx. 110% at 120 mmHg.

In conclusion, SMC-specific *Fto* deficiency significantly impaired development of myogenic tone in mesenteric arteries which was caused by significantly increased relative lumen diameter in the active curve.

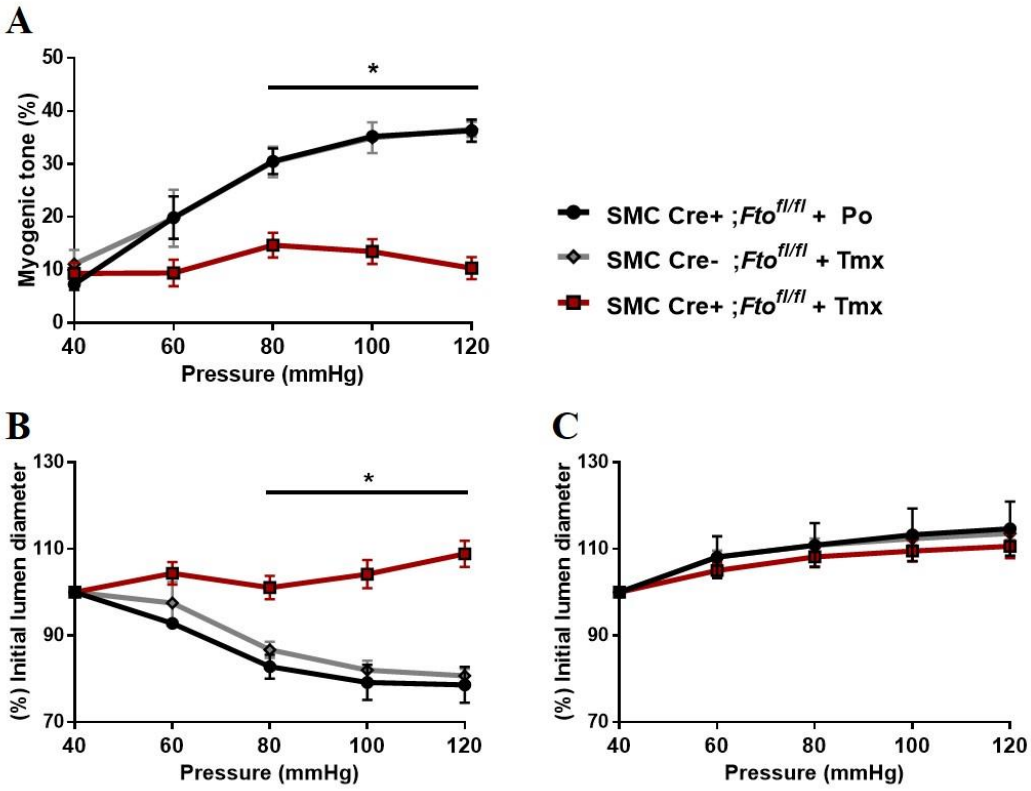

Fig. 24: Myogenic tone analysis in mesenteric arteries of SMC Cre+/- ;*Fto*$^{fl/fl}$ mice
3rd order mesenteric arteries were isolated from 20 week old SMC Cre+ ;*Fto*$^{fl/fl}$ +Po, SMC Cre- ;*Fto*$^{fl/fl}$ +Tmx and SMC Cre+ ;*Fto*$^{fl/fl}$ +Tmx mice and used for pressure myography. After equilibration and tone development, a pressure curve was first performed in presence of Ca^{2+} (active curve) and then without Ca^{2+} (passive curve) and myogenic tone was calculated using respective lumen diameter at each pressure step (n=3, 5, 7). (A) Myogenic tone analysis showed that mesenteric arteries of both control groups (SMC Cre+ ;*Fto*$^{fl/fl}$ +Po, SMC Cre- ;*Fto*$^{fl/fl}$ +Tmx) developed up to 35% myogenic tone at 120 mmHg. In comparison, mesenteric arteries of SMC-specific *Fto* deficient mice developed significantly less myogenic tone between 80 mmHg and 120 mmHg with a mean of approx. 10% myogenic tone at 120 mmHg. (B) Lumen diameter of active curve measurements are plotted in percentage to the initial lumen diameter at 40 mmHg. While in mesenteric arteries of both control groups SMC Cre+ ;*Fto*$^{fl/fl}$ +Po and SMC Cre- ;*Fto*$^{fl/fl}$ +Tmx lumen diameter was decreased at higher pressures, mesenteric arteries of SMC Cre+ ;*Fto*$^{fl/fl}$ +Tmx mice had a significantly increased lumen diameter between 80 mmHg and 120 mmHg. (C) Lumen diameter of passive curve measurements is plotted as percentage of initial lumen diameter (40 mmHg) and showed no significant differences between all three genotypes.
Data represent mean ± SEM, for statistical analysis one-way ANOVA with Tukey's post-hoc test was performed; $p<0.05$ was defined as significant.

5.3.2.2 Agonist-induced vasoactive analysis

As myogenic tone development was significantly impaired in mesenteric arteries of SMC Cre- ;*Fto*$^{fl/fl}$ +Tmx mice, analysis should investigate if only pressure-induced contraction or general contractility was affected by smooth muscle *Fto* deficiency. Therefore, mesenteric arteries of SMC Cre+ ;*Fto*$^{fl/fl}$ +Po, SMC Cre- ;*Fto*$^{fl/fl}$ +Tmx and SMC Cre+ ;*Fto*$^{fl/fl}$ +Tmx mice were isolated, equilibrated at 80 mmHg and contraction to 40 mM KCl assessed which induced non-agonist dependent depolarization of SMCs and

subsequent contraction. To verify that the isolated mesenteric arteries were alive, vasodilation in response to NS309 was measured.

Interestingly, mesenteric arteries of SMC-specific *Fto* deficient mice showed a tendency to decreased KCl-induced contraction, while NS309-dependent vasodilation was not affected. Mesenteric arteries of both control groups (SMC Cre+ ;$Fto^{fl/fl}$ +Po, SMC Cre- ;$Fto^{fl/fl}$ +Tmx) constricted approx. 25% in response to KCl (Fig.25 A). In contrast, mesenteric arteries of SMC Cre+ ;$Fto^{fl/fl}$ +Tmx mice constricted to approx. 8% showing a trend to reduced contraction in comparison to respective control vessels (p=0.08 and p=0.07). Contrary to KCl-induced contraction, NS309 induced approx. 90% vasodilation in mesenteric arteries of all mice revealing that all vessels were alive (Fig.25 B).

Together with the myogenic tone data, these data revealed that SMC-specific *Fto*-deficiency generally impaired SMC contraction in response to both intraluminal pressure and KCl.

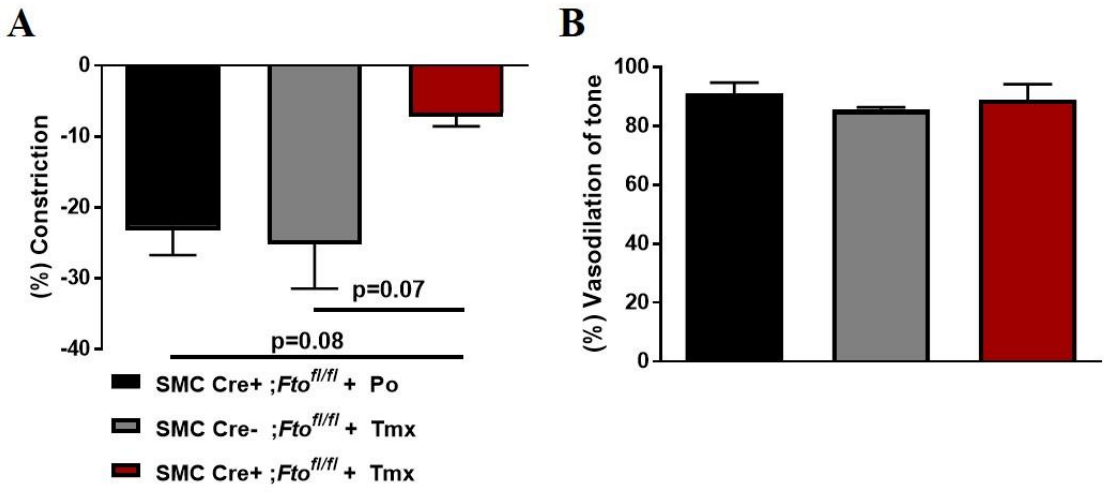

Fig. 25: Analysis of vasoactive properties in mesenteric arteries of SMC Cre+/-;$Fto^{fl/fl}$ mice

3rd order mesenteric arteries were isolated from 20 week old SMC Cre+ ;$Fto^{fl/fl}$ +Po, SMC Cre- ;$Fto^{fl/fl}$ +Tmx and SMC Cre+ ;$Fto^{fl/fl}$ +Tmx mice, equilibrated at 80 mmHg until myogenic tone developed. After myogenic tone plateaued, vasoconstriction in response to 40 mM KCl (A) or vasodilation in response to 1 µM NS309 (B) was assessed (n=4, 3, 3). (A) KCl induced contraction of approx. 25% in mesenteric arteries of both control groups (SMC Cre+ ;$Fto^{fl/fl}$ +Po, SMC Cre- ;$Fto^{fl/fl}$ +Tmx and SMC Cre+ ;$Fto^{fl/fl}$ +Tmx) which tended to be decreased to 8% in mesenteric arteries of SMC Cre+ ;$Fto^{fl/fl}$ +Tmx mice (p=0.08 and 0.07) (B) In comparison, the IK_{Ca} and SK_{Ca} channel activator induced in all three groups mean vasodilation around 90% of tone and showed no significant differences.

Data represent mean ± SEM, for statistical analysis one-way ANOVA with Tukey's post-hoc test was performed; $p<0.05$ was defined as significant.

5.3.3 Measurement of cellular metabolism in human coronary smooth muscle cells after siRNA-mediated *FTO* knockdown

As SMC-specific *Fto* deficiency significantly reduced myogenic tone in mesenteric arteries, further analysis should identify the cellular mechanism. As mitochondria are known to be important in SMC contraction, analysis should reveal if loss of smooth muscle *Fto* may affect mitochondrial function leading to changes in myogenic tone.

To assess if FTO affects mitochondrial function, human coronary smooth muscle cells (HCoSMCs) were used and transfected with either *FTO* or scrambled siRNA. For successful downregulation of *FTO* transcript expression, qRT-PCR was performed comparing relative transcript expression of *FTO* in *FTO* and scrambled siRNA transfected cells. These data revealed that transcript expression of *FTO* was significantly reduced to approx. 30% in *FTO* siRNA-transfected HCoSMCs (Fig.26 A). In turn, *FTO* and scrambled siRNA-transfected HCoSMCs were used for seahorse assays to analyze mitochondrial respiration. However, these data revealed that downregulation of *FTO* did not affect mitochondrial function (Fig. 26 B). Neither basal respiration, ATP-dependent respiration, maximal respiration nor non-mitochondrial respiration were significantly altered by *FTO* knockdown.

These data suggest that SMC-specific *Fto* deficiency affected myogenic tone independent of mitochondrial respiration, as *FTO* knockdown did not influence respiration in HCoSMCs.

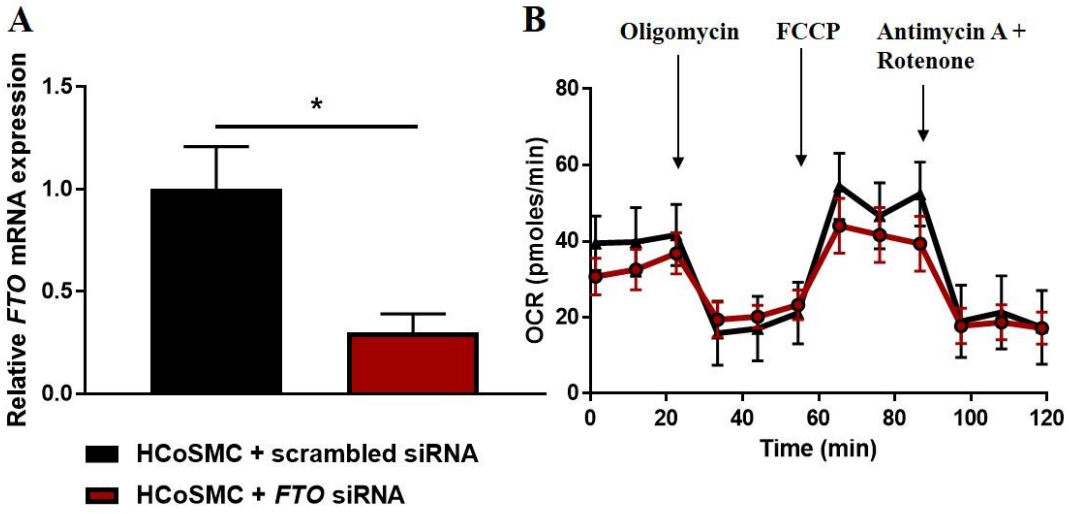

Fig. 26: Analysis of *FTO* knockdown on mitochondrial function in siRNA-transfected HCoSMCs
HCoSMCs were transfected with either *FTO* siRNA or scrambled siRNA. 48 h after transfection, RNA was isolated from cells and *FTO* knockdown efficiency analyzed by comparing *FTO* transcript expression levels to *GAPDH* transcript expression levels using qRT-PCR and the delta-delta Ct method. In parallel, 48 h after transfection, mitochondrial function was assessed in either *FTO* siRNA or scrambled siRNA transfected

cells (n=5, 5). Oxygen consumption rate (OCR) was measured under basal conditions. Also, ATP-dependent respiration (inhibited by oligomycin), maximal respiration (induced by FCCP) and non-mitochondrial respiration (Antimycin A + rotenone) inhibit mitochondrial-dependent respiration) were analyzed. (A) qRT-PCR analysis revealed that *FTO* was significantly downregulated in *FTO* siRNA-transfected cells compared to respective scrambled siRNA-transfected cells (n=3, 3). (B) Seahorse assay revealed that neither basal respiration, ATP-dependent respiration, maximal respiration as well as non-mitochondrial respiration was significantly different between *FTO* cells and respective scrambled siRNA-transfected cells (n=5, 5).
Data represent mean ± SEM, for statistical analysis either unpaired, two-tailed t-test (A) or 2-way RM ANOVA (B) was performed; $p<0.05$ was defined as significant.

5.3.4 Analysis of Fto-dependent effects on cytoskeletal proteins in smooth muscle cells

Loss of smooth muscle *Fto* reduced myogenic tone in mice independent of mitochondrial function. To unravel the cellular mechanism inducing this effect, bioinformatic analyses of microarray data from thoracic aortae of $Fto^{+/+}$ and $Fto^{-/-}$ mice were performed to identify pathways which are affected by *Fto* deficiency. Interestingly, upstream regulator analyses revealed that transcript expression of the transcription factor *Serum response factor* (*Srf*) and 14 downstream targets of Srf were changed in expression in thoracic aortae of $Fto^{-/-}$ mice (Fig. 27 A). As Srf is known to induce a more contractile phenotype in SMCs, we wanted to analyze the cellular localization of different cytoskeletal proteins in *Fto*-deficient SMCs. Therefore, primary SMCs were isolated from thoracic aortae of global $Fto^{+/+}$ and $Fto^{-/-}$ mice, cultivated and the cellular localization of filamentous actin (F-actin) and alpha-smooth muscle actin (α-SMA) analyzed using immunofluorescence. Interestingly, SMCs isolated from *Fto*-wildtypic mice showed filamentous structure of both F-actin and α-SMA staining (Fig. 27 B). SMCs from $Fto^{-/-}$ mice showed also a filamentous, although less intense staining of F-actin. α-SMA staining showed a more perinuclear and less filamentous localization.

Collectively, these data suggest that loss of *Fto* in SMCs affected the cellular localization of α-SMA indicating a putative role of altered *Srf* expression leading to the observed effects on myogenic tone and blood pressure by SMC-specific *Fto* deficiency.

A

Name	Expr. fold change	p-value	Downstream targets affected
Srf	-1.582	$1.56E^{-3}$	14
Ddx17	1.308	$1.43E^{-2}$	2
Cdkn1c	1.704	$4.89E^{-2}$	2

B

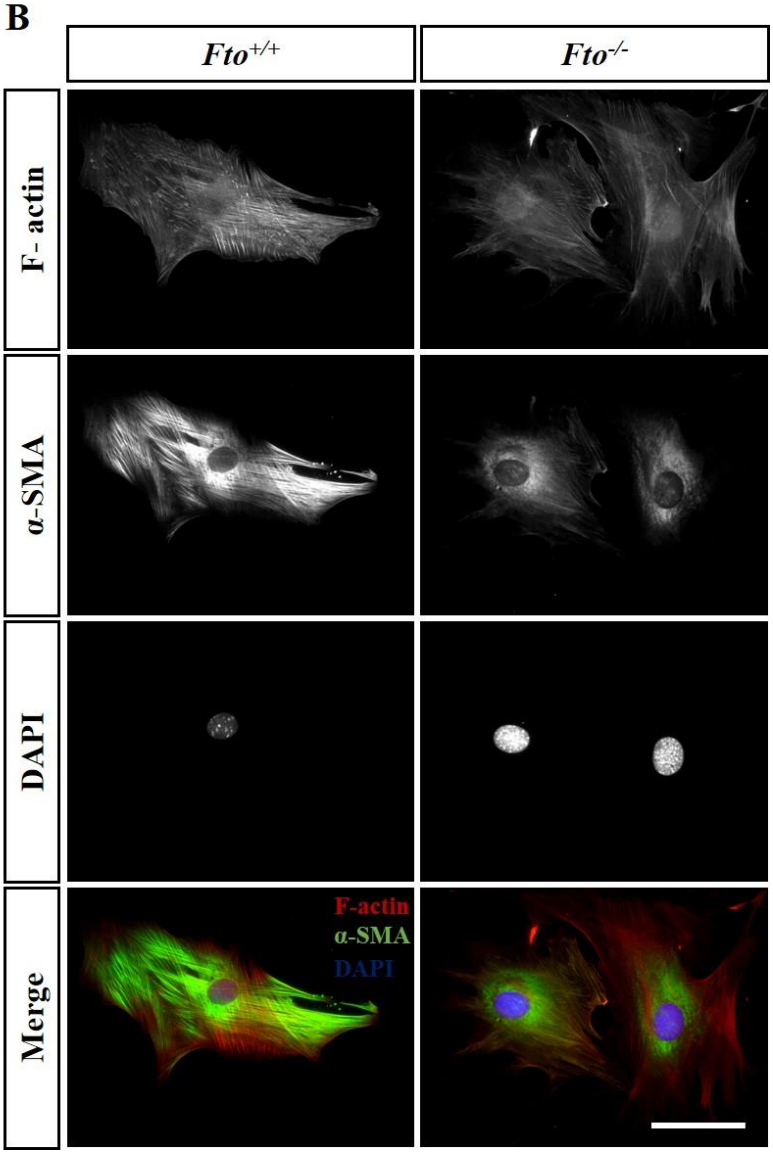

Fig. 27: Analysis of *Fto* dependent effects on cytoskeletal proteins in primary smooth muscle cells
(A) Bioinformatical upstream analysis of microarray data from thoracic aortae of global $Fto^{+/+}$ and $Fto^{-/-}$ mice using Ingenuity Pathway Analysis (IPA) revealed that the transcription factor *Serum response factor* (*Srf*) and 17 of its downstream targets were significantly altered in expression between both genotypes (n=4, 4). *Srf* transcript levels were 1.6-fold downregulated in thoracic aortae of $Fto^{-/-}$ mice. (B) As Srf is known to affect cytoskeletal properties of SMCs, primary smooth muscle cells were derived from thoracic aortae of global $Fto^{+/+}$ and $Fto^{-/-}$ mice (n=3 per genotype, pooled), fixed and stained for filamentous actin, α-SMA and cell nuclei using DAPI. From top to bottom, filamentous actin staining, α-SMA localization, cell nuclei and a merge of all channels are visualized. While SMCs derived from $Fto^{+/+}$ mice (left panel) showed filamentous staining of actin and α-SMA, SMCs derived from $Fto^{-/-}$ mice revealed a less filamentous, but more perinuclear localization of α-SMA. Scale bar represents 100 µm.

6 Discussion

The aim of this project was to analyze whether vascular Fto influences myogenic tone of resistance arteries, as myogenic tone participates in regulation of vascular resistance and blood pressure. A possible role of vascular Fto in regulation of myogenic tone was indicated by microarray data from thoracic aortae of global $Fto^{+/+}$ and $Fto^{-/-}$ mice. As ECs and SMCs have divergent roles in regulation of vascular tone, tamoxifen inducible, cell-type specific *Fto* deficient mice were generated revealing no effect of vascular *Fto* deficiency on body weight. Subsequent analysis of myogenic tone in EC- and SMC-specific *Fto* deficient mice revealed that EC-specific *Fto* deficiency protected from HFD-induced changes on myogenic tone. In contrast, SMC-specific *Fto* deficiency decreased myogenic tone in NC-fed mice. As endothelial *Fto* deficiency protected from HFD-induced changes in myogenic tone and ECs are known to be important in progression of obesity-induced comorbidities, metabolic parameters in HFD-fed mice with and without endothelial *Fto* were analyzed. These data demonstrated that EC-specific *Fto* deficiency significantly amerliorated glucose homeostasis in HFD-fed mice by improving glucose and insulin tolerance while dyslipidemia was not affected.

Collectively, these data reveal that vascular Fto has cell-type specific functions in regulation of myogenic tone. As myogenic tone influences vascular resistance, endothelial and smooth muscle *Fto* may be important in regulation of blood pressure. Furthermore, endothelial *Fto* deficiency significantly improved glucose homeostasis in HFD-fed mice suggesting that endothelial Fto may be important in the development of obesity-induced metabolic comorbidities.

6.1 Vascular Fto in regulation of body weight

As global $Fto^{-/-}$ mice have reduced body weight, body length and epigonadal fat weight, these parameters were measured in EC- and SMC-specific *Fto* deficient mice [187]. Although SMCs are not known to influence body weight, ECs have been shown to affect body weight and to increase adipose tissue in murine models of obesity by regulating neovascularization [253]. However, in contrast to global *Fto* deficiency, vascular cell-type specific *Fto* deficiency did not affect any of the analyzed parameters (Fig. 13 and Fig. 23). Thus, it can be concluded that *Fto* exerts its effects on body weight independently from its expression in ECs and SMCs.

Previous studies showed that neuron-specific *Fto* deficiency reduces body weight in mice suggesting that Fto exerts its effect on obesity at least partially by neuronal regulation [223]. However, neuron-specific *Fto* deficiency did contribute to reduced body weight by reducing rather lean mass than epigonadal fat mass [252]. This phenotype is in contrast to mice with global *Fto* deficiency which were characterized by a significantly reduced fat mass accumulation [187]. These data suggest that Fto is affecting body weight not only by its expression in neurons, but by a cooperative effect of different cell types. However it remains unknown, which other cell types contribute to a reduced body mass in global $Fto^{-/-}$ mice, but it seems to be independent of its expression in ECs and SMCs.

6.2 Vascular Fto in regulation of myogenic tone

As human GWAS reveal a correlation of genetic variations of *FTO* with hypertension and aortic rings of $Fto^{-/-}$ mice show impaired ACh-induced vasodilation, we hypothesized that vascular Fto affects myogenic tone in resistance arteries to influence blood pressure (Stefanie Seehaus, unpublished data) [12, 230]. Therefore, myogenic tone was measured in mesenteric arteries of EC- and SMC- specific *Fto* deficient mice. Furthermore, as ECs are known to be important in obesity-induced hypertension, myogenic tone was also investigated in EC-specific *Fto* deficient HFD-fed mice.

6.2.1 Endothelial Fto in regulation of myogenic tone

Interestingly, we could reveal that EC-specific *Fto* deficiency did not influence myogenic tone in mesenteric arteries of NC-fed mice, but protected from HFD-induced decrease of myogenic tone (Fig. 14 A). The HFD-induced decrease of myogenic tone was caused by reduced pressure-induced constriction, as vessel stiffness was not influenced (Fig. 14 B, C). As depolarization-induced contraction was not impaired, HFD specifically impaired myogenic tone by decreased pressure-induced contractility, which was absent if endothelial *Fto* was not expressed (Fig. 14 B, C and Fig. 15 C).

Although no other study has investigated the role of Fto in regulation of myogenic tone, different studies analyzed the influence of obesity on myogenic tone in resistance arteries with divergent results. Sweazea et al. reported decreased myogenic tone caused by impaired SMC contraction in mesenteric arteries isolated from rats after six weeks of HFD [180]. Similarly, Ogalla et al. reported decreased myogenic tone in mesenteric arteries after 20 weeks of HFD [254]. In contrast, Sauve et al reported unaltered myogenic tone in mesenteric arteries of HFD-fed mice [255]. Other studies measured myogenic

tone in resistance vessels of diabetic rats which mainly showed increased myogenic tone, although this was induced by different mechanisms. While some studies suggested that obesity-induced increase in myogenic tone was caused by augmented pressure-induced contraction, others proposed that obesity-induced alterations in vessel stiffness affected myogenic tone. For example, Frisbee et al. showed in obese zucker rats, a genetic mouse model of type II diabetes, increased myogenic tone by augmented pressure-induced contraction [256]. Also, Osmond et al. reported increased myogenic tone in resistance arteries of obese zucker rats, but caused by increased vascular stiffness [257].

As obesity itself is a heterogenous disease, it is possible that metabolic differences *in vivo* such as free fatty acid levels or adiponectin levels differently affect resistance arteries leading to the heterogenous results of myogenic tone [139, 143]. Furthermore, glucose levels are known to influence vascular tone which were not analyzed in every study [181]. Independent of metabolic variations, genetic differences between the models of obesity may have affected the results. These data emphasize the complexity of obesity-induced effects on vascular tone. Further studies specifically focusing on the influence of different metabolic parameters on vascular tone would help to better understand obesity-induced effects on myogenic tone and endothelial dysfunction.

6.2.2 Smooth muscle Fto in regulation of myogenic tone

Similar to EC-specific *Fto* deficiency, SMC-specific *Fto* deficiency also decreased myogenic tone development by impairing pressure-induced and depolarization-induced contraction in mesenteric arteries (Fig. 24 A, B and Fig. 25 A).

That SMC-specific gene inactivation can influence SMC-contractility and myogenic tone has been shown before. Similar to SMC-specific *Fto* deficiency, also SMC-specific deletion of the *mineralocorticoide receptor* or the *Serum response factor* (*Srf*) were shown to significantly impair SMC contractility and the development of myogenic tone in resistance arteries [258]. These effects were primarily caused by impairment of cellular pathways such as MLCK or cytoskeletal proteins, which are important in both pressure- and depolarization-induced contraction [22]. These data reveal the importance of proper cellular signaling within SMCs to allow myogenic tone development.

6.3 Endothelial Fto in regulation of obesity-induced metabolic comorbidities

Endothelial dysfunction is known to occur early in the development of obesity-induced metabolic comorbidities [126]. However, its role in the progress of hyperglycemia, insulin resistance and dyslipidemia is not well understood. As global *Fto* deficiency has been shown to improve glucose homeostasis, analyses were performed to investigate whether EC-specific *Fto* deficiency may alter glucose homeostasis or dyslipidemia in HFD-fed mice. Interestingly, EC-specific *Fto* deficiency significantly improved both glucose and insulin tolerance in HFD-fed mice, while serum lipid levels were unaltered (Fig. 17 and 18). Also, fasting glucose levels were significantly reduced in HFD-fed EC-specific *Fto* deficient mice (Fig. 18). These data suggest that the loss of endothelial *Fto* specifically improved glucose homeostasis without influencing serum lipids and revealed that altered cellular signaling in ECs can significantly improve the outcome of obesity-induced metabolic changes.

The importance of ECs in glucose homeostasis has been shown previously. Kanda et al. could show that the endothelial-specific loss of the transcription factor *Ppar-γ* significantly improved glucose and insulin tolerance in HFD-fed mice [259]. Kubota et al. revealed that impaired insulin-signaling within ECs decreased glucose uptake in the skeletal muscle. In detail, a decreased expression of the insulin receptor substrate 2 (Irs2) and decreased insulin-dependent activation of eNOS in ECs reduced insulin-mediated glucose uptake in the skeletal muscle by affecting capillary recruitment [133]. Interestingly, although we have not investigated eNOS phosphorylation or Irs2 expression in ECs of EC-specific *Fto* deficient mice, microarray analysis of thoracic aortae point to a role of vascular Fto in insulin signaling (Tab. 19). Though this hypothesis has to be verified, it would explain how endothelial Fto may exert its effect on glucose and insulin tolerance.

Interestingly, in contrast to EC-specific loss of *Fto*, global *Fto* deficiency in *Lep* $^{ob/ob}$ mice improved glucose tolerance without affecting insulin resistance [229]. As leptin and insulin share some intracellular signaling cascades, leptin-resistance in *Lep* $^{ob/ob}$ mice may affect these signaling cascades. In detail, leptin-dependent activation of the leptin-receptor has been shown to decrease insulin-mediated phosphorylation of Irs2 [260]. Furthermore, leptin and insulin can both induce phosphorylation of eNOS which is known to be important in EC-dependent development of insulin resistance in skeletal muscle in

conjunction with Irs2 [133, 261]. Therefore, a putative crosstalk between leptin and insulin signaling may explain the difference in insulin resistance between both mouse models. Further analysis in HFD-fed global *Fto* deficient mice as well as analysis of Irs2 expression levels and eNOS phosphorylation in ECs of all mouse models would allow conclusions about the role of Fto in glucose homeostasis. In addition, comparing glucose and insulin tolerance between HFD-fed global and EC-specific *Fto* deficient mice would allow to specifically analyze the role of endothelial Fto in this process.

In conclusion, these data verify that ECs are important in regulation of glucose homeostasis and revealed that endothelial Fto is important in regulation of glucose metabolism. Furthermore, these data demonstrate that Fto can exert effects on obesity-induced comorbidities independently from its role in body weight regulation.

6.4 Vascular Fto in regulation of blood pressure

6.4.1 Endothelial Fto in regulation of blood pressure

EC-specific *Fto* deficiency protected from HFD-induced changes on myogenic tone and as alterations on myogenic tone are known to influence blood pressure, we hypothesized that EC-specific *Fto* deficiency influenced blood pressure in HFD-fed mice. Therefore, blood pressure was measured in HFD-fed mice with and without endothelial *Fto* in collaboration with B. Isakson (University of Virginia, USA). These data revealed that HFD-fed EC specific *Fto* deficient mice had a significantly reduced MAP and heart rate (Suppl. Fig. 4).

Usually, increased myogenic tone and thus augmented vascular resistance induce a subsequent increase of blood pressure. However, HFD-fed EC specific *Fto* deficient mice had significantly increased myogenic tone compared to HFD-fed control mice while blood pressure was significantly reduced (Fig. 14 and Suppl. Fig. 4). A putative explanation would be that myogenic tone was measured *ex vivo*. Thus, it is possible that *in vivo* vascular tone was influenced by external factors leading to a higher vascular tone in mesenteric arteries of HFD-fed control mice compared to EC-specific *Fto* deficient mice.

As obesity is known to influence levels of adipokines, blood glucose and insulin, it is possible that loss of endothelial *Fto* deficiency either 1) altered the vasoactive response to the respective factor or 2) the respective factor was influenced in its expression level

[126, 162, 262]. Indeed, HFD-fed EC-specific *Fto* deficient mice had improved glucose and insulin tolerance (Fig. 18) implying that mesenteric arteries of HFD-fed EC-specific *Fto* deficient mice may be still insulin sensitive. Thus, it is possible that mesenteric arteries of HFD-fed EC-specific *Fto* deficient mice still show insulin-dependent vasodilation, while the response is impaired in mesenteric arteries of HFD-fed control mice. This would increase vascular tone in mesenteric arteries of HFD-control mice *in vivo*. Furthermore, altered blood glucose levels are known to influence vascular tone. As HFD-fed EC-specific *Fto* deficient mice had significantly reduced fasting blood glucose levels, this could also influence vascular tone *in vivo* (Fig. 18 D).

Independent of its metabolic effects, obesity is known to increase sympathetic nerve activity [153]. Therefore, a putative explanation could be that HFD induced a decrease of pressure-induced myogenic tone as a control mechanism to compensate for increased sympathetic tone. Similarly, myogenic tone was decreased in mesenteric arteries of hypertensive rats after a high sodium diet, although high sodium diet is known to increase blood pressure [263]. Furthermore, it is possible that EC-specific *Fto* deficiency affected the vasoactive response to NE. Interestingly, global *Fto* deficient mice were shown to have altered serum NE and E levels pointing to either 1) altered sympathetic nerve activity or 2) vasoactive response to these factors [187]. Therefore, it is possible that EC-specific *Fto* deficiency impaired the vasoactive response to NE and myogenic tone was not decreased as a control mechanism to obesity-induced increases of sympathetic nerve activity. Thus, it would be interesting to perform vasoactive analyses in mesenteric arteries in response to NE, E, insulin or glucose in mesenteric arteries of HFD-fed mice with and without *Fto*. Furthermore, measurement of serum NE and E levels in HFD-fed EC-specific *Fto* deficient mice could help to understand the cellular mechanism of this paradox phenomenon.

In conclusion, independent of the unknown mechanism being responsible for the invers correlation of myogenic tone and blood pressure, EC-specific *Fto* deficiency has been shown to significantly reduce blood pressure in HFD-fed mice. Further blood pressure measurement in respective NC-fed mice would allow to conclude if endothelial *Fto* only affected blood pressure in HFD-fed mice or if EC-specific *Fto* deficiency also influences blood pressure in NC-fed mice. Furthermore, these data would allow to specifically analyze if HFD-fed mice are hypertensive in comparison to respective NC-fed mice and if EC-specific *Fto* deficiency protects from HFD-induced changes of blood pressure.

In addition to changes in blood pressure, HFD-fed EC specific *Fto* deficient mice had a significantly reduced heart rate (Suppl. Fig. 4 D). Interestingly, EC-derived factors have been shown before to not only influence vascular tone, but also the heart rate. Endothelial dysfunction and subsequent altered release of EC-derived factors have been shown to affect baroreceptor sensitivity which influences their function in regulation of the heart rate [264]. Therefore, it is possible that EC-specific *Fto* deficiency affected EC-derived factors and subsequently led to a decreased heart rate. However, further analysis of serum levels of different EC-factors, especially prostaglandins, in HFD-fed mice with and without *Fto* would help to unravel the cellular mechanism of this effect.

Interestingly, a similar effect of a gene inactivation in ECs has been reported for *Ppar-γ,* as EC- specific *Ppar-γ* deficiency has been shown to increase blood pressure and heart rate in mice [265]. Thus, a putative explanation would be that loss of endothelial *Fto* not only affected myogenic tone, but also heart rate by an altered release of EC-derived factors in HFD-fed mice. However, further analysis would be necessary to identify these factors.

6.4.2 Smooth muscle Fto in regulation of blood pressure

As SMC-specific *Fto* deficient mice had a decreased myogenic tone in mesenteric arteries (Fig. 24 A), we hypothesized that vascular resistance was decreased and caused a reduction of blood pressure. Therefore, blood pressure was measured in collaboration with B. Isakson (University of Virginia) and revealed that SMC-specific *Fto* deficient mice had a significantly reduced MAP, systolic and diastolic blood pressure while the heart rate was unaltered (Suppl. Fig. 5). These data support our hypothesis that SMC-specific *Fto* deficiency decreased vascular resistance which in turn reduced blood pressure. A positive correlation of reduced myogenic tone and blood pressure is supported by Pouseuille's law stating that small changes in the lumen diameter of resistance arteries can influence blood pressure.

Collectively, these data show that vascular Fto influenced myogenic tone cell-type specifically and also respective blood pressure *in vivo*. Furthermore, while EC-specific *Fto* deficiency has been shown to reduce blood pressure in HFD-fed mice, SMC-specific *Fto* deficiency decreased blood pressure in NC-fed mice. Thus, these data demonstrate a functional role of vascular Fto in regulation of blood pressure, which is most likely induced by changes in pressure-induced myogenic tone. Until now, different GWAS could only identify a correlation of genetic variations within the *FTO* locus with blood

pressure, but no causative effect. Furthermore, GWAS were inconsistent regarding the effect of BMI on the correlation of genetic variations of *FTO* with hypertension. While a meta-analysis reported that genetic variations within *FTO* were associated with obesity-dependent hypertension in humans [237], other GWAS showed a correlation with hypertension independent of the BMI [230, 231]. Thus, the blood pressure data of EC- and SMC-specific *Fto* deficient mice support the hypothesis that *Fto* influences blood pressure in both obese and non-obese subjects.

6.5 Cellular effects of Fto in the vascular system

Fto is a m6A-specific RNA demethylase, which is assumed to be important for mediating the cellular effects of Fto [192]. Interestingly, microarray analysis of thoracic aortae of global $Fto^{+/+}$ and $Fto^{-/-}$ mice revealed that 1997 transcripts were altered in expression which is possibly caused by increased m6A-levels by *Fto* deficiency. However, verification of transcript expression levels via qRT-PCR as well as MeRIP-sequencing would be necessary to verify that vascular Fto mediate its effects on cellular processes by influencing m6A-levels. Interestingly, although microarray data were not verified by q-RT PCR, bioinformatical analysis pointed to a role of Fto in vascular smooth muscle cell contraction and insulin signaling (Tab. 19). Both processes could be revealed to be affected by *Fto* deficiency in later experiments, as we could show that vascular Fto was important in pressure-induced contraction (Fig. 14 and 24) and glucose homeostasis (Fig. 19). Therefore, further analysis of other bioinformatically identified pathway may reveal additional functions of vascular Fto.

6.5.1 Endothelial Fto in HFD-induced endothelial dysfunction and vascular tone

Different cellular pathways in resistance vessels are known to be affected in HFD-fed mice leading to subsequent effects on vascular tone. The most prominent vascular damage caused by HFD is endothelial dysfunction which is characterized by an imbalance of endothelial vasodilators and vasoconstrictors [126]. One hallmark of endothelial dysfunction is reduced NO-bioavailability which leads to significantly decreased ACh-induced vasodilation in resistance arteries in obese mouse models [126]. Interestingly, EC-specific *Fto* deficiency did not improve NO-bioavailability, as ACh-induced vasodilation was similar between mesenteric arteries of all HFD-fed mice (Fig. 16). In line, also a seahorse assay could not reveal differences in mitochondrial respiration

suggesting that *Fto* did not affect ROS production and subsequently NO bioavailability (Fig. 19). In addition to reduced NO-bioavailability, also altered EDH-mediated vasodilation has been described in mesenteric arteries of HFD-fed mice. Climent et al. reported an increased expression of IK_{Ca} and SK_{Ca} channels in obese zucker rats and hypothesized that this was induced to compensate for reduced NO bioavailability in early obesity [266]. Concurrent with this finding, they could show that in obese zucker rats EDH gained importance in ACh-mediated vasodilation and that NS309-induced vasodilation was significantly increased compared to vessels of lean rats [266]. In contrast, Haddock et al. revealed that endothelial IK_{Ca} and K_{ir} channel expression was decreased in mesenteric arteries of HFD-fed mice implying a reduced EDH-mediated vasodilation and supporting the heterogenous nature of endothelial dysfunction [267]. Despite differentially reported effects of obesity on EDH, we investigated IK_{Ca}, SK_{Ca} and K_{ir} channel function by measuring the vasoactive response to NS309 and Ba^{2+}. However, neither *Fto* deficiency nor HFD did influence NS309-dependent vasodilation or Ba^{2+}-induced constriction in mesenteric arteries (Fig. 15 A and B). Although the contribution of EDH to ACh-induced vasodilation was not assessed, these data suggest that EDH-mediated signaling was not affected between mesenteric arteries of NC-fed and HFD-fed mice. In conclusion, loss of endothelial *Fto* did not mediate its effect on myogenic tone by affecting NO- or EDH-mediated vasodilation.

Similar to NO and EDH, prostaglandins are also known to be altered in endothelial dysfunction [176]. Interestingly, microarray analysis revealed that the transcript of one prostaglandin synthase, *Pgds,* was upregulated in thoracic aortae of global $Fto^{-/-}$ mice (Fig. 20 A). Although the influence of Pgd2 on pressure-induced myogenic tone was not analyzed before, previous studies investigated the influence of Pgd2 injection on blood pressure. In anaesthetized cats, infusion of Pgd2 decreased blood pressure and heart rate, while increasing carotid blood flow [268]. Similarly, Town et al. were able to show that intravenous injection of BW 245 C, a selective agonist of the DP1 receptor, significantly lowered systolic and diastolic blood pressure in spontaneously hypertensive rats [269]. These data suggest that Pgd2 may influence pressure-induced myogenic tone in resistance arteries by activating DP1 receptors on SMCs leading to a subsequent decrease in blood pressure.

To analyze if altered Pgd2 levels may be responsible for increased myogenic tone in mesenteric arteries of HFD-fed EC-specific *Fto* deficient mice, myogenic tone was measured after addition of Pgd2 or an inhibitor of its respective synthase (Fig. 20 B and

C). Strikingly, exogenously added Pgd2 could increase myogenic tone of mesenteric arteries from HFD-fed control mice to comparable levels of mesenteric arteries from HFD-fed EC-specific *Fto* deficient mice (Fig. 20 B). Vice versa, inhibition of Pgds in mesenteric arteries of HFD-fed EC-specific *Fto* deficient mice could decrease myogenic tone, although this effect was less pronounced (Fig. 20 C). Interestingly, these data reveal that altered levels of Pgd2 affect pressure-induced myogenic tone in mesenteric arteries of HFD-fed mice. Although the Pgd2-induced increase in myogenic tone in mesenteric arteries of HFD-fed control mice exactly correlated with myogenic tone in mesenteric arteries of respective EC-specific *Fto* deficient mice, it did not prove a causative effect. Comparative analysis of Pgd2 levels in lysates of mesenteric arteries of NC-fed and HFD-fed mice with and without *Fto* would allow to conclude whether Fto affected Pgd2 expression levels and if HFD may influence Pgd2 levels. As *Pgds* expression has been shown to be decreased in thoracic aortae of spontaneously hypertensive rats, it is possible that *Fto* deficiency increases *Pgds* expression which could rescue HFD-induced decreased Pgd2 levels and subsequent decreases in myogenic tone [270]. Furthermore, Pgd2 injection into NC-fed and HFD-fed mice with and without *Fto* and respective analysis of blood pressure would allow to unravel the influence of Fto on Pgd2-induced effects on myogenic tone and blood pressure *in vivo*.

Interestingly, independent from its function in blood pressure, Pgds is also known to be important in glucose homeostasis, as *Pgds*-deficient mice have significantly impaired glucose and insulin tolerance [271]. As Pgd2 is known to be spontaneously converted to the Pgj2 series of prostaglandins which are activators of Ppar-γ in ECs, it is possible that Fto influences glucose homeostasis by affecting Ppar-γ activity [259, 272]. Therefore, it would be interesting to analyze if EC-specific *Fto* deficiency influences glucose homeostasis by affecting Pgd2 levels and subsequently Ppar-γ activation. That Fto can influence Ppar-γ expression was shown in $Lep^{ob/ob}$ mice, as global *Fto* deficiency rescued obesity-induced transcriptional decrease of *Ppar-γ* in adipose tissue [229]. However, further analysis of expression levels of Ppar-γ, Pgd2 and Pgj2 in mesenteric arteries of NC-fed and HFD-fed mice with and without endothelial *Fto* would be necessary to analyze this hypothesis.

6.5.2 Smooth muscle Fto in regulation of vascular tone

As pressure-induced and depolarization-induced contraction were significantly impaired in mesenteric arteries of SMC-specific *Fto* deficient mice (Fig. 24 B and 25 A), we

analyzed different factors which are known to influence general SMC contraction. Mitochondrial function has been shown to influence both pressure- and depolarization-induced contraction of resistance arteries, so we investigated if smooth muscle *Fto* influences mitochondrial respiration [273]. However, an effect of *FTO* on mitochondria function could not be revealed (Fig. 26). To identify other factors which could influence SMC contraction, we performed bioinformatical analysis of microarray data from thoracic aortae of $Fto^{+/+}$ and $Fto^{-/-}$ mice and could identify that the transcription factor *Srf* and 14 of its regulated transcripts were altered in expression (Fig. 27 A). As smooth muscle-specific *Srf* deficiency is known to reduce pressure-induced myogenic tone and KCl-induced constriction by affecting cytoskeletal properties, it is possible that SMC-specific effects of *Fto* on myogenic tone are mediated by Srf [22, 252]. Because Srf is a regulator of different cytoskeletal proteins, we investigated *Fto*-dependent effects on cytoskeletal properties in murine SMCs and could show that *Fto*-deficiency induced a more perinuclear and less filamentous localization of α-SMA. As *Srf* is known to regulate α-SMA expression and stress fibers containing α-SMA are known to generate a greater contractile force, it is possible that Fto regulates *Srf* expression which affects α-SMA localization and in turn myogenic tone [274, 275]. Although *Srf* transcript expression was only 1.6-fold downregulated in microarray analysis, *Srf* transcript expression was also decreased to only 50% in vessels of SMC-specific *Srf* deficient mice suggesting that already slight changes in *Srf* expression level can affect myogenic tone (Fig. 27 A) [252]. However, to verify that smooth muscle Fto regulated *Srf* transcript expression, it would be necessary to analyze *Srf* transcript expression in isolated SMCs with and without *Fto*. Furthermore, as Fto is known to be a RNA demethylase, it would be interesting to analyze if *Srf* is m6A-methylated in SMCs and if this is affected by *Fto*-deficiency. That *Srf* can be m6A-methylated has been shown for human U2OS and HepG2 cells, but a putative role of *Fto* in Srf-dependent demethylation was not yet investigated [199, 216]. Furthermore, m6A methylation has been shown to have tissue-specific differences. Therefore, it would be important to analyze m6A-methylation of *Srf* in SMCs with and without *Fto*. Interestingly, Fto was shown to regulate another transcription factor by m6A methylation. In adipose tissue, *Fto* deficiency increased m6A methylation of the transcription factor Runx1 which was shown to influence adipogenesis [276]. Similarly, Srf is known to regulate a contractile phenotype of SMCs so it is possible that Fto influences myogenic tone and contractility by influencing *Srf* m6A methylation [20]. However, further analysis would be necessary to verify this hypothesis.

6.6 Conclusion

The data reveal that vascular Fto has cell type-specific functions in regulation of myogenic tone in resistance arteries. Its biological importance was underlined by respective blood pressure measurements which verified a significant effect of EC- or SMC-specific *Fto* deficiency on blood pressure. Furthermore, loss of endothelial *Fto* significantly improved glucose homeostasis in HFD-fed mice.

While EC-specific *Fto* deficiency did not affect myogenic tone in mesenteric arteries of NC-fed mice, it protected vessels from HFD-induced changes on myogenic tone. Further analysis in HFD-fed mice showed that EC-specific *Fto* deficiency significantly decreased blood pressure and improved glucose tolerance as well as insulin sensitivity. Thus, the data suggest that loss of endothelial *Fto* might be of importance in the development of obesity-induced comorbidities such as hypertension, insulin resistance and hyperglycemia. Although the underlying cellular mechanisms remain unknown, EC-specific *Fto* deficiency induced its effect on myogenic tone independent of NO- or EDH-mediated vasodilation. Presumably, increased Pgd2 levels might be important in the protective effect of EC-specific *Fto* deficiency as higher Pgd2 levels significantly increased myogenic tone in mesenteric arteries of HFD-fed control mice to levels of vessels of HFD-fed EC-specific *Fto* deficient mice. However, to verify this hypothesis, further studies are necessary to confirm that Fto regulates *Pgds* expression e.g. by analyzing transcript expression of *Pgds* in ECs of mesenteric arteries of NC-fed and HFD-fed mice with and without endothelial *Fto*.

In contrast, SMC-specific *Fto* deficiency was shown to significantly decrease pressure-induced myogenic tone and depolarization-induced constriction in mesenteric arteries of NC-fed mice. SMC-specific *Fto* deficient mice had a significantly decreased blood pressure supporting the biological importance. Similar to EC-specific *Fto* deficiency, the cellular mechanism of SMC-specific *Fto* deficiency on myogenic tone and blood pressure have to be further analyzed. However, preliminary data point to altered cytoskeletal properties in SMCs without *Fto,* which might be caused by altered *Srf* expression. Further analysis of *Srf* transcript expression and its m6A-methylation in SMCs with and without *Fto* would be important to verify that Fto regulates *Srf* transcript expression. Additionally, further immunofluorescence analysis of different cytoskeletal proteins as well as their expression levels in SMCs with and without *Fto* could identify the cellular mechanism explaning how smooth muscle *Fto* influences myogenic tone.

In conclusion, the data reveal for the first time that vascular Fto is important in regulation of myogenic tone and blood pressure. Furthermore, these data demonstrate that vascular Fto regulated blood pressure in both, NC-fed and HFD-fed mice, although the cellular mechanisms are different. Additionally, we could show that EC-specific *Fto* deficiency significantly improved glucose and insulin tolerance in HFD-fed mice. Although further studies would be necessary, these data suggest that *Fto* may be a promising pharmaceutical target to treat obesity- induced comorbidities such as hypertension, insulin resistance and hyperglycemia.

7 References

1. Alexander, R.W., *Theodore Cooper Memorial Lecture. Hypertension and the pathogenesis of atherosclerosis. Oxidative stress and the mediation of arterial inflammatory response: a new perspective.* Hypertension, 1995. **25**(2): p. 155-61.
2. Kannel, W.B., M.J. Schwartz, and P.M. McNamara, *Blood pressure and risk of coronary heart disease: the Framingham study.* Dis Chest, 1969. **56**(1): p. 43-52.
3. Wolf, P.A., et al., *Probability of stroke: a risk profile from the Framingham Study.* Stroke, 1991. **22**(3): p. 312-8.
4. WHO. *Cardiovascular Diseases (CVDs) Fact Sheet*. [cited 2016 25.10.]; Available from: http://www.who.int/mediacentre/factsheets/fs317/en/.
5. OpenStax. *OpenStax, Anatomy & Physiology*. [cited 2016 26.02.].
6. Klabunde, R.E. *Cardiovascular Physiology Concepts*. [cited 2016 01.10.]; Available from: http://www.cvphysiology.com/Blood%20Flow/BF004.htm.
7. Straub, A.C., A.C. Zeigler, and B.E. Isakson, *The myoendothelial junction: connections that deliver the message.* Physiology (Bethesda), 2014. **29**(4): p. 242-9.
8. Young, D.B., in *Control of Cardiac Output*. 2010: San Rafael (CA).
9. Bayliss, W.M., *On the local reactions of the arterial wall to changes of internal pressure.* J Physiol, 1902. **28**(3): p. 220-31.
10. Davis, M.J., *Myogenic response gradient in an arteriolar network.* Am J Physiol, 1993. **264**(6 Pt 2): p. H2168-79.
11. Uchida, E. and D.F. Bohr, *Myogenic tone in isolated perfused vessels. Occurrence among vascular beds and along vascular trees.* Circ Res, 1969. **25**(5): p. 549-55.
12. Davis, M.J. and M.A. Hill, *Signaling mechanisms underlying the vascular myogenic response.* Physiol Rev, 1999. **79**(2): p. 387-423.
13. Ishiguro, M., et al., *Enhanced myogenic tone in cerebral arteries from a rabbit model of subarachnoid hemorrhage.* Am J Physiol Heart Circ Physiol, 2002. **283**(6): p. H2217-25.
14. Plus, P. *Influence of resistance artery radius on blood flow*. [cited 2016 01.10.]; Available from: http://physiologyplus.com/arterioles/.
15. Ikebe, M. and D.J. Hartshorne, *Phosphorylation of smooth muscle myosin at two distinct sites by myosin light chain kinase.* J Biol Chem, 1985. **260**(18): p. 10027-31.
16. Martinez-Lemus, L.A., M.A. Hill, and G.A. Meininger, *The plastic nature of the vascular wall: a continuum of remodeling events contributing to control of arteriolar diameter and structure.* Physiology (Bethesda), 2009. **24**: p. 45-57.
17. Mehta, D. and S.J. Gunst, *Actin polymerization stimulated by contractile activation regulates force development in canine tracheal smooth muscle.* J Physiol, 1999. **519 Pt 3**: p. 829-40.
18. Cipolla, M.J. and G. Osol, *Vascular smooth muscle actin cytoskeleton in cerebral artery forced dilatation.* Stroke, 1998. **29**(6): p. 1223-8.
19. Tseng, S., et al., *F-actin disruption attenuates agonist-induced [Ca2+], myosin phosphorylation, and force in smooth muscle.* Am J Physiol, 1997. **272**(6 Pt 1): p. C1960-7.
20. Miano, J.M., X. Long, and K. Fujiwara, *Serum response factor: master regulator of the actin cytoskeleton and contractile apparatus.* Am J Physiol Cell Physiol, 2007. **292**(1): p. C70-81.

21. Schildmeyer, L.A., et al., *Impaired vascular contractility and blood pressure homeostasis in the smooth muscle alpha-actin null mouse.* FASEB J, 2000. **14**(14): p. 2213-20.
22. Retailleau, K., et al., *Selective involvement of serum response factor in pressure-induced myogenic tone in resistance arteries.* Arterioscler Thromb Vasc Biol, 2013. **33**(2): p. 339-46.
23. Chrissobolis, S. and C.G. Sobey, *Evidence that Rho-kinase activity contributes to cerebral vascular tone in vivo and is enhanced during chronic hypertension: comparison with protein kinase C.* Circ Res, 2001. **88**(8): p. 774-9.
24. Schubert, R., V.U. Kalentchuk, and U. Krien, *Rho kinase inhibition partly weakens myogenic reactivity in rat small arteries by changing calcium sensitivity.* Am J Physiol Heart Circ Physiol, 2002. **283**(6): p. H2288-95.
25. Drummond, H.A., D. Gebremedhin, and D.R. Harder, *Degenerin/epithelial Na+ channel proteins: components of a vascular mechanosensor.* Hypertension, 2004. **44**(5): p. 643-8.
26. Welsh, D.G., et al., *Transient receptor potential channels regulate myogenic tone of resistance arteries.* Circ Res, 2002. **90**(3): p. 248-50.
27. Brayden, J.E. and M.T. Nelson, *Regulation of arterial tone by activation of calcium-dependent potassium channels.* Science, 1992. **256**(5056): p. 532-5.
28. Kauffenstein, G., et al., *Emerging role of G protein-coupled receptors in microvascular myogenic tone.* Cardiovasc Res, 2012. **95**(2): p. 223-32.
29. Martinez-Lemus, L.A., et al., *alphavbeta3- and alpha5beta1-integrin blockade inhibits myogenic constriction of skeletal muscle resistance arterioles.* Am J Physiol Heart Circ Physiol, 2005. **289**(1): p. H322-9.
30. Mederos y Schnitzler, M., U. Storch, and T. Gudermann, *AT1 receptors as mechanosensors.* Curr Opin Pharmacol, 2011. **11**(2): p. 112-6.
31. Furchgott, R.F. and J.V. Zawadzki, *The obligatory role of endothelial cells in the relaxation of arterial smooth muscle by acetylcholine.* Nature, 1980. **288**(5789): p. 373-6.
32. Ledoux, J., et al., *Calcium-activated potassium channels and the regulation of vascular tone.* Physiology (Bethesda), 2006. **21**: p. 69-78.
33. Burnham, M.P., et al., *Characterization of an apamin-sensitive small-conductance Ca(2+)-activated K(+) channel in porcine coronary artery endothelium: relevance to EDHF.* Br J Pharmacol, 2002. **135**(5): p. 1133-43.
34. Bychkov, R., et al., *Characterization of a charybdotoxin-sensitive intermediate conductance Ca2+-activated K+ channel in porcine coronary endothelium: relevance to EDHF.* Br J Pharmacol, 2002. **137**(8): p. 1346-54.
35. Kohler, R., et al., *Expression and function of endothelial Ca(2+)-activated K(+) channels in human mesenteric artery: A single-cell reverse transcriptase-polymerase chain reaction and electrophysiological study in situ.* Circ Res, 2000. **87**(6): p. 496-503.
36. Strobaek, D., et al., *Activation of human IK and SK Ca2+ -activated K+ channels by NS309 (6,7-dichloro-1H-indole-2,3-dione 3-oxime).* Biochim Biophys Acta, 2004. **1665**(1-2): p. 1-5.
37. Sonkusare, S.K., et al., *Elementary Ca2+ signals through endothelial TRPV4 channels regulate vascular function.* Science, 2012. **336**(6081): p. 597-601.
38. von Beckerath, N., et al., *Inwardly rectifying K+ channels in freshly dissociated coronary endothelial cells from guinea-pig heart.* J Physiol, 1996. **491 (Pt 2)**: p. 357-65.

39. Crane, G.J., et al., *Evidence for a differential cellular distribution of inward rectifier K channels in the rat isolated mesenteric artery.* J Vasc Res, 2003. **40**(2): p. 159-68.
40. Nelson, M.T. and J.M. Quayle, *Physiological roles and properties of potassium channels in arterial smooth muscle.* Am J Physiol, 1995. **268**(4 Pt 1): p. C799-822.
41. Sonkusare, S.K., et al., *Inward rectifier potassium (Kir2.1) channels as end-stage boosters of endothelium-dependent vasodilators.* J Physiol, 2016. **594**(12): p. 3271-85.
42. Papapetropoulos, A., et al., *Nitric oxide synthase inhibitors attenuate transforming-growth-factor-beta 1-stimulated capillary organization in vitro.* Am J Pathol, 1997. **150**(5): p. 1835-44.
43. Forstermann, U., et al., *Calmodulin-dependent endothelium-derived relaxing factor/nitric oxide synthase activity is present in the particulate and cytosolic fractions of bovine aortic endothelial cells.* Proc Natl Acad Sci U S A, 1991. **88**(5): p. 1788-92.
44. Pollock, J.S., et al., *Purification and characterization of particulate endothelium-derived relaxing factor synthase from cultured and native bovine aortic endothelial cells.* Proc Natl Acad Sci U S A, 1991. **88**(23): p. 10480-4.
45. Cristina de Assis, M., et al., *Expression of inducible nitric oxide synthase in human umbilical vein endothelial cells during primary culture.* Nitric Oxide, 2002. **7**(4): p. 254-61.
46. Palmer, R.M., A.G. Ferrige, and S. Moncada, *Nitric oxide release accounts for the biological activity of endothelium-derived relaxing factor.* Nature, 1987. **327**(6122): p. 524-6.
47. Palmer, R.M., et al., *L-arginine is the physiological precursor for the formation of nitric oxide in endothelium-dependent relaxation.* Biochem Biophys Res Commun, 1988. **153**(3): p. 1251-6.
48. Knowles, R.G. and S. Moncada, *Nitric oxide synthases in mammals.* Biochem J, 1994. **298 (Pt 2)**: p. 249-58.
49. Matouk, C.C. and P.A. Marsden, *Epigenetic regulation of vascular endothelial gene expression.* Circ Res, 2008. **102**(8): p. 873-87.
50. Andrew, P.J. and B. Mayer, *Enzymatic function of nitric oxide synthases.* Cardiovasc Res, 1999. **43**(3): p. 521-31.
51. Hofmann, F., et al., *Function of cGMP-dependent protein kinases as revealed by gene deletion.* Physiol Rev, 2006. **86**(1): p. 1-23.
52. Rapoport, R.M. and F. Murad, *Agonist-induced endothelium-dependent relaxation in rat thoracic aorta may be mediated through cGMP.* Circ Res, 1983. **52**(3): p. 352-7.
53. Soff, G.A., et al., *Smooth muscle cell expression of type I cyclic GMP-dependent protein kinase is suppressed by continuous exposure to nitrovasodilators, theophylline, cyclic GMP, and cyclic AMP.* J Clin Invest, 1997. **100**(10): p. 2580-7.
54. Geiselhoringer, A., et al., *IRAG is essential for relaxation of receptor-triggered smooth muscle contraction by cGMP kinase.* EMBO J, 2004. **23**(21): p. 4222-31.
55. Tang, K.M., et al., *Regulator of G-protein signaling-2 mediates vascular smooth muscle relaxation and blood pressure.* Nat Med, 2003. **9**(12): p. 1506-12.
56. Lee, M.R., L. Li, and T. Kitazawa, *Cyclic GMP causes Ca2+ desensitization in vascular smooth muscle by activating the myosin light chain phosphatase.* J Biol Chem, 1997. **272**(8): p. 5063-8.

57. Albertini, M., G. Vanelli, and M.G. Clement, *PGI2 and nitric oxide involvement in the regulation of systemic and pulmonary basal vascular tone in the pig.* Prostaglandins Leukot Essent Fatty Acids, 1996. **54**(4): p. 273-8.
58. Furfine, E.S., et al., *Selective inhibition of constitutive nitric oxide synthase by L-NG-nitroarginine.* Biochemistry, 1993. **32**(33): p. 8512-7.
59. Pfeifer, A., et al., *Defective smooth muscle regulation in cGMP kinase I-deficient mice.* EMBO J, 1998. **17**(11): p. 3045-51.
60. Chataigneau, T., et al., *Acetylcholine-induced relaxation in blood vessels from endothelial nitric oxide synthase knockout mice.* Br J Pharmacol, 1999. **126**(1): p. 219-26.
61. Brandes, R.P., et al., *An endothelium-derived hyperpolarizing factor distinct from NO and prostacyclin is a major endothelium-dependent vasodilator in resistance vessels of wild-type and endothelial NO synthase knockout mice.* Proc Natl Acad Sci U S A, 2000. **97**(17): p. 9747-52.
62. Huang, P.L., et al., *Hypertension in mice lacking the gene for endothelial nitric oxide synthase.* Nature, 1995. **377**(6546): p. 239-42.
63. Smyth, E.M., et al., *Prostanoids in health and disease.* J Lipid Res, 2009. **50 Suppl**: p. S423-8.
64. Mohan, S., et al., *Putative role of prostaglandin receptor in intracerebral hemorrhage.* Front Neurol, 2012. **3**: p. 145.
65. DeWitt, D.L., et al., *Concentrations of prostaglandin endoperoxide synthase and prostaglandin I2 synthase in the endothelium and smooth muscle of bovine aorta.* J Clin Invest, 1983. **72**(6): p. 1882-8.
66. Potter, C.M., et al., *Role of shear stress in endothelial cell morphology and expression of cyclooxygenase isoforms.* Arterioscler Thromb Vasc Biol, 2011. **31**(2): p. 384-91.
67. Vane, J.R. and R.M. Botting, *Pharmacodynamic profile of prostacyclin.* Am J Cardiol, 1995. **75**(3): p. 3A-10A.
68. Nakahata, N., *Thromboxane A2: physiology/pathophysiology, cellular signal transduction and pharmacology.* Pharmacol Ther, 2008. **118**(1): p. 18-35.
69. Sugimoto, Y., et al., *Two isoforms of the EP3 receptor with different carboxyl-terminal domains. Identical ligand binding properties and different coupling properties with Gi proteins.* J Biol Chem, 1993. **268**(4): p. 2712-8.
70. Sugimoto, Y. and S. Narumiya, *Prostaglandin E receptors.* J Biol Chem, 2007. **282**(16): p. 11613-7.
71. Wong, S.L., et al., *Cyclooxygenase-2-derived prostaglandin F2alpha mediates endothelium-dependent contractions in the aortae of hamsters with increased impact during aging.* Circ Res, 2009. **104**(2): p. 228-35.
72. Ketsawatsomkron, P., et al., *Does peroxisome proliferator-activated receptor-gamma (PPAR gamma) protect from hypertension directly through effects in the vasculature?* J Biol Chem, 2010. **285**(13): p. 9311-6.
73. De Mey, J.G., M. Claeys, and P.M. Vanhoutte, *Endothelium-dependent inhibitory effects of acetylcholine, adenosine triphosphate, thrombin and arachidonic acid in the canine femoral artery.* J Pharmacol Exp Ther, 1982. **222**(1): p. 166-73.
74. Taylor, S.G. and A.H. Weston, *Endothelium-derived hyperpolarizing factor: a new endogenous inhibitor from the vascular endothelium.* Trends Pharmacol Sci, 1988. **9**(8): p. 272-4.
75. Garland, C.J. and K.A. Dora, *EDH: Endothelium-dependent hyperpolarization and microvascular signaling.* Acta Physiol (Oxf), 2016.

76. Zygmunt, P.M. and E.D. Hogestatt, *Role of potassium channels in endothelium-dependent relaxation resistant to nitroarginine in the rat hepatic artery.* Br J Pharmacol, 1996. **117**(7): p. 1600-6.
77. Adeagbo, A.S. and C.R. Triggle, *Varying extracellular [K+]: a functional approach to separating EDHF- and EDNO-related mechanisms in perfused rat mesenteric arterial bed.* J Cardiovasc Pharmacol, 1993. **21**(3): p. 423-9.
78. Holzmann, S., et al., *Pharmacologic differentiation between endothelium-dependent relaxations sensitive and resistant to nitro-L-arginine in coronary arteries.* J Cardiovasc Pharmacol, 1994. **23**(5): p. 747-56.
79. Busse, R., et al., *EDHF: bringing the concepts together.* Trends Pharmacol Sci, 2002. **23**(8): p. 374-80.
80. Edwards, G., et al., *K+ is an endothelium-derived hyperpolarizing factor in rat arteries.* Nature, 1998. **396**(6708): p. 269-72.
81. Feletou, M. and P.M. Vanhoutte, *Endothelium-derived hyperpolarizing factor: where are we now?* Arterioscler Thromb Vasc Biol, 2006. **26**(6): p. 1215-25.
82. Johnstone, S., B. Isakson, and D. Locke, *Biological and biophysical properties of vascular connexin channels.* Int Rev Cell Mol Biol, 2009. **278**: p. 69-118.
83. Isakson, B.E., S.I. Ramos, and B.R. Duling, *Ca2+ and inositol 1,4,5-trisphosphate-mediated signaling across the myoendothelial junction.* Circ Res, 2007. **100**(2): p. 246-54.
84. Yamamoto, Y., K. Imaeda, and H. Suzuki, *Endothelium-dependent hyperpolarization and intercellular electrical coupling in guinea-pig mesenteric arterioles.* J Physiol, 1999. **514 (Pt 2)**: p. 505-13.
85. Figueroa, X.F. and B.R. Duling, *Dissection of two Cx37-independent conducted vasodilator mechanisms by deletion of Cx40: electrotonic versus regenerative conduction.* Am J Physiol Heart Circ Physiol, 2008. **295**(5): p. H2001-7.
86. de Wit, C., et al., *Impaired conduction of vasodilation along arterioles in connexin40-deficient mice.* Circ Res, 2000. **86**(6): p. 649-55.
87. Haddock, R.E., et al., *Endothelial coordination of cerebral vasomotion via myoendothelial gap junctions containing connexins 37 and 40.* Am J Physiol Heart Circ Physiol, 2006. **291**(5): p. H2047-56.
88. Lang, N.N., et al., *Connexin 43 mediates endothelium-derived hyperpolarizing factor-induced vasodilatation in subcutaneous resistance arteries from healthy pregnant women.* Am J Physiol Heart Circ Physiol, 2007. **292**(2): p. H1026-32.
89. Matchkov, V.V., et al., *Analysis of effects of connexin-mimetic peptides in rat mesenteric small arteries.* Am J Physiol Heart Circ Physiol, 2006. **291**(1): p. H357-67.
90. Rath, G., et al., *Vascular hypoxic preconditioning relies on TRPV4-dependent calcium influx and proper intercellular gap junctions communication.* Arterioscler Thromb Vasc Biol, 2012. **32**(9): p. 2241-9.
91. Straub, A.C., et al., *Compartmentalized connexin 43 s-nitrosylation/denitrosylation regulates heterocellular communication in the vessel wall.* Arterioscler Thromb Vasc Biol, 2011. **31**(2): p. 399-407.
92. Garland, C.J., et al., *Endothelium-dependent hyperpolarization: a role in the control of vascular tone.* Trends Pharmacol Sci, 1995. **16**(1): p. 23-30.
93. Shimokawa, H., et al., *The importance of the hyperpolarizing mechanism increases as the vessel size decreases in endothelium-dependent relaxations in rat mesenteric circulation.* J Cardiovasc Pharmacol, 1996. **28**(5): p. 703-11.

94. Hwa, J.J., et al., *Comparison of acetylcholine-dependent relaxation in large and small arteries of rat mesenteric vascular bed.* Am J Physiol, 1994. **266**(3 Pt 2): p. H952-8.
95. Sandow, S.L. and C.E. Hill, *Incidence of myoendothelial gap junctions in the proximal and distal mesenteric arteries of the rat is suggestive of a role in endothelium-derived hyperpolarizing factor-mediated responses.* Circ Res, 2000. **86**(3): p. 341-6.
96. Haynes, W.G. and D.J. Webb, *Endothelin as a regulator of cardiovascular function in health and disease.* J Hypertens, 1998. **16**(8): p. 1081-98.
97. Xu, D., et al., *ECE-1: a membrane-bound metalloprotease that catalyzes the proteolytic activation of big endothelin-1.* Cell, 1994. **78**(3): p. 473-85.
98. Rubanyi, G.M. and M.A. Polokoff, *Endothelins: molecular biology, biochemistry, pharmacology, physiology, and pathophysiology.* Pharmacol Rev, 1994. **46**(3): p. 325-415.
99. Wagner, O.F., et al., *Polar secretion of endothelin-1 by cultured endothelial cells.* J Biol Chem, 1992. **267**(23): p. 16066-8.
100. Bohm, F. and J. Pernow, *The importance of endothelin-1 for vascular dysfunction in cardiovascular disease.* Cardiovasc Res, 2007. **76**(1): p. 8-18.
101. de Nucci, G., et al., *Pressor effects of circulating endothelin are limited by its removal in the pulmonary circulation and by the release of prostacyclin and endothelium-derived relaxing factor.* Proc Natl Acad Sci U S A, 1988. **85**(24): p. 9797-800.
102. Guyenet, P.G., *The sympathetic control of blood pressure.* Nat Rev Neurosci, 2006. **7**(5): p. 335-46.
103. Raven, P.B., *Recent advances in baroreflex control of blood pressure during exercise in humans: an overview.* Med Sci Sports Exerc, 2008. **40**(12): p. 2033-6.
104. Gericke, A., et al., *Role of M1, M3, and M5 muscarinic acetylcholine receptors in cholinergic dilation of small arteries studied with gene-targeted mice.* Am J Physiol Heart Circ Physiol, 2011. **300**(5): p. H1602-8.
105. Furchgott, R.F., *Introduction to EDRF research.* J Cardiovasc Pharmacol, 1993. **22 Suppl 7**: p. S1-2.
106. Fleming, I. and R. Busse, *Molecular mechanisms involved in the regulation of the endothelial nitric oxide synthase.* Am J Physiol Regul Integr Comp Physiol, 2003. **284**(1): p. R1-12.
107. Sonkusare, S.K., et al., *AKAP150-dependent cooperative TRPV4 channel gating is central to endothelium-dependent vasodilation and is disrupted in hypertension.* Sci Signal, 2014. **7**(333): p. ra66.
108. Dinenno, F.A. and M.J. Joyner, *Alpha-adrenergic control of skeletal muscle circulation at rest and during exercise in aging humans.* Microcirculation, 2006. **13**(4): p. 329-41.
109. Guimaraes, S. and D. Moura, *Vascular adrenoceptors: an update.* Pharmacol Rev, 2001. **53**(2): p. 319-56.
110. Ferrario, C.M. and W.B. Strawn, *Role of the renin-angiotensin-aldosterone system and proinflammatory mediators in cardiovascular disease.* Am J Cardiol, 2006. **98**(1): p. 121-8.
111. Higuchi, S., et al., *Angiotensin II signal transduction through the AT1 receptor: novel insights into mechanisms and pathophysiology.* Clin Sci (Lond), 2007. **112**(8): p. 417-28.

112. Falcone, J.C., L. Kuo, and G.A. Meininger, *Endothelial cell calcium increases during flow-induced dilation in isolated arterioles.* Am J Physiol, 1993. **264**(2 Pt 2): p. H653-9.
113. Mendoza, S.A., et al., *TRPV4-mediated endothelial Ca2+ influx and vasodilation in response to shear stress.* Am J Physiol Heart Circ Physiol, 2010. **298**(2): p. H466-76.
114. Rubanyi, G.M., J.C. Romero, and P.M. Vanhoutte, *Flow-induced release of endothelium-derived relaxing factor.* Am J Physiol, 1986. **250**(6 Pt 2): p. H1145-9.
115. Hull, S.S., Jr., et al., *Endothelium-dependent flow-induced dilation of canine femoral and saphenous arteries.* Blood Vessels, 1986. **23**(4-5): p. 183-98.
116. Koller, A. and G. Kaley, *Endothelial regulation of wall shear stress and blood flow in skeletal muscle microcirculation.* Am J Physiol, 1991. **260**(3 Pt 2): p. H862-8.
117. Mozaffarian, D., et al., *Heart disease and stroke statistics--2015 update: a report from the American Heart Association.* Circulation, 2015. **131**(4): p. e29-322.
118. Eckel, R.H. and R.M. Krauss, *American Heart Association call to action: obesity as a major risk factor for coronary heart disease. AHA Nutrition Committee.* Circulation, 1998. **97**(21): p. 2099-100.
119. Yusuf, S., et al., *Obesity and the risk of myocardial infarction in 27,000 participants from 52 countries: a case-control study.* Lancet, 2005. **366**(9497): p. 1640-9.
120. Organization, W.H. *Obesity and overweight fact sheet No. 311*. [cited 2016 05.10.]; Available from: http://www.who.int/mediacentre/factsheets/fs311/en/.
121. Lau, D.C., et al., *2006 Canadian clinical practice guidelines on the management and prevention of obesity in adults and children [summary]*. CMAJ, 2007. **176**(8): p. S1-13.
122. Keith, S.W., et al., *Putative contributors to the secular increase in obesity: exploring the roads less traveled.* Int J Obes (Lond), 2006. **30**(11): p. 1585-94.
123. Locke, A.E., et al., *Genetic studies of body mass index yield new insights for obesity biology.* Nature, 2015. **518**(7538): p. 197-206.
124. Loos, R.J., *Genetic determinants of common obesity and their value in prediction.* Best Pract Res Clin Endocrinol Metab, 2012. **26**(2): p. 211-26.
125. Poirier, P., et al., *Obesity and cardiovascular disease: pathophysiology, evaluation, and effect of weight loss: an update of the 1997 American Heart Association Scientific Statement on Obesity and Heart Disease from the Obesity Committee of the Council on Nutrition, Physical Activity, and Metabolism.* Circulation, 2006. **113**(6): p. 898-918.
126. Bakker, W., et al., *Endothelial dysfunction and diabetes: roles of hyperglycemia, impaired insulin signaling and obesity.* Cell Tissue Res, 2009. **335**(1): p. 165-89.
127. Pessin, J.E. and A.R. Saltiel, *Signaling pathways in insulin action: molecular targets of insulin resistance.* J Clin Invest, 2000. **106**(2): p. 165-9.
128. Petersen, K.F., et al., *The role of skeletal muscle insulin resistance in the pathogenesis of the metabolic syndrome.* Proc Natl Acad Sci U S A, 2007. **104**(31): p. 12587-94.
129. Grundy, S.M., *Metabolic complications of obesity.* Endocrine, 2000. **13**(2): p. 155-65.
130. Muniyappa, R. and M.J. Quon, *Insulin action and insulin resistance in vascular endothelium.* Curr Opin Clin Nutr Metab Care, 2007. **10**(4): p. 523-30.

131. Polonsky, K.S., et al., *Quantitative study of insulin secretion and clearance in normal and obese subjects.* J Clin Invest, 1988. **81**(2): p. 435-41.
132. Grundy, S.M., *Obesity, metabolic syndrome, and cardiovascular disease.* J Clin Endocrinol Metab, 2004. **89**(6): p. 2595-600.
133. Kubota, T., et al., *Impaired insulin signaling in endothelial cells reduces insulin-induced glucose uptake by skeletal muscle.* Cell Metab, 2011. **13**(3): p. 294-307.
134. Hutley, L. and J.B. Prins, *Fat as an endocrine organ: relationship to the metabolic syndrome.* Am J Med Sci, 2005. **330**(6): p. 280-9.
135. Diamant, M., et al., *The association between abdominal visceral fat and carotid stiffness is mediated by circulating inflammatory markers in uncomplicated type 2 diabetes.* J Clin Endocrinol Metab, 2005. **90**(3): p. 1495-501.
136. Hotamisligil, G.S., *The role of TNFalpha and TNF receptors in obesity and insulin resistance.* J Intern Med, 1999. **245**(6): p. 621-5.
137. Bastard, J.P., et al., *Adipose tissue IL-6 content correlates with resistance to insulin activation of glucose uptake both in vivo and in vitro.* J Clin Endocrinol Metab, 2002. **87**(5): p. 2084-9.
138. Orshal, J.M. and R.A. Khalil, *Reduced endothelial NO-cGMP-mediated vascular relaxation and hypertension in IL-6-infused pregnant rats.* Hypertension, 2004. **43**(2): p. 434-44.
139. Shimabukuro, M., et al., *Hypoadiponectinemia is closely linked to endothelial dysfunction in man.* J Clin Endocrinol Metab, 2003. **88**(7): p. 3236-40.
140. Ryo, M., et al., *Adiponectin as a biomarker of the metabolic syndrome.* Circ J, 2004. **68**(11): p. 975-81.
141. Heptulla, R., et al., *Temporal patterns of circulating leptin levels in lean and obese adolescents: relationships to insulin, growth hormone, and free fatty acids rhythmicity.* J Clin Endocrinol Metab, 2001. **86**(1): p. 90-6.
142. Randle, P.J., et al., *The glucose fatty-acid cycle. Its role in insulin sensitivity and the metabolic disturbances of diabetes mellitus.* Lancet, 1963. **1**(7285): p. 785-9.
143. Steinberg, H.O., et al., *Elevated circulating free fatty acid levels impair endothelium-dependent vasodilation.* J Clin Invest, 1997. **100**(5): p. 1230-9.
144. Wilkins, K., et al., *Blood pressure in Canadian adults.* Health Rep, 2010. **21**(1): p. 37-46.
145. Emerging Risk Factors, C., et al., *Separate and combined associations of body-mass index and abdominal adiposity with cardiovascular disease: collaborative analysis of 58 prospective studies.* Lancet, 2011. **377**(9771): p. 1085-95.
146. Bonetti, P.O., L.O. Lerman, and A. Lerman, *Endothelial dysfunction: a marker of atherosclerotic risk.* Arterioscler Thromb Vasc Biol, 2003. **23**(2): p. 168-75.
147. Heitzer, T., et al., *Endothelial dysfunction, oxidative stress, and risk of cardiovascular events in patients with coronary artery disease.* Circulation, 2001. **104**(22): p. 2673-8.
148. Echahidi, N., et al., *Obesity and metabolic syndrome are independent risk factors for atrial fibrillation after coronary artery bypass graft surgery.* Circulation, 2007. **116**(11 Suppl): p. I213-9.
149. Moebus, S., et al., *Regional differences in the prevalence of the metabolic syndrome in primary care practices in Germany.* Dtsch Arztebl Int, 2008. **105**(12): p. 207-13.
150. Ford, E.S., W.H. Giles, and W.H. Dietz, *Prevalence of the metabolic syndrome among US adults: findings from the third National Health and Nutrition Examination Survey.* JAMA, 2002. **287**(3): p. 356-9.

151. Alberti, K.G., et al., *Harmonizing the metabolic syndrome: a joint interim statement of the International Diabetes Federation Task Force on Epidemiology and Prevention; National Heart, Lung, and Blood Institute; American Heart Association; World Heart Federation; International Atherosclerosis Society; and International Association for the Study of Obesity.* Circulation, 2009. **120**(16): p. 1640-5.
152. Alberti, K.G. and P.Z. Zimmet, *Definition, diagnosis and classification of diabetes mellitus and its complications. Part 1: diagnosis and classification of diabetes mellitus provisional report of a WHO consultation.* Diabet Med, 1998. **15**(7): p. 539-53.
153. Rahmouni, K., et al., *Obesity-associated hypertension: new insights into mechanisms.* Hypertension, 2005. **45**(1): p. 9-14.
154. Luscher, T.F., *Heterogeneity of endothelial dysfunction in hypertension.* Eur Heart J, 1992. **13 Suppl D**: p. 50-5.
155. Perticone, F., et al., *Obesity and body fat distribution induce endothelial dysfunction by oxidative stress: protective effect of vitamin C.* Diabetes, 2001. **50**(1): p. 159-65.
156. Klotz, L.O., P. Schroeder, and H. Sies, *Peroxynitrite signaling: receptor tyrosine kinases and activation of stress-responsive pathways.* Free Radic Biol Med, 2002. **33**(6): p. 737-43.
157. Barrett, E.J. and Z. Liu, *The endothelial cell: an "early responder" in the development of insulin resistance.* Rev Endocr Metab Disord, 2013. **14**(1): p. 21-7.
158. de Jongh, R.T., et al., *Impaired microvascular function in obesity: implications for obesity-associated microangiopathy, hypertension, and insulin resistance.* Circulation, 2004. **109**(21): p. 2529-35.
159. Steinberg, H.O., et al., *Obesity/insulin resistance is associated with endothelial dysfunction. Implications for the syndrome of insulin resistance.* J Clin Invest, 1996. **97**(11): p. 2601-10.
160. Edgley, A.J., et al., *In vivo regulation of endothelium-dependent vasodilation in the rat renal circulation and the effect of streptozotocin-induced diabetes.* Am J Physiol Regul Integr Comp Physiol, 2008. **295**(3): p. R829-39.
161. Serne, E.H., et al., *Microvascular function relates to insulin sensitivity and blood pressure in normal subjects.* Circulation, 1999. **99**(7): p. 896-902.
162. Erdei, N., et al., *High-fat diet-induced reduction in nitric oxide-dependent arteriolar dilation in rats: role of xanthine oxidase-derived superoxide anion.* Am J Physiol Heart Circ Physiol, 2006. **291**(5): p. H2107-15.
163. Du, X.L., et al., *Hyperglycemia-induced mitochondrial superoxide overproduction activates the hexosamine pathway and induces plasminogen activator inhibitor-1 expression by increasing Sp1 glycosylation.* Proc Natl Acad Sci U S A, 2000. **97**(22): p. 12222-6.
164. Nishikawa, T., et al., *Normalizing mitochondrial superoxide production blocks three pathways of hyperglycaemic damage.* Nature, 2000. **404**(6779): p. 787-90.
165. Laursen, J.B., et al., *Endothelial regulation of vasomotion in apoE-deficient mice: implications for interactions between peroxynitrite and tetrahydrobiopterin.* Circulation, 2001. **103**(9): p. 1282-8.
166. Schmidt, H.H., et al., *No .NO from NO synthase.* Proc Natl Acad Sci U S A, 1996. **93**(25): p. 14492-7.

167. Huang, A., et al., *In eNOS knockout mice skeletal muscle arteriolar dilation to acetylcholine is mediated by EDHF.* Am J Physiol Heart Circ Physiol, 2000. **278**(3): p. H762-8.
168. Taddei, S., et al., *Identification of a cytochrome P450 2C9-derived endothelium-derived hyperpolarizing factor in essential hypertensive patients.* J Am Coll Cardiol, 2006. **48**(3): p. 508-15.
169. Katakam, P.V., et al., *Enhanced endothelin-1 response and receptor expression in small mesenteric arteries of insulin-resistant rats.* Am J Physiol Heart Circ Physiol, 2001. **280**(2): p. H522-7.
170. Potenza, M.A., et al., *Insulin resistance in spontaneously hypertensive rats is associated with endothelial dysfunction characterized by imbalance between NO and ET-1 production.* Am J Physiol Heart Circ Physiol, 2005. **289**(2): p. H813-22.
171. Du, X., et al., *Insulin resistance reduces arterial prostacyclin synthase and eNOS activities by increasing endothelial fatty acid oxidation.* J Clin Invest, 2006. **116**(4): p. 1071-80.
172. Rutkai, I., et al., *Activation of prostaglandin E2 EP1 receptor increases arteriolar tone and blood pressure in mice with type 2 diabetes.* Cardiovasc Res, 2009. **83**(1): p. 148-54.
173. Gluais, P., et al., *Acetylcholine-induced endothelium-dependent contractions in the SHR aorta: the Janus face of prostacyclin.* Br J Pharmacol, 2005. **146**(6): p. 834-45.
174. Lagaud, G.J., et al., *Influence of type II diabetes on arterial tone and endothelial function in murine mesenteric resistance arteries.* J Vasc Res, 2001. **38**(6): p. 578-89.
175. Schofield, I., et al., *Vascular structural and functional changes in type 2 diabetes mellitus: evidence for the roles of abnormal myogenic responsiveness and dyslipidemia.* Circulation, 2002. **106**(24): p. 3037-43.
176. Bagi, Z., et al., *Type 2 diabetic mice have increased arteriolar tone and blood pressure: enhanced release of COX-2-derived constrictor prostaglandins.* Arterioscler Thromb Vasc Biol, 2005. **25**(8): p. 1610-6.
177. Harrison, B.C., et al., *Skeletal muscle adaptations in response to voluntary wheel running in myosin heavy chain null mice.* J Appl Physiol (1985), 2002. **92**(1): p. 313-22.
178. Gluais, P., P.M. Vanhoutte, and M. Feletou, *Mechanisms underlying ATP-induced endothelium-dependent contractions in the SHR aorta.* Eur J Pharmacol, 2007. **556**(1-3): p. 107-14.
179. Gluais, P., et al., *In SHR aorta, calcium ionophore A-23187 releases prostacyclin and thromboxane A2 as endothelium-derived contracting factors.* Am J Physiol Heart Circ Physiol, 2006. **291**(5): p. H2255-64.
180. Sweazea, K.L. and B.R. Walker, *Impaired myogenic tone in mesenteric arteries from overweight rats.* Nutr Metab (Lond), 2012. **9**(1): p. 18.
181. Ito, I., et al., *Myogenic tone and reactivity of rat ophthalmic artery in acute exposure to high glucose and in a type II diabetic model.* Invest Ophthalmol Vis Sci, 2006. **47**(2): p. 683-92.
182. Frayling, T.M., et al., *A common variant in the FTO gene is associated with body mass index and predisposes to childhood and adult obesity.* Science, 2007. **316**(5826): p. 889-94.
183. Cornes, B.K., et al., *Replication of the association of common rs9939609 variant of FTO with increased BMI in an Australian adult twin population but no evidence*

for gene by environment (G x E) interaction. Int J Obes (Lond), 2009. **33**(1): p. 75-9.
184. Hotta, K., et al., *Variations in the FTO gene are associated with severe obesity in the Japanese.* J Hum Genet, 2008. **53**(6): p. 546-53.
185. Tan, J.T., et al., *FTO variants are associated with obesity in the Chinese and Malay populations in Singapore.* Diabetes, 2008. **57**(10): p. 2851-7.
186. Peters, T., K. Ausmeier, and U. Ruther, *Cloning of Fatso (Fto), a novel gene deleted by the Fused toes (Ft) mouse mutation.* Mamm Genome, 1999. **10**(10): p. 983-6.
187. Fischer, J., et al., *Inactivation of the Fto gene protects from obesity.* Nature, 2009. **458**(7240): p. 894-8.
188. Robbens, S., et al., *The FTO gene, implicated in human obesity, is found only in vertebrates and marine algae.* J Mol Evol, 2008. **66**(1): p. 80-4.
189. Gerken, T., et al., *The obesity-associated FTO gene encodes a 2-oxoglutarate-dependent nucleic acid demethylase.* Science, 2007. **318**(5855): p. 1469-72.
190. Falnes, P.O., R.F. Johansen, and E. Seeberg, *AlkB-mediated oxidative demethylation reverses DNA damage in Escherichia coli.* Nature, 2002. **419**(6903): p. 178-82.
191. Sanchez-Pulido, L. and M.A. Andrade-Navarro, *The FTO (fat mass and obesity associated) gene codes for a novel member of the non-heme dioxygenase superfamily.* BMC Biochem, 2007. **8**: p. 23.
192. Jia, G., et al., *N6-methyladenosine in nuclear RNA is a major substrate of the obesity-associated FTO.* Nat Chem Biol, 2011. **7**(12): p. 885-7.
193. Dubin, D.T. and R.H. Taylor, *The methylation state of poly A-containing messenger RNA from cultured hamster cells.* Nucleic Acids Res, 1975. **2**(10): p. 1653-68.
194. Beemon, K. and J. Keith, *Localization of N6-methyladenosine in the Rous sarcoma virus genome.* J Mol Biol, 1977. **113**(1): p. 165-79.
195. Bodi, Z., et al., *Yeast targets for mRNA methylation.* Nucleic Acids Res, 2010. **38**(16): p. 5327-35.
196. Horowitz, S., et al., *Mapping of N6-methyladenosine residues in bovine prolactin mRNA.* Proc Natl Acad Sci U S A, 1984. **81**(18): p. 5667-71.
197. Desrosiers, R., K. Friderici, and F. Rottman, *Identification of methylated nucleosides in messenger RNA from Novikoff hepatoma cells.* Proc Natl Acad Sci U S A, 1974. **71**(10): p. 3971-5.
198. Perry, R.P. and D.E. Kelley, *Existence of methylated messenger RNA in mouse L cells.* Cell. **1**(1): p. 37-42.
199. Dominissini, D., et al., *Topology of the human and mouse m6A RNA methylomes revealed by m6A-seq.* Nature, 2012. **485**(7397): p. 201-6.
200. Meyer, K.D., et al., *Comprehensive analysis of mRNA methylation reveals enrichment in 3' UTRs and near stop codons.* Cell, 2012. **149**(7): p. 1635-46.
201. He, C. *Effectors of m6a-RNA methylation*. [cited 2016 30.09.]; Available from: http://chemistry.uchicago.edu/faculty/faculty/person/member/chuan-he.html.
202. Bokar, J.A., et al., *Characterization and partial purification of mRNA N6-adenosine methyltransferase from HeLa cell nuclei. Internal mRNA methylation requires a multisubunit complex.* J Biol Chem, 1994. **269**(26): p. 17697-704.
203. Liu, J., et al., *A METTL3-METTL14 complex mediates mammalian nuclear RNA N6-adenosine methylation.* Nat Chem Biol, 2014. **10**(2): p. 93-5.
204. Wang, Y., et al., *N6-methyladenosine modification destabilizes developmental regulators in embryonic stem cells.* Nat Cell Biol, 2014. **16**(2): p. 191-8.

205. Ping, X.L., et al., *Mammalian WTAP is a regulatory subunit of the RNA N6-methyladenosine methyltransferase.* Cell Res, 2014. **24**(2): p. 177-89.
206. Bokar, J.A., et al., *Purification and cDNA cloning of the AdoMet-binding subunit of the human mRNA (N6-adenosine)-methyltransferase.* RNA, 1997. **3**(11): p. 1233-47.
207. Wang, X., et al., *N6-methyladenosine-dependent regulation of messenger RNA stability.* Nature, 2014. **505**(7481): p. 117-20.
208. Xu, C., et al., *Structures of human ALKBH5 demethylase reveal a unique binding mode for specific single-stranded N6-methyladenosine RNA demethylation.* J Biol Chem, 2014. **289**(25): p. 17299-311.
209. Zheng, G., et al., *ALKBH5 is a mammalian RNA demethylase that impacts RNA metabolism and mouse fertility.* Mol Cell, 2013. **49**(1): p. 18-29.
210. Feng, C., et al., *Crystal structures of the human RNA demethylase Alkbh5 reveal basis for substrate recognition.* J Biol Chem, 2014. **289**(17): p. 11571-83.
211. Aik, W., et al., *Structure of human RNA N(6)-methyladenine demethylase ALKBH5 provides insights into its mechanisms of nucleic acid recognition and demethylation.* Nucleic Acids Res, 2014. **42**(7): p. 4741-54.
212. Zou, S., et al., *N(6)-Methyladenosine: a conformational marker that regulates the substrate specificity of human demethylases FTO and ALKBH5.* Sci Rep, 2016. **6**: p. 25677.
213. Geula, S., et al., *Stem cells. m6A mRNA methylation facilitates resolution of naive pluripotency toward differentiation.* Science, 2015. **347**(6225): p. 1002-6.
214. Fu, Y., et al., *Gene expression regulation mediated through reversible m(6)A RNA methylation.* Nat Rev Genet, 2014. **15**(5): p. 293-306.
215. Alarcon, C.R., et al., *N6-methyladenosine marks primary microRNAs for processing.* Nature, 2015. **519**(7544): p. 482-5.
216. Fustin, J.M., et al., *RNA-methylation-dependent RNA processing controls the speed of the circadian clock.* Cell, 2013. **155**(4): p. 793-806.
217. Zhao, X., et al., *FTO-dependent demethylation of N6-methyladenosine regulates mRNA splicing and is required for adipogenesis.* Cell Res, 2014. **24**(12): p. 1403-19.
218. Zhou, J., et al., *Dynamic m(6)A mRNA methylation directs translational control of heat shock response.* Nature, 2015. **526**(7574): p. 591-4.
219. Hess, M.E., et al., *The fat mass and obesity associated gene (Fto) regulates activity of the dopaminergic midbrain circuitry.* Nat Neurosci, 2013. **16**(8): p. 1042-8.
220. Church, C., et al., *Overexpression of Fto leads to increased food intake and results in obesity.* Nat Genet, 2010. **42**(12): p. 1086-92.
221. Church, C., et al., *A mouse model for the metabolic effects of the human fat mass and obesity associated FTO gene.* PLoS Genet, 2009. **5**(8): p. e1000599.
222. McMurray, F., et al., *Adult onset global loss of the fto gene alters body composition and metabolism in the mouse.* PLoS Genet, 2013. **9**(1): p. e1003166.
223. Gao, X., et al., *The fat mass and obesity associated gene FTO functions in the brain to regulate postnatal growth in mice.* PLoS One, 2010. **5**(11): p. e14005.
224. Cecil, J.E., et al., *An obesity-associated FTO gene variant and increased energy intake in children.* N Engl J Med, 2008. **359**(24): p. 2558-66.
225. Speakman, J.R., K.A. Rance, and A.M. Johnstone, *Polymorphisms of the FTO gene are associated with variation in energy intake, but not energy expenditure.* Obesity (Silver Spring), 2008. **16**(8): p. 1961-5.

226. Haupt, A., et al., *Variation in the FTO gene influences food intake but not energy expenditure.* Exp Clin Endocrinol Diabetes, 2009. **117**(4): p. 194-7.
227. Smemo, S., et al., *Obesity-associated variants within FTO form long-range functional connections with IRX3.* Nature, 2014. **507**(7492): p. 371-5.
228. Stratigopoulos, G., et al., *Regulation of Fto/Ftm gene expression in mice and humans.* Am J Physiol Regul Integr Comp Physiol, 2008. **294**(4): p. R1185-96.
229. Ikels, K., et al., *FTO is a relevant factor for the development of the metabolic syndrome in mice.* PLoS One, 2014. **9**(8): p. e105349.
230. Sjogren, M., et al., *The search for putative unifying genetic factors for components of the metabolic syndrome.* Diabetologia, 2008. **51**(12): p. 2242-51.
231. Pausova, Z., et al., *A common variant of the FTO gene is associated with not only increased adiposity but also elevated blood pressure in French Canadians.* Circ Cardiovasc Genet, 2009. **2**(3): p. 260-9.
232. Timpson, N.J., et al., *Does greater adiposity increase blood pressure and hypertension risk?: Mendelian randomization using the FTO/MC4R genotype.* Hypertension, 2009. **54**(1): p. 84-90.
233. Ahmad, T., et al., *The fat-mass and obesity-associated (FTO) gene, physical activity, and risk of incident cardiovascular events in white women.* Am Heart J, 2010. **160**(6): p. 1163-9.
234. Hotta, K., et al., *Association of variations in the FTO, SCG3 and MTMR9 genes with metabolic syndrome in a Japanese population.* J Hum Genet, 2011. **56**(9): p. 647-51.
235. Xi, B., et al., *Associations of obesity susceptibility loci with hypertension in Chinese children.* Int J Obes (Lond), 2013. **37**(7): p. 926-30.
236. Kumar, R., et al., *Interactions between the FTO and GNB3 genes contribute to varied clinical phenotypes in hypertension.* PLoS One, 2013. **8**(5): p. e63934.
237. He, D., et al., *FTO gene variant and risk of hypertension: a meta-analysis of 57,464 hypertensive cases and 41,256 controls.* Metabolism, 2014. **63**(5): p. 633-9.
238. Freathy, R.M., et al., *Common variation in the FTO gene alters diabetes-related metabolic traits to the extent expected given its effect on BMI.* Diabetes, 2008. **57**(5): p. 1419-26.
239. Liu, C., S. Mou, and C. Pan, *The FTO gene rs9939609 polymorphism predicts risk of cardiovascular disease: a systematic review and meta-analysis.* PLoS One, 2013. **8**(8): p. e71901.
240. Pluthero, F.G., *Rapid purification of high-activity Taq DNA polymerase.* Nucleic Acids Res, 1993. **21**(20): p. 4850-1.
241. Kuhn, R., et al., *Inducible gene targeting in mice.* Science, 1995. **269**(5229): p. 1427-9.
242. Lohman, A.W., et al., *Pannexin 1 channels regulate leukocyte emigration through the venous endothelium during acute inflammation.* Nat Commun, 2015. **6**: p. 7965.
243. Billaud, M., et al., *A molecular signature in the pannexin1 intracellular loop confers channel activation by the alpha1 adrenoreceptor in smooth muscle cells.* Sci Signal, 2015. **8**(364): p. ra17.
244. Wirth, A., et al., *G12-G13-LARG-mediated signaling in vascular smooth muscle is required for salt-induced hypertension.* Nat Med, 2008. **14**(1): p. 64-8.
245. DMT. *Mounted artery on Pressure Myograph Setup*. 13.10. [cited 2016 13.10.]; DMT cannulated vessel]. Available from: http://www.dmt.dk/pressure-myograph---general.html.

246. DMT. *Pressure myograph setup*. [cited 2016 03.04.]; Available from: http://www.dmt.dk/files/drawings/pressure_setup.jpg.
247. Technologies, A. *Seahorse assay*. [cited 2016 14.10.]; Available from: http://www.agilent.com/en-us/products/cell-analysis-(seahorse)/mitochondrial-respiration-the-xf-cell-mito-stress-test.
248. Laker, R.C., et al., *A novel MitoTimer reporter gene for mitochondrial content, structure, stress, and damage in vivo.* J Biol Chem, 2014. **289**(17): p. 12005-15.
249. Kenwood, B.M., et al., *Identification of a novel mitochondrial uncoupler that does not depolarize the plasma membrane.* Mol Metab, 2014. **3**(2): p. 114-23.
250. LaFave, L.M., et al., *Loss of BAP1 function leads to EZH2-dependent transformation.* Nat Med, 2015. **21**(11): p. 1344-9.
251. Huang da, W., B.T. Sherman, and R.A. Lempicki, *Systematic and integrative analysis of large gene lists using DAVID bioinformatics resources.* Nat Protoc, 2009. **4**(1): p. 44-57.
252. Galmiche, G., et al., *Inactivation of serum response factor contributes to decrease vascular muscular tone and arterial stiffness in mice.* Circ Res, 2013. **112**(7): p. 1035-45.
253. Rupnick, M.A., et al., *Adipose tissue mass can be regulated through the vasculature.* Proc Natl Acad Sci U S A, 2002. **99**(16): p. 10730-5.
254. Ogalla, E., et al., *Structural, mechanical and myogenic properties of small mesenteric arteries from ApoE KO mice: characterization and effects of virgin olive oil diets.* Atherosclerosis, 2015. **238**(1): p. 55-63.
255. Sauve, M., et al., *Tumor Necrosis Factor/Sphingosine-1-Phosphate Signaling Augments Resistance Artery Myogenic Tone in Diabetes.* Diabetes, 2016. **65**(7): p. 1916-28.
256. Frisbee, J.C., K.G. Maier, and D.W. Stepp, *Oxidant stress-induced increase in myogenic activation of skeletal muscle resistance arteries in obese Zucker rats.* Am J Physiol Heart Circ Physiol, 2002. **283**(6): p. H2160-8.
257. Osmond, J.M., et al., *Obesity increases blood pressure, cerebral vascular remodeling, and severity of stroke in the Zucker rat.* Hypertension, 2009. **53**(2): p. 381-6.
258. McCurley, A., et al., *Direct regulation of blood pressure by smooth muscle cell mineralocorticoid receptors.* Nat Med, 2012. **18**(9): p. 1429-33.
259. Kanda, T., et al., *PPARgamma in the endothelium regulates metabolic responses to high-fat diet in mice.* J Clin Invest, 2009. **119**(1): p. 110-24.
260. Szanto, I. and C.R. Kahn, *Selective interaction between leptin and insulin signaling pathways in a hepatic cell line.* Proc Natl Acad Sci U S A, 2000. **97**(5): p. 2355-60.
261. Konner, A.C. and J.C. Bruning, *Selective insulin and leptin resistance in metabolic disorders.* Cell Metab, 2012. **16**(2): p. 144-52.
262. Rask-Madsen, C., et al., *Tumor necrosis factor-alpha inhibits insulin's stimulating effect on glucose uptake and endothelium-dependent vasodilation in humans.* Circulation, 2003. **108**(15): p. 1815-21.
263. Matrougui, K., et al., *High sodium intake decreases pressure-induced (myogenic) tone and flow-induced dilation in resistance arteries from hypertensive rats.* Hypertension, 1998. **32**(1): p. 176-9.
264. Chapleau, M.W., et al., *Structural versus functional modulation of the arterial baroreflex.* Hypertension, 1995. **26**(2): p. 341-7.
265. Wang, N., et al., *Vascular PPARgamma controls circadian variation in blood pressure and heart rate through Bmal1.* Cell Metab, 2008. **8**(6): p. 482-91.

266. Climent, B., et al., *Upregulation of SK3 and IK1 channels contributes to the enhanced endothelial calcium signaling and the preserved coronary relaxation in obese Zucker rats.* PLoS One, 2014. **9**(10): p. e109432.
267. Haddock, R.E., et al., *Diet-induced obesity impairs endothelium-derived hyperpolarization via altered potassium channel signaling mechanisms.* PLoS One, 2011. **6**(1): p. e16423.
268. Hemker, D.P. and J.W. Aiken, *Modulation of autonomic neurotransmission by PGD2: comparison with effects of other prostaglandins in anesthetized cats.* Prostaglandins, 1980. **20**(2): p. 321-32.
269. Town, M.H., J. Casals-Stenzel, and E. Schillinger, *Pharmacological and cardiovascular properties of a hydantoin derivative, BW 245 C, with high affinity and selectivity for PGD2 receptors.* Prostaglandins, 1983. **25**(1): p. 13-28.
270. Tang, E.H. and P.M. Vanhoutte, *Gene expression changes of prostanoid synthases in endothelial cells and prostanoid receptors in vascular smooth muscle cells caused by aging and hypertension.* Physiol Genomics, 2008. **32**(3): p. 409-18.
271. Ragolia, L., et al., *Accelerated glucose intolerance, nephropathy, and atherosclerosis in prostaglandin D2 synthase knock-out mice.* J Biol Chem, 2005. **280**(33): p. 29946-55.
272. Ide, T., et al., *Activation of nuclear receptors by prostaglandins.* Thromb Res, 2003. **110**(5-6): p. 311-5.
273. Narayanan, D., et al., *Mitochondria control functional CaV1.2 expression in smooth muscle cells of cerebral arteries.* Circ Res, 2010. **107**(5): p. 631-41.
274. Hinz, B., et al., *Mechanical tension controls granulation tissue contractile activity and myofibroblast differentiation.* Am J Pathol, 2001. **159**(3): p. 1009-20.
275. Mack, C.P., et al., *Smooth muscle alpha-actin CArG elements coordinate formation of a smooth muscle cell-selective, serum response factor-containing activation complex.* Circ Res, 2000. **86**(2): p. 221-32.
276. Merkestein, M., et al., *FTO influences adipogenesis by regulating mitotic clonal expansion.* Nat Commun, 2015. **6**: p. 6792.

8 Supplements

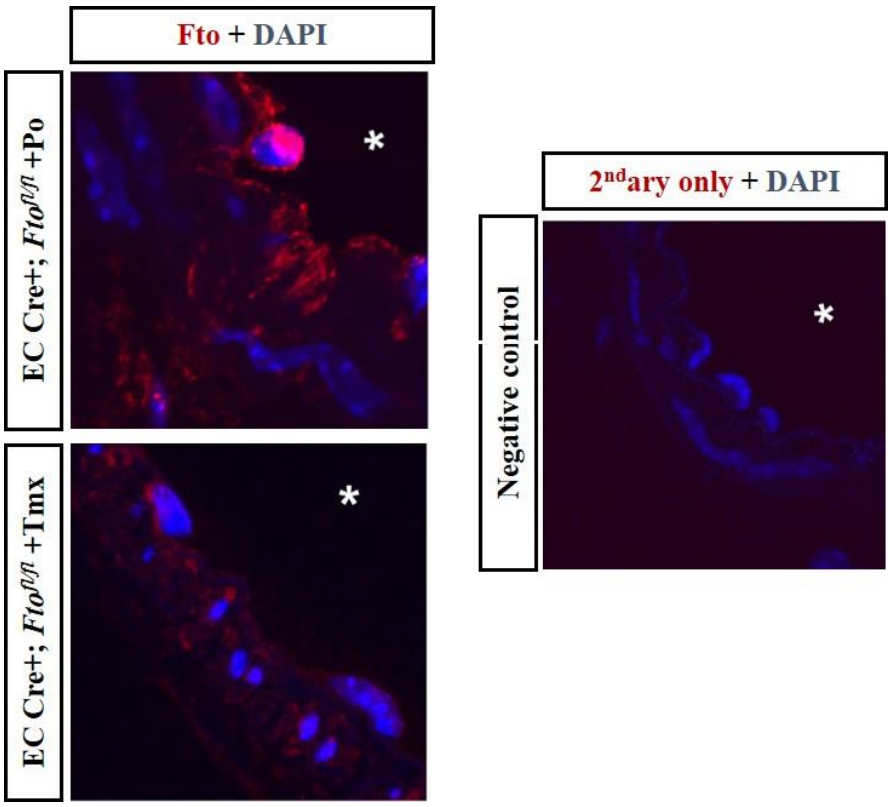

Suppl. Fig. 1: Immunofluorescence analysis of endothelial Fto expression in mesenteric arteries of EC Cre+ ;Fto$^{fl/fl}$ +Po and EC Cre+ ;Fto$^{fl/fl}$ +Tmx mice

3rd order mesenteric arteries were isolated from 20 week old EC Cre+; *Fto*$^{fl/fl}$ +PO and EC Cre+; *Fto*$^{fl/fl}$ +Tmx mice, paraffin-embedded, sectioned and fluorescently stained for Fto (red) and cell nuclei (blue). Negative control was performed on vessels with secondary antibody only and DAPI. Lumen of the vessel was indicated with an asterisk

Immunofluorescence analysis of mesenteric arteries of EC Cre+; *Fto*$^{fl/fl}$ +Tmx mice showed reduced Fto staining in ECs compared to respective ECs of mesenteric arteries of EC Cre+; *Fto*$^{fl/fl}$ +Po mice while no Fto staining was visible in the negative control.

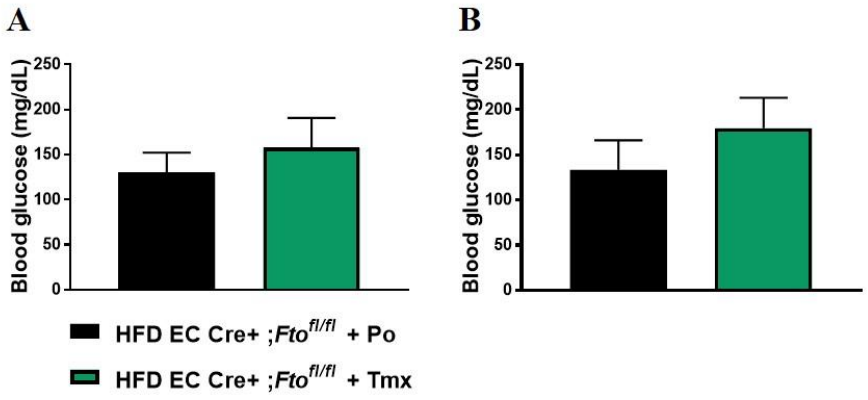

Suppl. Fig. 2: Measurement of blood glucose levels of unfasted and 5 h fasted HFD-fed EC Cre+; *Fto*$^{fl/fl}$ +Po and EC Cre+; *Fto*$^{fl/fl}$ +Tmx mice

Blood glucose levels were analyzed in 20- 23 week old HFD-fed EC Cre+; *Fto*$^{fl/fl}$ +Po and EC Cre+; *Fto*$^{fl/fl}$ +Tmx mice (A) Measurement of unfasted blood glucose levels revealed no significant differences between both genotypes (n=6, 6). (B) Similarly, blood glucose levels were unaltered between mice of both genotypes if the mice were fasted for 5 h (n=3 for HFD-fed EC Cre+; *Fto*$^{fl/fl}$ +Po, n=6 for HFD-fed EC Cre+; *Fto*$^{fl/fl}$ +Tmx).

Data represent mean ± SEM, for statistical analysis unpaired, two-tailed t-test was performed; $p<0.05$ was defined as significant.

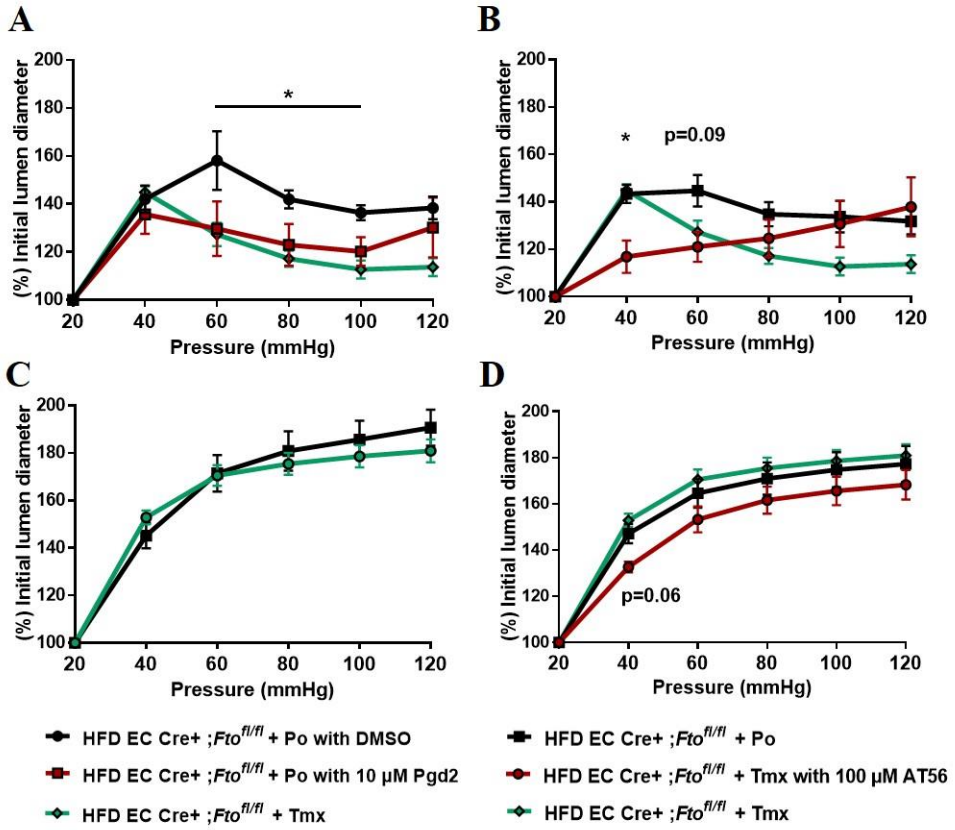

Suppl. Fig. 3: Analysis of active and passive pressure curves in mesenteric arteries in dependence of altered Pgd2 levels

Pressure curves were performed on 3rd order mesenteric arteries of 20 week old HFD-fed EC Cre+; *Fto*$^{fl/fl}$ +Po and EC Cre+; *Fto*$^{fl/fl}$ +Tmx mice in presence of Ca^{2+} (A and B) and without Ca^{2+} (C and D). Lumen diameter at each pressure is shown as percentage of initial lumen diameter at 20mmHg. In A and C mesenteric arteries of HFD-fed EC Cre+; *Fto*$^{fl/fl}$ +Po were analyzed in either the presence of 10 µM Pgd2 (dissolved in DMSO) or DMSO alone and compared to mesenteric arteries of EC Cre+; *Fto*$^{fl/fl}$ +Tmx mice

(n=3, 3, 3). In contrast, Pgds was inhibited by adding 100 µM AT56 to mesenteric arteries of EC Cre+; *Fto*$^{fl/fl}$ +Tmx mice and pressure curves compared to mesenteric arteries of HFD-fed EC Cre+; *Fto*$^{fl/fl}$ +Po and EC Cre+; *Fto*$^{fl/fl}$ +Tmx mice (n=3, 6, 3) (B and D). (A) Active curve measurement revealed significantly reduced lumen diameter between 60 mmHg and 100 mmHg in mesenteric arteries of HFD-fed EC Cre+; *Fto*$^{fl/fl}$ +Po mice with 10 µM Pgd2 levels compared to respective vessels treated with DMSO alone. (B) 100 µM AT 56 induced a significantly reduced lumen diameter at 40 mmHg and a trend at 60 mmHg (p=0.09) compared to respective mesenteric arteries of HFD-fed EC Cre+; *Fto*$^{fl/fl}$ +Po and EC Cre+; *Fto*$^{fl/fl}$ +Tmx mice without inhibitor in the active curve. (C) Passive pressure curves showed no significant effect of either DMSO alone or 10 µM Pgd2 dissolved in DMSO. (D) Analysis of passive curves in mesenteric arteries revealed that addition of AT56 to mesenteric arteries of HFD-fed EC Cre+; *Fto*$^{fl/fl}$ +Tmx mice showed a trend to reduced lumen diameter compared to respective vessels without AT56 addition at 40 mmHg (p=0.06).
Data represent mean ± SEM, for statistical analysis either ordinary 2-way ANOVA (A and C) or 1-way ANOVA (B and D) were performed; p<0.05 was defined as significant.

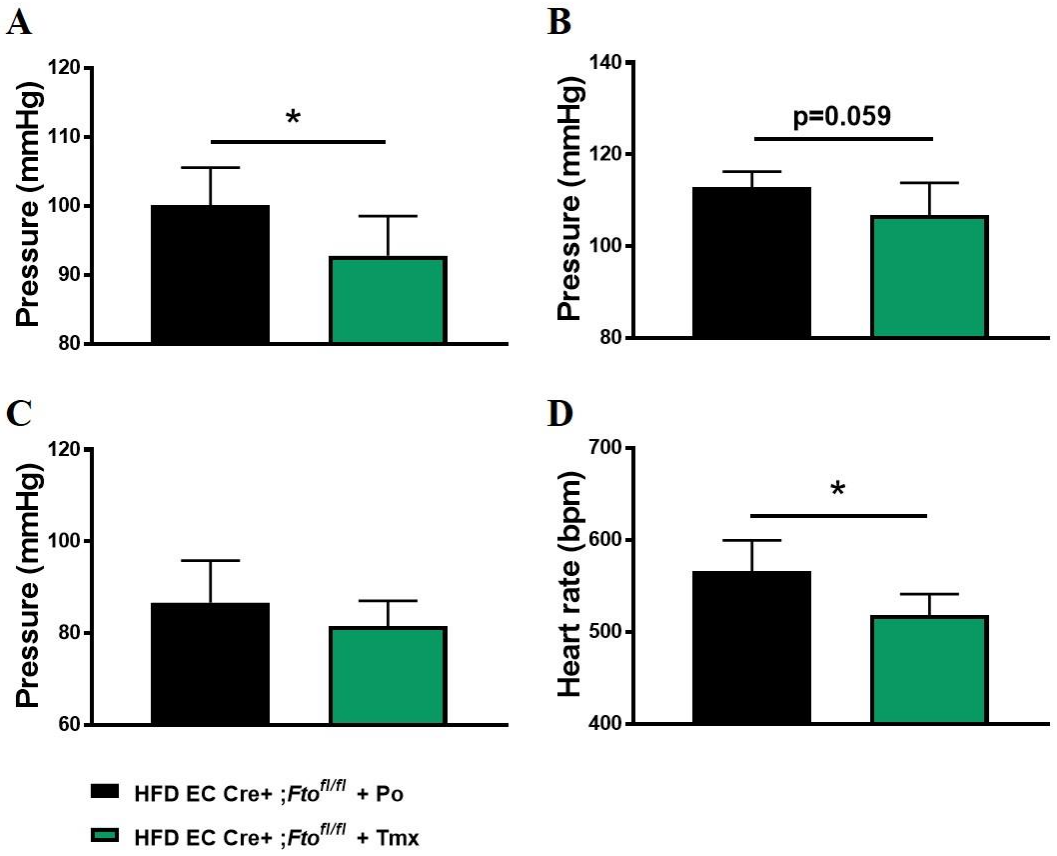

Suppl. Fig. 4: Blood pressure analysis in HFD-fed EC Cre+; *Fto*$^{fl/fl}$ +Po and EC Cre+; *Fto*$^{fl/fl}$ +Tmx mice

Blood pressure was measured in 20 week old HFD-fed EC Cre+; *Fto*$^{fl/fl}$ +Po and EC Cre+; *Fto*$^{fl/fl}$ +Tmx mice for 7 following days using radiotelemetry. Systolic and diastolic blood pressure as well as heart rate were assessed and mean arterial pressure calculated (n=7, 9). (A) Day time mean arterial pressure was significantly reduced in HFD-fed EC Cre+; *Fto*$^{fl/fl}$ +Tmx mice compared to HFD-fed EC Cre+; *Fto*$^{fl/fl}$ +Po mice. (B) Day time systolic blood pressure showed a trend to reduced blood pressure in HFD-fed EC Cre+; *Fto*$^{fl/fl}$ +Tmx mice compared to HFD-fed EC Cre+; *Fto*$^{fl/fl}$ +Po mice (p=0.059). (C) Diastolic blood pressure showed no significant differences between both genotypes. (D) Heart rate was significantly reduced by endothelial *Fto*-deficiency compared to Po-injected litters in HFD-fed mice.
Data represent mean ± SEM, for statistical analysis unpaired, two-tailed t-test was performed; p<0.05 was defined as significant.

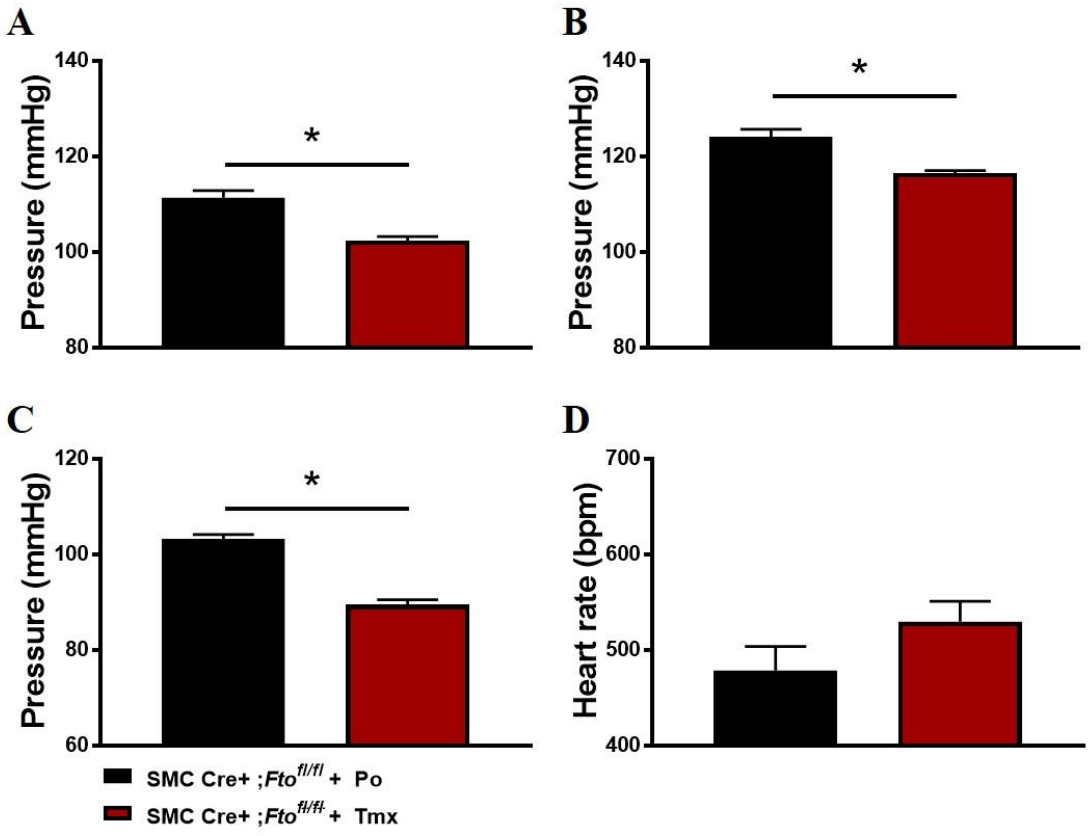

Suppl. Fig. 5: Blood pressure analysis in SMC Cre+; *Fto*$^{fl/fl}$ +Po and SMC Cre+; *Fto*$^{fl/fl}$ +Tmx mice
Blood pressure was measured in 20 week old SMC Cre+; *Fto*$^{fl/fl}$ +Po and SMC Cre+; *Fto*$^{fl/fl}$ +Tmx mice for 7 following days using radiotelemetry (n=3, 3). Systolic and diastolic blood pressure as well as heart rate were assessed and mean arterial pressure calculated. (A) 24 h mean arterial pressure (MAP) was significantly reduced in SMC-specific *Fto*-deficient mice compared to SMC Cre+; *Fto*$^{fl/fl}$ +Po mice. (B) 24 h systolic blood pressure was also significantly reduced in SMC Cre+; *Fto*$^{fl/fl}$ +Tmx mice compared to respective Po-injected litters. (C) Similar to systolic blood pressure, 24 h diastolic blood pressure was also significantly reduced in SMC Cre+; *Fto*$^{fl/fl}$ +Tmx mice compared to SMC Cre+; *Fto*$^{fl/fl}$ +Po mice. (D) 24 h analysis of heart rate revealed no significant differences between both groups.
Data represent mean ± SEM for statistical analysis unpaired, two-tailed t-test was performed; $p<0.05$ was defined as significant.